Using Knockout Mice to Study the Molecular Mechanisms that Shape Auditory Nerve Responses

by

Annette M. Taberner

B.S. Electrical Engineering
Florida International University, 1996

M.S. Computer Engineering
Florida International University, 1998

Submitted to the Harvard-M.I.T. Division of Health Sciences and Technology in partial fulfillment of the requirements for the degree of

DOCTOR OF PHILOSOPHY

at the

MASSACHUSETTS INSTITUTE OF TECHNOLOGY

February 2005

Signature of Author: .....
Harvard-M.I.T. Division of Health Sciences and Technology
January 11, 2005

Certified by: .....
M. Charles Liberman, Ph.D.
Professor of Otology and Laryngology, Harvard Medical School
Thesis Supervisor

Accepted By: .....
Martha L. Gray, Ph.D.
Edward Hood Taplin Professor of Medical and Electrical Engineering
Co-Director, Harvard-M.I.T. Division of Health Sciences and Technology

Using Knockout Mice to Study the Molecular Mechanisms that Shape Auditory Nerve Responses

by

Annette M. Taberner

Submitted to the Harvard-M.I.T Division of Health Sciences and Technology on January 14, 2005 in partial fulfillment of the requirements for the degree of Doctor of Philosophy

ABSTRACT

The ease of targeted genetic modification makes the mouse a valuable model to study hearing and deafness. A powerful window into cochlear function can be obtained by recording from single auditory (AN) fibers, primary afferents connecting cochlear inner hair cells to the brain. This thesis provides the first systematic analysis of fundamental response properties of the mouse AN, including rate and timing of spontaneous and sound-evoked discharge, frequency selectivity, dynamic range, and the relations between spontaneous rate and these other response properties. Three wildtype strains were compared: CBA/CaJ (because it retains normal cochlear sensitivity as it ages); and C57BL/6 and 129/SvJ (because they are used in "knockout" generation). Two lines with targeted deletion of inner ear genes were also studied.

The cochlea in mouse responds to frequencies octaves higher than in humans or most other mammals; nevertheless, most other AN characteristics were fundamentally similar to those in well-studied mammals. The only significant differences were 1) smaller dynamic ranges in all three strains; and 2) high-frequency threshold elevation and tuning degradation in C57BL/6 and 129/SvJ, consistent with early-onset degeneration of basal-turn sensory cells in these strains.

The mutant lines studied included deletion of 1) Calcitonin-Gene-Related Peptide (CGRP), a neurotransmitter expressed by cochlear efferent fibers, or 2) the α subunit of BK channels, a large-conductance K^+ channel, expressed in hair cells and AN fibers, and implicated in cochlear tuning in lower vertebrates. Loss of CGRP had no detectable effect on AN responses, suggesting a minimal role in cochlear processing. Loss of BK channels led to dramatic decreases in sound-evoked discharge rates and spike synchronization, without changes in frequency selectivity. The degraded spike synchronization likely arises from slowing rise-times of inner hair cell receptor potentials observed *in vitro*; the decreased steady-state rates likely arise from depolarization block in the AN fibers themselves.

Thesis Supervisor: M. Charles Liberman, Ph.D.
Title: Professor of Otology and Laryngology, Harvard Medical School

Acknowledgements

I would like to acknowledge the contributions made by so many people towards my development as a scientist and as a human being in general. This thesis work could not have been done without their support and kindness.

I would like to begin by thanking my thesis supervisor, Dr. M. Charles Liberman, who has dedicated much of his busy time to helping me to develop into an independent scientist. I am grateful to him for all that he has taught me and for his patience in my growing process. I would also like to thank my committee members: Dr. M. Christian Brown, Dr. Stefan Heller and Dr. Herbert Voigt. They have been with me since my oral exam and have quite literally seen me "grow up" as a scientist. I am grateful for their direction and support.

Throughout my tenure at EPL, I have sought the advice of every professor that works in the lab. I am grateful to all of them, but would like to extend a special thanks to Dr. John Guinan, Jr. and Dr. Christopher Shera, who gave generously of their time to help me. I went to them so often with my questions that they really ought to be honorary thesis committee members.

I would also like thank my academic advisor, Dr. John Rosowski; a true father figure who was not only a great advisor, but also a source of much hope and encouragement for me. I am grateful for his kindness, support, and belief in me. In a long and difficult journey, John has helped me to see that I had something of value to contribute to the world, and that I should be proud of my hard work.

I have learned an enormous amount and have grown as a scientist in the Liberman lab. Much of the learning came from my interaction with my co-lab members, Dr. Stephane Maison and Keith Darrow, who were always available to talk about my thesis work and provide me with suggestions. I am also grateful to Connie Miller and Leslie Liberman who helped me do histology and provided the much needed words of encouragement throughout the ups and downs of doing experimental research.

I think that every student who comes to EPL finds in our Research Administrator, Dianna Sands, an advocate who cares about them. Going to Dianna with a problem was very much like going to my mom with a problem: I always left knowing that everything was going to be O.K. I am grateful to her for all the times she has gone to bat for me. Quick with a joke, a story, or an explanation, I have the greatest respect and admiration for her work and feel privileged to have known her.

Doing research at EPL would be very difficult if not for the help of our engineers: Ish Stefanov-Wagner, Chris Scarpino, and Frank Cardarelli. They are the ones that help maintain our recording chambers and computer equipment. In my years at EPL, they have always been more than happy to discuss any of my numerous problems with experimental equipment. I feel that much of my experimental work was made possible because of their hard work.

Many friends in the Speech and Hearing Bioscience and Technology program contributed to my thesis work through their availability and encouragement. I would like to especially thank Bradford Backus, Becky Poon, Teresa Santos, and Jocelyn Songer, who gave generously of their time by sitting through countless practice talks and helping me think through my research.

Without the sacrifice and love of my parents I would not have reached this stage in my life. Words cannot describe how grateful I am for all they have done to help me get an education and to help me grow as a human being. Their lessons about the importance of hard work,

responsibility, gratitude, and love, are lessons that translate today into the success of this thesis (among other things).

The prayers of all my family members and close friends were also a source of encouragement and peace. The love of my family and friends is a constant reminder of all that is beautiful and worth living for in my life. I'd like to thank my sister Barbara, my nieces Barbie and Stephanie, my brother-in-law Manolo, my cousins Baldo, Elena, Aida, and Ramon, and my close friends that are like family, Sylvia, Cristina, Nick, Letty, Regina, and Norma, for their love and support in every moment of my life. I love them all deeply and am grateful for their love.

On our wedding day, my husband offered to help share my load whenever I felt overburdened. During the crazy times before my thesis defense he did just that by helping me get things into perspective and letting me know how much I was loved. I cannot explain how grateful I am for having the opportunity to spend the rest of my life with such a loving, integrated, and truly exceptional human being. It is my hope that he will see in me what I already see in him: a source of peace, hope, and love.

Table of Contents

List of Figures

Chapter 2

Chapter 3

Chapter 4

Chapter 5

Chapter 6

Chapter 1

Introduction

The availability of transgenic and mutant lines with interesting cochlear phenotypes makes the mouse a valuable model for the study of the auditory system. Minimally invasive measures of auditory function are often used to assess cochlear phenotype in mice. Such measures include distortion product otoacoustic emissions (DPOAEs), auditory brainstem responses (ABRs), and compound action potentials (CAPs) (Maison et al. 2003; Ruttiger et al. 2004; Vetter et al. 1999). Although these measures can rapidly provide useful information about cochlear sensitivity as a function of cochlear location, there are many aspects of cochlear physiology that cannot be unambiguously inferred from these gross responses, because they represent the summed activity of numerous cochlear generators.

Although requiring more invasive procedures, recordings from single auditory nerve (AN) fibers can provide more detailed insight into the functional state of the inner ear. The vast majority of AN fibers in the mammalian ear make synaptic contact with only a single inner hair cell, by means of one synaptic complex (Liberman 1980; Spoendlin 1969; Spoendlin and Schrott 1988). Thus, recording from a single AN provides a sensitive window into the microenvironment of a single sensory cell in the inner ear and a sensitive functional metric of the transducer apparatus on the specific inner hair cell contacted and the neighboring outer hair cells that influence its local cochlear mechanics. Analysis of the fine timing patterns of spike discharges (e.g. the degree of phase locking or the response adaptation) can provide insight into the processes involved in synaptic transmission between the hair cell and its primary sensory neuron. By sampling from numerous fibers in the same animal or mutant strain, a detailed picture can be assembled of the outputs of the sensory transduction and synaptic transmission machinery all along the cochlear duct.

There have been only two previous reports of single-fiber activity from the mouse AN. These pioneering studies were not primarily interested in understanding cochlear mechanisms. One was aimed at validating the use of the galvanic skin response as a minimally invasive measure of cochlear sensitivity (Finck and Berlin 1965) and thus collected mainly data on single-fiber thresholds. The other was aimed at understanding the neurophysiological bases for critical bands and thus collected data on single fiber thresholds and on the masking of tone responses by noise bands (Ehret and Moffat 1984). In contrast, an aim of this thesis was to describe those fundamental aspects of auditory nerve response that may provide the most insight into the mechanisms of transduction and synaptic transmission in the inner ear, especially when coupled with the use of targeted genetic modification in the mouse model. Thus, in chapter 3, a systematic description is provided of all the most fundamental response properties of the mouse AN response, including the distribution of spontaneous rates, tuning curves, rate-vs-level functions, dynamic range, response adaptation, degree of phase-locking and the relations between spontaneous rate and the aforementioned response properties. Because the CBA/CaJ mouse strain is commonly used in auditory research and has excellent cochlear sensitivity

throughout its life span (Jimenez et al. 1999; Li and Borg 1991; Zheng et al. 1999), it was chosen for this initial study.

Comparisons between mouse AN physiology and that of other mammals is of interest, because the mouse cochlea is specialized for higher frequency stimuli than cat, guinea pig, chinchilla, or gerbil, the other mammalian species in which AN response has been well studied. It will be shown in chapter 3 that despite the difference in hearing ranges, AN responses in mouse are qualitatively similar to that found in other mammals. This is an important finding since it indicates that the mouse falls within the general mammalian plan as it applies to the coding of sound in the auditory nerve. Therefore, changes in AN function observed in transgenic and mutant lines of mice are likely to be seen in other mammalian species with similar genetic phenotypes. This makes the mouse a valuable model for the study of the molecular mechanisms of auditory health and disease.

A common technique used to create transgenic mice favor the use of C57BL/6 and 129/SvJ mouse strains. In this technique, pluripotent mouse embryonic stem (ES) cells are removed from the inner cell mass of early embryos (blastocyst) and placed in a culture dish containing a medium which allows them to reproduce but not differentiate (Watson et al. 1998). Multiple copies of a mutant gene are introduced into the stem cells through transfection and a screening process is applied to identify ES cells in which homologous recombination of the mutant gene occurred (Watson et al. 1998). The 129 strains are the most favored for recombinant genetics because their ES cells reproduce well in culture and are more tolerant of transfection and selection procedures than ES cells derived from other strains (Mullen and Ryan 2001). After transfection, ES cells with homologous recombination are introduced into the embryos of mice that have a different coat color. For example, ES cells from the 129 strain (agouti colored coats) are usually injected into C57BL/6 mouse embryos (black colored coats). Germline chimeras are identified by mating chimeric male offspring with C57BL/6 females. The offspring of germline chimeras would have coats that display a mixture of agouti (from 129/SvJ) and black (from C57BL/6) colors. Finally, subsequent generations are produced by interbreeding among the hybrid offspring.

Interpretation of AN phenotypes in transgenic or mutant mice having C57BL/6 or 129/SvJ backgrounds is complicated by the presence of cochlear pathology in the wildtype strains. C57BL/6 mice are commonly used as animal models for the study of age-related hearing loss (AHL); they display a severe hearing loss that starts at high-frequencies and progresses to low-frequencies with age (Hequembourg and Liberman 2001). Studies on the morphological correlates of age-related hearing loss in the C57BL/6 cochlea describe a base-to-apical degeneration of hair cells, with the outer hair cells leading, along with AN fiber degeneration (Hequembourg and Liberman 2001; Spongr et al. 1997). Physiologic correlates of age-related hearing loss in the C57BL/6 strain include progressive elevations of CAP and ABR responses, along with decreases in DPOAE amplitudes (Hequembourg and Liberman 2001) (Jimenez et al. 1999; Lang et al. 2002). Similar to the C57BL/6, the 129/SvJ strain displays AHL that progresses from high-to-low frequencies (Zheng et al. 1999a). In chapter 4, the spontaneous and sound-evoked discharge properties of AN fibers recorded from the CBA/CaJ strain, are compared to recordings in the C57BL/6 and 129/SvJ strains. It will be shown that setting aside differences in hearing sensitivity, AN fiber responses are qualitatively and quantitatively similar among the three strains.

The last two chapters of the thesis provide examples of how single-fiber recordings in knockout mice can offer insights into the molecular mechanisms that shape auditory nerve

responses. The mutant mice studied are Calcitonin-Gene Related Peptide (CGRP) knockouts and BK-Channel knockouts. Both knockouts have genetic mutations that affect the expression of proteins that are found in cells thought to be important for auditory function (Maison et al. 2003; Ruttiger et al. 2004) and have expected auditory phenotypes that can best be captured from single AN fiber recordings. Results from these studies confirm the power of the single-fiber approach and provides a basis on which future studies using knockout mice can be built.

Chapter 2

Methods

2.1 Animals, anesthesia, and surgical approach

Single-fiber recordings were made from the auditory nerve in CBA/CaJ mice aged 8 - 17 weeks, and in two knockout mouse lines with targeted gene deletion: 1) CGRP, the Calcitonin gene related peptide (Lu et al. 1999) and 2) BK, the α subunit of the large-conductance K^+ channel (Ruttiger et al. 2004). The CGRP knockout mice have a genotype that differs from that of C57BL/6 only at the CGRP gene locus (i.e., they are congenic). Animals from the CGRP knockout line were studied at ages 16-17 weeks, as were their wildtype littermates. The BK-channel knockout mice are congenic with a 129/SvJ background. Animals from the BK channel knockout line, and their wildtype littermates, were studied at ages 7 –17 weeks.

Animals were anesthetized with 10% xylazine (5 mg/kg i.p.) and 20% urethane (1.32 mg/kg i.p.). Animal temperature was maintained near 38^0C with a heating pad and by maintaining the ambient temperature in the experimental chamber at about 33^0 C.

For the surgical approach, the cartilaginous ear canals were removed, scalp reflected, skull opened, and a semi-cerebellectomy performed to expose the left cochlear nucleus. Glass microelectrodes filled with 2M KCL and 4% methyl blue were directed at the surface of the cochlear nucleus, ~1 mm medial to the edge of the temporal bone, angled anteriorly at 24^o in the sagittal plane and laterally at 10^o in the coronal plane. All animal procedures were approved by the IACUC of the Massachusetts Eye and Ear Infirmary.

2.2 Acoustic System

The sound system comprised dual electrostatic sound sources (TDT ED-1) and a Knowles electret microphone coupled to a probe tube. The sensitivity of the probe-tube microphone was calibrated for frequencies between 1.0 and 73 kHz using a calibrated Bruel & Kjaer 1/4" condenser microphone in a coupler. In every experiment, the calibrated acoustic assembly was fitted within the opening of the mouse ear canal. In-animal sensitivity analysis was performed before each experiment to determine the maximum sound pressure level that could be delivered to the mouse ear for test frequencies ranging between 1.0 and 73 kHz.

2.3 Distortion-Product Otoacoustic Emissions and Preparation Stability

Distortion-product otoactoustic emissions (DPOAEs) were monitored throughout the experiments to assess cochlear stability. DPOAEs can be used to assess cochlear function since the cochlea, under normal conditions, is a non-linear system that produces DPOAEs when two pure tones (f_1,f_2) are simultaneously presented. A decrease in cochlear sensitivity will be reflected in a decrease in DPOAE amplitude. Of the distortion products produced by the cochlea, the $2f_1$-f_2 has the largest amplitude and is the one monitored in this study. DPOAEs were measured at the beginning of each experiment, before cerebellar aspiration, using f_2 frequencies from 5.6 to 45.2 kHz in half-octave steps.

The DPOAE was recorded in response to primary tones f_1 and f_2, with f_2/f_1=1.2 and $L_2 = L_1$ - 10 dB. The ear-canal sound pressure waveform was amplified and digitally sampled at 4 μs intervals. Fast-Fourier transforms were computed from averaged sound pressure waveforms, and the DPOAE and surrounding noise floor were extracted. Because the noise floor amplitude is a function of the primary-tone frequencies used, DPOAE threshold was defined differently based on the f_2 frequency used. "Threshold" was defined as the primary-tone level necessary to produce a $2f_1$-f_2 DPOAE of 0 dB (f_2 = 5.6 kHz, 8 kHz, 11.3 kHz, or 16 kHz), 5 dB (f_2 = 22.6 kHz), 10 dB (for f_2 = 32 kHz) or 15 dB (f_2 = 45.2 kHz).

During single-fiber recordings, the DPOAEs were re-checked at the f_2 nearest the characteristic frequency (CF) of each fiber studied. Data are included in the final database for CBA/CaJ if DPOAE threshold shifts, using an f_2 nearest fiber CF, were $\leq$ 5 dB re initial values. For CGRP knockout mice, and their wildtype littermates, data are included if DPOAE threshold shifts at $2f_1$-f_2 were $\leq$ 10 dB re initial values. A larger DPOAE threshold shift criterion was used, because the data pool was relatively small compared to CBA/CaJ. DPOAEs could not always be used to monitor cochlear condition in the BK channel knockouts, since most animals had initial DPOAE threshold values too high to be able to monitor threshold changes (see Chapter 6).

2.4 Stimuli and Response Measures

50-msec noise bursts were used as search stimuli. Tone bursts were used for all other sound-evoked measures (except phase-locking): they were 50 msec in duration, with 2.5 msec rise-fall and a repetition rate of 10/sec. Tuning curves were measured under computer control, and represent isorate contours for response magnitude of 10 sp/sec > spontaneous rate (Liberman 1978). Spontaneous rates were calculated from 10 sec samples.

Rate-level functions were measured at CF with 10 - 40 tone bursts per level. Levels (in 5 dB steps) were presented in random order. Rate-level functions were fit using a modified version of a previously published model (Sachs et al. 1989). The published model has three components. The first component (equation 1) passes the input sound pressure "*P*" through a nonlinear attenuator to obtain a value $\hat{P}$ that is the input to a saturating non-linearity that represents the inner ear transfer function (equation 1). θ_I in equation 1 represents the "compression threshold" of the model and the point when $\hat{P}$ stops being a linear function of the sound pressure "P". The parameter α was fixed as 0.27. The second component (equation 2) obtains a value for the driven rate (R_d) by passing $\hat{P}$ through a saturating non-linearity. As will be shown in later chapters, mouse rate-level functions are generally steeper than those found in cat, the species used by Sachs et. al. to create their model. Therefore, a modification was made to the model in order to fit mouse rate-level functions. Namely, the input to the saturating non-linearity was given an exponential β (a free parameter) which allowed the function to have steeper slopes (equation 2). In equation 2, R_M represents the driven saturation rate of the fiber and θ_E gives the value of $\hat{P}$ at which the driven rate reaches half of its maximum value. The last component (equation 3) of the model obtains the total discharge (R_{TOT}) rate by adding the spontaneous rate (R_{sp}) to the driven rate (R_d).

$$\hat{P} = P \cdot \left(\frac{1}{\left(1 + \frac{P}{\theta_I}\right)^2} \right)^{\alpha} \qquad (1)$$

$$R_d = \frac{R_m \left(\frac{\hat{P}^{\beta}}{\theta_E} \right)^{1.77}}{1 + \left(\frac{\hat{P}^{\beta}}{\theta_E} \right)^{1.77}} \qquad (2)$$

$$R_{TOT} = R_d + R_{sp} \qquad (3)$$

The fitting procedure was done in Matlab® using the function *fminsearch*, which performs a multidimensional, unconstrained, nonlinear minimization (Nelder-Mead (Nelder and Mead

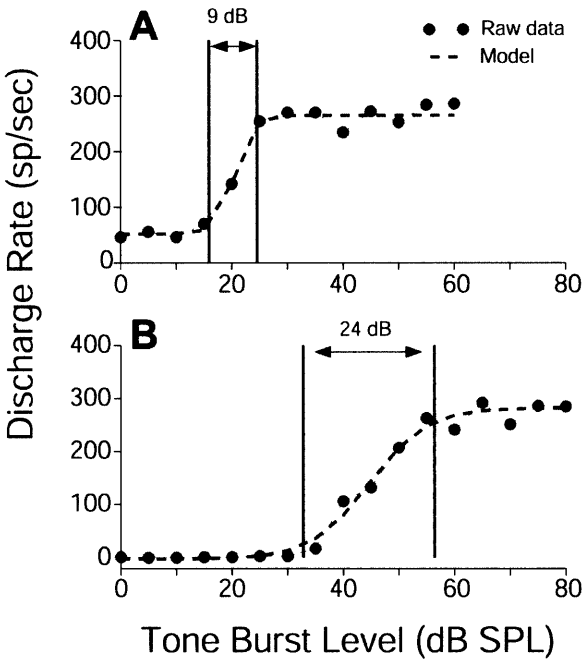

Figure 2.1: Model fitting of rate-level functions using a modification of the formula developed by Sachs et al (1989). **Panels A and B**: raw data (filled symbols) and model fit (dashed lines) for the rate-level function for a fiber with CF = 18.8 kHz and SR = 47.6 sp/sec (**A**) and CF = 23.7 kHz and SR = 0.1 sp/sec (**B**). Dynamic range (paired vertical lines in each panel) was defined as the difference between SPLs evoking 10% and 90% of the (model fit) maximum driven rate. The root-mean-square-errors for the model fits were 13.2 sp/sec and 13.9 sp/sec in panels A and B, respectively.

1965)). Dynamic range was defined as the difference between SPLs evoking 10% and 90% of the (model fit) maximum driven rate (Figure 2.1).

Measures of synchrony were obtained from post-zero-crossing (PZC) histograms derived from the presentation of tones of 15 sec duration. The tone frequencies were constrained (f = 1.0, 1.6, 2.0, 2.5 or 4 kHz) so that an integer number of cycles fit in the digital buffer. The degree of phase-locking was examined using the synchronization index calculated as described by Johnson (Johnson 1980).

When measuring phase-locking in AN response, care was taken to eliminate artifactual synchrony due to microelectrode pick-up of cochlear microphonic potentials. A model developed by Johnson (Johnson 1978) was used to compute a *synchrony noise floor* below which synchrony may be artifactual. According to the model, the synchronization index (SI) due to the microphonic artifact is given by:

$$SI_{artifact} = \sqrt{8}\,\pi f\,\gamma t \qquad (4)$$

assuming a randomly-distributed spike train contaminated by an additive sine wave at frequency f; γ is the ratio of the rms stimulus artifact amplitude to the peak spike amplitude, and t is the rise time of the spikes. Rise time t and ratio γ were calculated from measurements of digitized spike trains obtained during each synchrony measurement: the amplitude of the sine wave (microphonic) component at the stimulus frequency was extracted via FFT. Only the data for which the measured SI was greater than $SI_{artifact}$ are included in this thesis.

2.5 Classifying Auditory Nerve Fibers

Because the auditory nerve (AN) in mouse is difficult to expose directly without compromising cochlear function, the AN was reached via electrode penetrations which first travel through the cochlear nucleus (CN), which can be readily exposed. Electrode angles and insertion area were chosen to avoid the anteroventral CN, which contains cells with AN-like responses in other mammalian species (Rouiller and Ryugo 1984). Based on surface landmarks, most electrode penetrations entered through the anterior portions of the DCN (figure 2.2A). Cell types encountered along the electrode track yielded post-stimulus-time (PST) histograms with "pauser/build-up", "chopper", "onset", "primary-like with notch", and "primary-like" shapes (Blackburn and Sachs 1989; Rhode and Smith 1986b; Rouiller and Ryugo 1984; Young et al. 1988) (figure 2.2B-F). As expected, non-primary like cells tended to be seen superficially in the electrode tracks, whereas "primary-like" (AN) responses were almost exclusively seen at electrodes sites deeper than 1 mm from the point of penetration.

A classification scheme based on PST shape, first spike latency (FSL), and the coefficient of variation (CV) of the interspike intervals, was adopted to distinguish AN and CN cell types. In cat, where AN and CN can be separately accessed by microelectrodes (with visible superficial landmarks identifying the Schwann-glial border separating these two structures), AN responses are more irregular (i.e., larger CV for interspike intervals) and show a smaller FSL than most CN cells with similar characteristic frequencies and spontaneous rates (Young et al. 1988). PST histograms used to characterize response type were based on 150-350 tone burst presentations at CF and were always presented at 30 dB above threshold. A measure of FSL, i.e. the mode of the

FSL distribution, and the CV, i.e. the ratio of the standard deviation to the mean of the interspike interval distribution, were both obtained from responses to 150 CF tone bursts at 30 dB above threshold. CV measures were derived only from spikes occurring 20-40 msec after tone-burst onset (i.e., excluding the initial and final 10 msec, where some spike intervals may include spontaneous discharge).

In early experiments to develop effective criteria for differentiating AN fibers from CN cells, tone-burst responses were obtained and analyzed from all fibers encountered along each electrode pass, Figure 2.3 shows the relationship between CV and FSL in fibers subjectively classified by PST shapes. Results suggest that mouse AN fibers have CVs ≥ 0.5 and FSLs ≤ 5 msec, which are similar to values reported for cat (Young et al. 1988). As in cat, there appears to be some overlap of CV and FSLs between AN and CN (e.g., for the "pri-notch" CN units) (Young et al. 1988). Nevertheless, the data in Figure 2.3 suggest that the following criteria adopted for classification as AN fiber should provide the best trade-off between sensitivity and

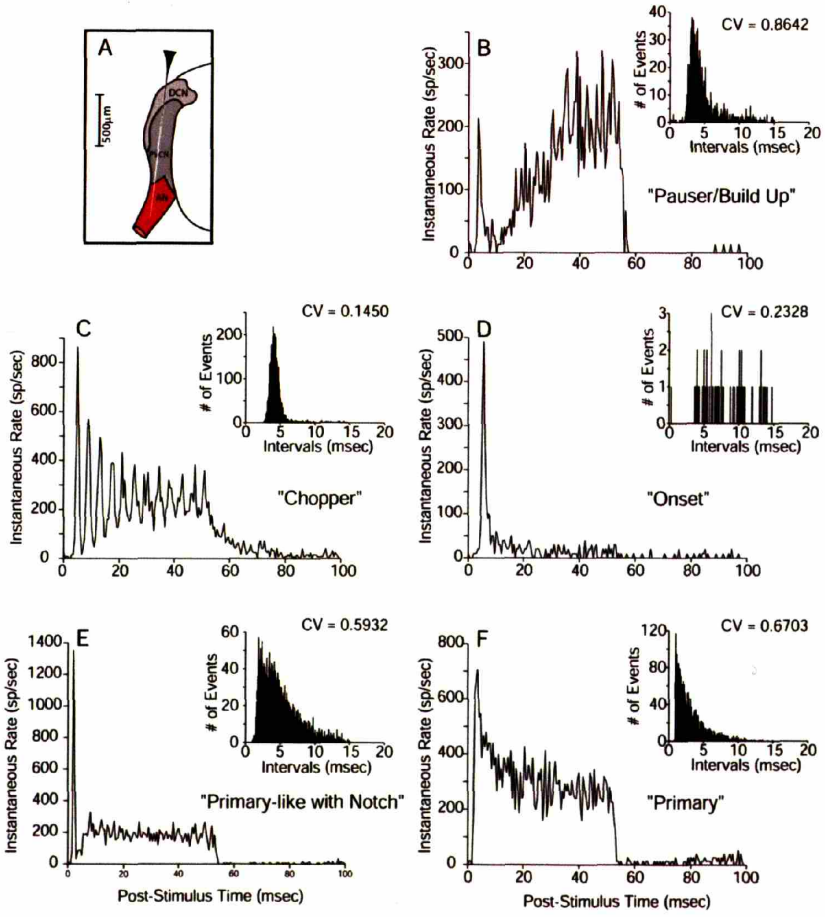

Figure 2.2: AN fibers in the mouse were reached via the cochlear nucleus. **Panel A**: recording electrode traverses the dorsal cochlear nucleus (DCN) and posteroventral cochlear nucleus (PVCN) before reaching the AN. **Panels B-F**: PST histograms of cells encountered along the electrode tract. PSTs were obtained from the presentation 150 CF tones 30 dB above response threshold. Histograms of the interspike intervals and their corresponding coefficient of variation (CV) values are shown as insets for each PST.

specificity: 1) CV $\geq$ 0.5, (2) FSL $\leq$ 5msec, (3) electrode depth $\geq$ 1000 and 4) "primary-like" PST.

In later experiments, the superficially located CN cells were bypassed in order to increase the yield of AN fibers in each animal studied. By the end of the experimental series, the mean yield of AN recordings had grown to 7/animal (with a maximum of 16/animal).

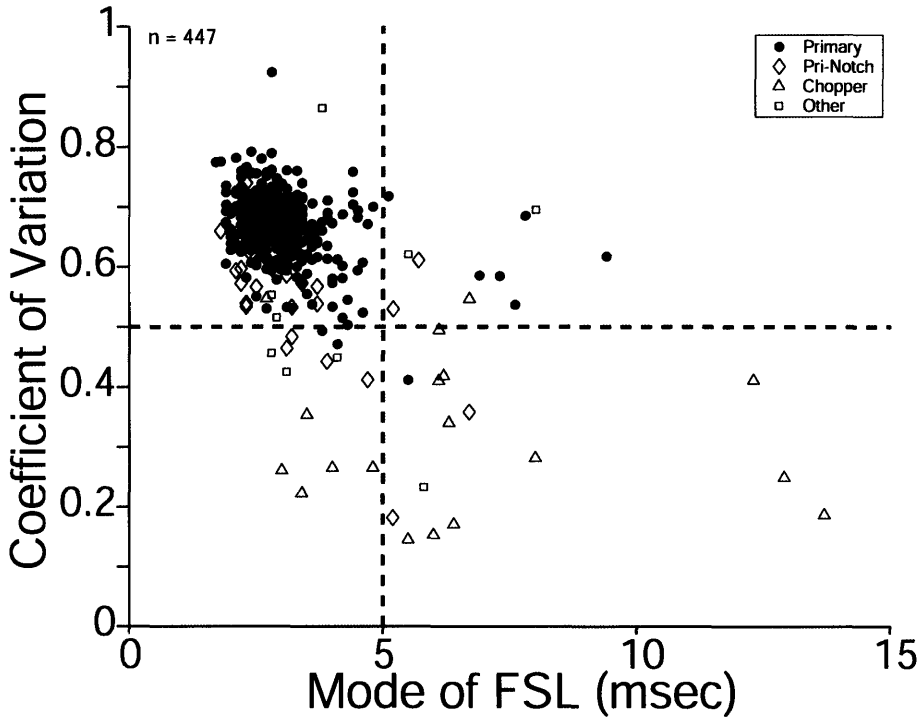

Figure 2.3: Criteria for distinguishing AN fiberss from cochlear nucleus (CN) cells. Relation between the coefficient of variation of the interspike intervals (CV) and the mode of the first spike latency (FSL) for all units, including from the preliminary study, encountered. CV is the ratio of the standard deviation to the mean of the interspike interval distribution obtained from responses to 150 CF tone bursts, 30 dB above threshold. Symbols represent the subjective classification based on PST shapes (see legend). An acoustic delay of 0.5 msec should be subtracted from the FSL values shown in order to obtain time re arrival of acoustic signal at the eardrum.

2.6 Robustness of criterion for identifying AN fibers

Based on the classification described in the previous section, the fiber population studied must be dominated by AN responses. However, CN units with "primary-like" responses could also be included, given that, in cat, there is some overlap in response latency and regularity measures between these CN cells and AN fibers (Young et al. 1988). CN cells that can generate primary-like responses include spherical and globular bushy cells (Blackburn and Sachs 1989) (Smith et al. 1993).

Spherical bushy cells are located in the anterior AVCN. They receive axosomatic synapses from AN fibers in the form of endbulbs of Held (Sento and Ryugo 1989) and are thought to be

important for low-frequency sound localization since they preserve temporal information and project to the medial superior olive bilaterally (Smith et al. 1993). In mouse, the spherical bushy cell area and the medial superior olive are small compared to other mammals (e.g., cat; (Irving and Harrison 1967); (Webster and Trune 1982)), consistent with the fact that mice are high frequency animals and likely do not depend heavily on localization of low-frequency sounds. Given the small size of the spherical cell area in mouse, and the fact that our electrode angle and insertion point in the DCN is such that anterior AVCN is not traversed, it is not likely that any of the present results are from spherical bushy cells.

Globular bushy cells are located more posteriorly in the AVCN and receive more numerous, smaller terminals from a larger number of AN fibers than spherical cells (Harrison and Irving 1966; Rouiller et al. 1986). They generate tone-burst PST histograms described as "primary-like with notch" (Smith et al. 1993) (Rhode and Smith 1986a). However, the distinctive notch, located ~2 msec after an initial peak, is not always present at 30 dB above threshold (Blackburn and Sachs 1989), the level used in this study. Because globular cells are located near the AN root in mouse (Webster and Trune 1982) and have tone burst FSLs comparable to AN fibers (Young et al. 1988), it is possible that some globular cell responses were classified as AN fibers in the present database. Such inclusion would have minimal affect on the conclusions, since their responses are generally so similar to those of AN fibers. The greatest differences include a tendency towards larger SRs, maximum driven rates and peak-to-steady state ratios in globular cells (Rhode and Smith 1986a). Thus, these aspects of mouse AN response may be slightly skewed towards higher values in the present study.

2.7 Genotyping

The CGRP knockout and the wildtype mice used in this thesis were bred and raised at the Massachusetts Eye and Ear Infirmary animal care facility. The original breeding pairs were generously given to us by Dr. Ronald Emeson, creator of the CGRP knockout line. A genotyping protocol developed by Dr. Emeson was used to confirm the presence or absence of the genetic mutation in each generation. The protocol required the use of the Extract-n-Amp PCR kit (Sigma ®) to prep the DNA for PCR amplification. DNA primers were used to amplify a segment of DNA corresponding to the CGRP gene:

(1) 5'-CCTCCCACTGCCCCATCCTGA-3' sense primer
(2) 5'-CATTCTGGGGCTGTTATCTGTTCA-3' antisense primer

The DNA segment amplified in CGRP knockout mice gave PCR products that were 224bp in length, while that in wild-type mice gave PCR products that were in 209bp in length. Figure 2.4 shows example PCR products obtained from 6 wildtype mice (underscored in light blue) and 4 CGRP knockouts (underscored in yellow). Because longer segments of DNA need more time to travel done the algarose gel than shorter ones, DNA segments from wildtype mice (209bp) are closer to the bottom than the knockout mice (224bp). A 100bp ladder, last column on the right, was included to serve as a reference.

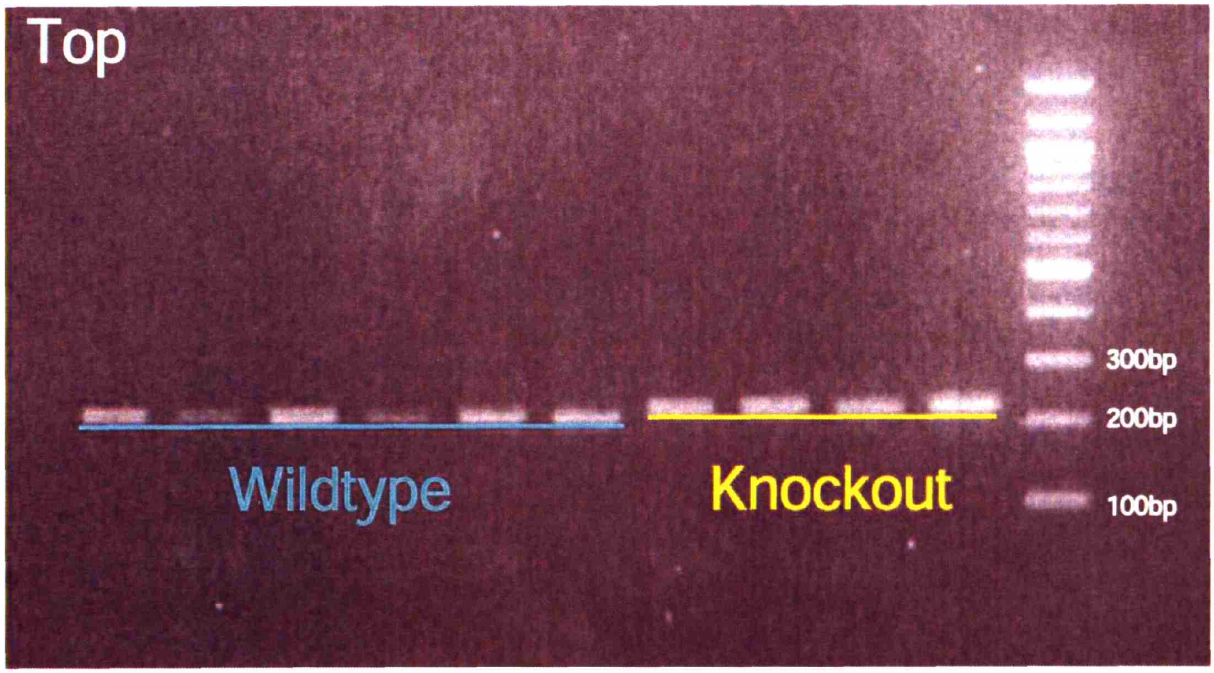

Figure 2.4: Genotyping using PCR. PCR products for 6 wildtype (underscored in light blue (209 bp)) and 4 CGRP knockout mice (underscored in light blue (224 bp)). Shown on the extreme right is a 100 bp ladder. Since smaller segments of DNA travel faster through the agarose gel, the segment of the ladder nearest the bottom of the image is 100bp in length.

Chapter 3

Recordings from Single Auditory Nerve Fibers in CBA/CaJ Mice

3.1 Introduction

In this chapter, the spontaneous and sound-evoked discharge properties of 196 AN fibers recorded from the CBA/CaJ strain are described. The characterization of CBA/CaJ single-unit AN physiology is important since CBA/CaJ mice are commonly used in studies of the auditory periphery. CBA/CaJ is popular for cochlear studies because their hearing sensitivity is relatively stable up to at least 15 months of age (Jimenez et al. 1999; Li and Borg 1991; Zheng et al. 1999a). Conversely, knockout mice are produced in a variety of strains known to have early onset age-related hearing loss. Therefore, it will be of additional use to characterize AN physiology in the CBA/CaJ strain in order to have data that can be used as one standard of comparison in studies performed in a number of knockout mice.

Physiologic measures commonly used to characterize AN responses are tuning curves, spontaneous discharge rates (SRs), and discharge rate-versus-level functions for characteristic frequency (CF) tone bursts. Fundamental features of AN response that can be extracted from these measures are presented in this chapter, including: 1) threshold sensitivity, 2) sharpness of tuning (Q_{10dB}), 3) the dynamic range and maximum rates of response, 4) response adaptation, 5) degree of phase-locking and 6) the relationships among SR, CF and all the aforementioned response properties.

Comparisons between mouse AN physiology and that of other mammals is also of interest, because the mouse cochlea is specialized for higher frequency stimuli than cat, guinea pig, chinchilla, or gerbil, the other mammalian species in which AN responses have been well studied. Despite this important difference, it will be shown that the fundamental aspects of AN response are qualitatively similar in the mouse. This finding increases the value of the mouse model, because it indicates that the mouse falls within the general mammalian plan and, as such, increases the likelihood that conclusions derived from the study of the molecular mechanisms of hearing and deafness in mouse are generalizable to all mammals.

3.2 Results

3.2.1 Rate Threshold and Tuning

A fundamental property of AN fibers is their frequency selectivity, which is often quantified via "threshold" tuning curves which track iso-response contours in the frequency-intensity plane (Figure 3.1). Tuning curves were obtained for all AN fibers encountered. As in other mammalian species, mouse AN tuning curves show sharply tuned "tips", defining a characteristic frequency (CF: frequency of maximum sensitivity) and broadly tuned low-frequency "tails". The data in Figure 3.1 show populations of tuning curves obtained from 28 CBA/CaJ mice, clustered

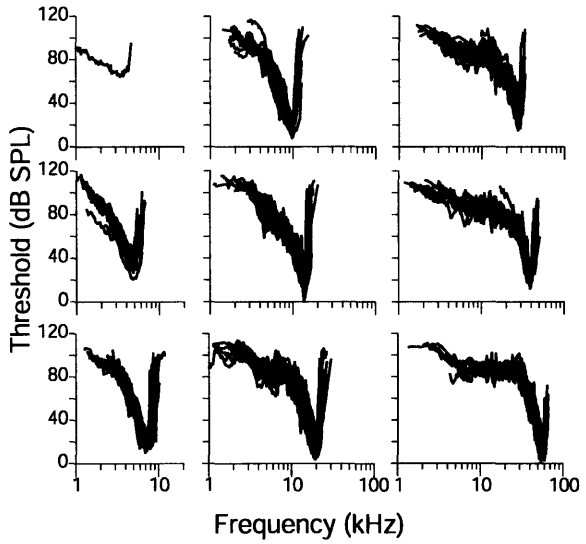

Figure 3.1: Tuning-curve shapes in different regions of characteristic frequency for AN fibers from CBA/CaJ. Data from 28 mice were segregated into groups according to characteristic frequency (half-octave bins) from 3.1 kHz (upper left) to 54 kHz (lower right). Each tuning curve was normalized by characteristic frequency and placed in the middle of its respective half-octave bin. Only data from fibers with high spontaneous rate (i.e., SR > 1 sp/sec) are shown.

according to CF. Tuning curve shapes are remarkably similar across animals. As reported for other species (Dallos and Harris 1978; Evans 1972; Liberman 1978; Ohlemiller and Echteler 1990), tuning curves from lower CF regions tend to be more "V-shaped", with a less obvious low-frequency tail.

Plotting thresholds at CF for all the AN fibers obtained in the present study provides an

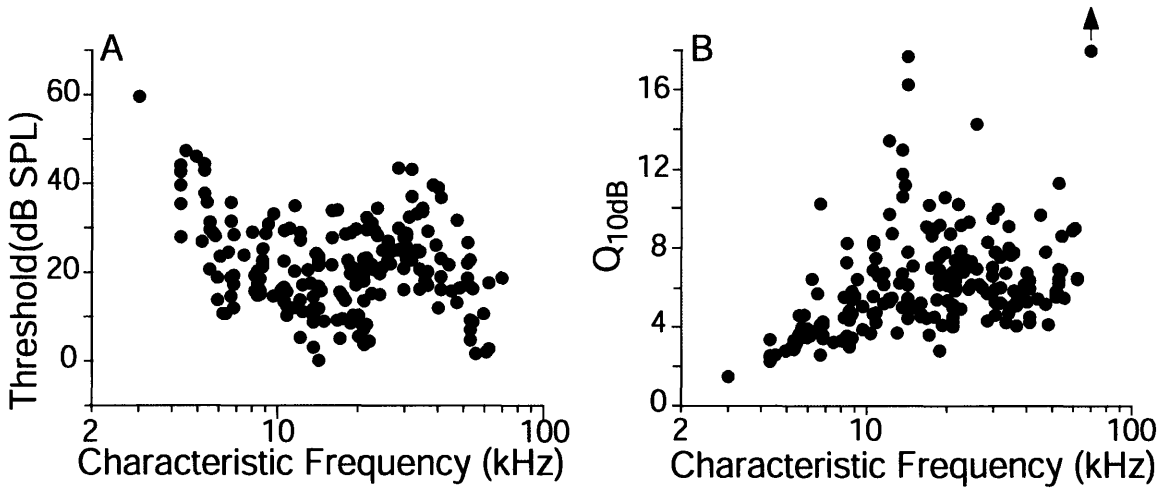

Figure 3.2: Thresholds at CF (**Panel A**) and sharpness of tuning (**Panel B**), as a function of characteristic frequency for 196 AN fibers from 28 CBA/CaJ mice. Arrow in panel B indicates a Q_{10dB} value that was off-scale.

overview of the sensitivity and frequency range of the peripheral auditory system in this strain. In this study, CFs ranged from 3.1 – 69.8 kHz for 196 fibers obtained in 28 animals (Figure 3.2A). A local threshold minimum was seen among fibers in the middle of that range. i.e. 12 - 24 kHz. In both strains, minimum thresholds rose for CFs below that region and the spread in thresholds at any one region of CF was on the order of 30 dB. Threshold sensitivity near 0 dB SPL could be seen in fibers with CF as high as 60 kHz.

The sharpness of AN tuning in mouse increased with CF. This relationship can be seen qualitatively in Figure 3.1 and quantitatively in Figure 3.2B, which shows Q_{10dB} (ratio of CF to bandwidth at 10 dB above threshold at CF) for all AN fibers in the present study.

3.2.2 Spontaneous Rate

Auditory nerve fibers discharge spontaneously in the absence of sound (Kiang et al. 1965). Figure 3.3A shows the spontaneous rate (SR) distribution for the fiber population. SRs ranged from 0 - 120 sp/sec with 49% of the fibers having SRs < 20 sp/sec. In contrast to many other mammalian species studied, e.g. cat (Kiang et al. 1965) or guinea pig (Tsuji and Liberman 1997), the SR distribution in mouse is not clearly bimodal. While there is no clear relationship between fiber SR and CF (Figure 3.3B), there is a clear relationship between fiber threshold and SR. As

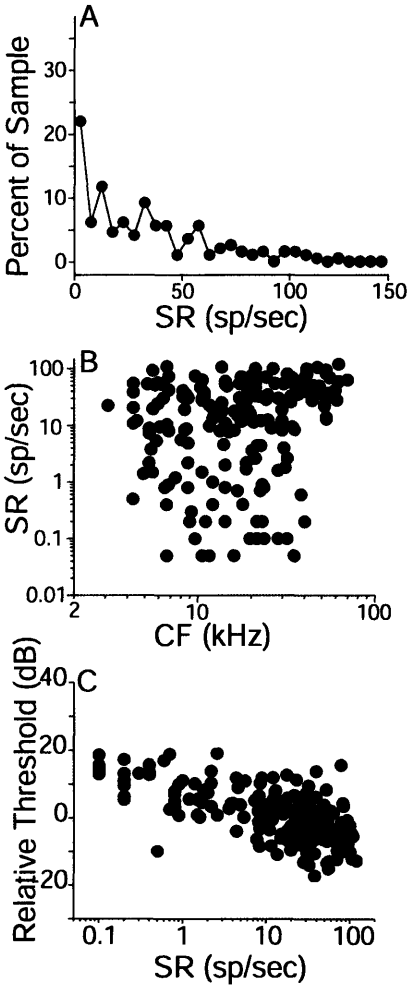

Figure 3.3: Spontaneous rate (SR) data from the same fiber populations shown in Figure 3.2. **Panel A**: distribution of SRs in the sample of AN fibers obtained. **Panel B**: SR as a function of characteristic frequency. **Panel C**: relation between SR and threshold. Relative threshold is defined by referring the threshold at CF of each fiber to the mean threshold of high-SR fibers (SR > 1 sp/sec) of similar CF. In this and all subsequent figures with SR on a logarithmic scale, SR values of 0 are plotted as 0.05 sp/sec.

seen in other mammalian species (e.g. Liberman, 1978), fibers with the lowest relative thresholds (with respect to the most sensitive fibers of similar CF) also had the highest SRs (Figure 3.3C).

3.2.3 Response Adaptation

PST histograms of AN fibers show a peak in discharge rate at tone-burst onset, which decays to a steady-state response (Kiang et al. 1965; Smith 1977). Response adaptation in auditory nerve fibers follows a multi-component time course with time constants varying from milliseconds to minutes (Chimento and Schreiner 1991; Javel 1996; Westerman and Smith 1984). In this study, the ratio of peak to steady-state rate was used as a measure of response adaptation; corresponding to the "short-term" component studied by Westerman and Smith (1984). Adaptation of mouse AN responses was studied using PST histograms of responses to

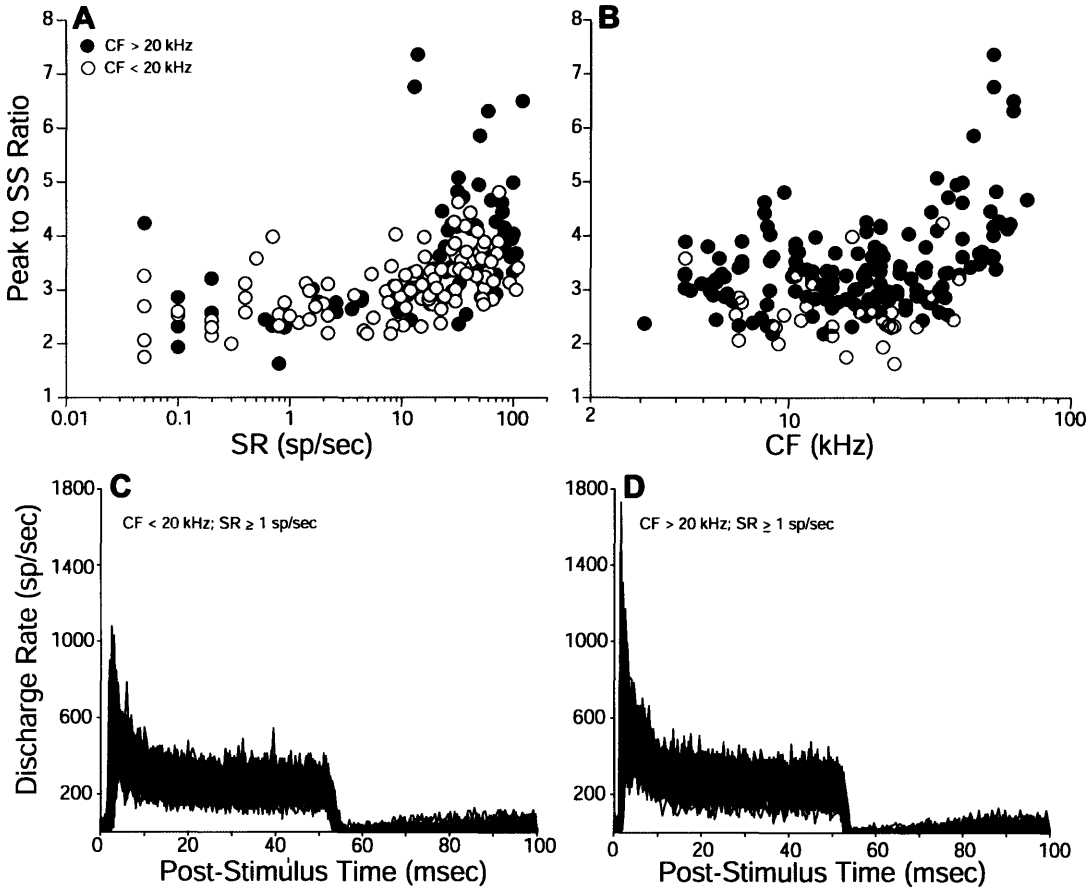

Figure 3.4: Response adaptation as a function of SR (**Panel A**) and CF (**Panel B**). Adaptation was derived from PST histograms based on 150-250 CF tone bursts, 30 dB above threshold. Peak to steady state (SS) ratio was obtained by dividing the maximum rate by the average rate during the last 10 msec of the tone burst. **Panels C and D:** superimposed PST histograms all from high-SR (> 1 sp/sec) fibers with CF < 20 kHz and CF > 20 kHz respectively. Histograms are normalized by the number of stimulus presentations and the histogram bin width (0.5 msec) to give instantaneous discharge rate.

CF tone bursts at 30 dB above threshold. The histograms were divided by the number of tone burst presentations and the histogram bin width (0.5 msec) to give the instantaneous discharge rate.

Response adaptation is a function of both SR and CF in the mouse AN (Figures 3.4A and B). In fibers with SR $\geq$ 1 sp/sec peak-to-steady-state ratios ranged from 2.2 - 7.4, while fibers with SR < 1 sp/sec had ratios between 1.6 and 4.2 (Figure 3.4A). Fibers with the largest peak-to-steady state ratios had CF > 20 kHz (Figure 3.4B). The increase in peak-to-steady state ratio is due to an increase peak rate with CF. This difference can be seen from the superimposed PST histograms for high-SR (SR $\geq$ 1) fibers with CF < 20 kHz vs. those with CF > 20 kHz (Figures 3.4C and D, respectively).

3.2.4 Rate-vs.-Level Functions and Dynamic Range

Maximum discharge rates and dynamic range of single AN fibers in mouse was investigated by measuring discharge rate vs. sound level for tone bursts at CF (Figure 3.5). Each level function was fit by a modified version of an existing model (Sachs et al. 1989) in order to get better estimates of dynamic range.

In data from guinea pig AN (Winter et al. 1990), rate-level functions were categorized as

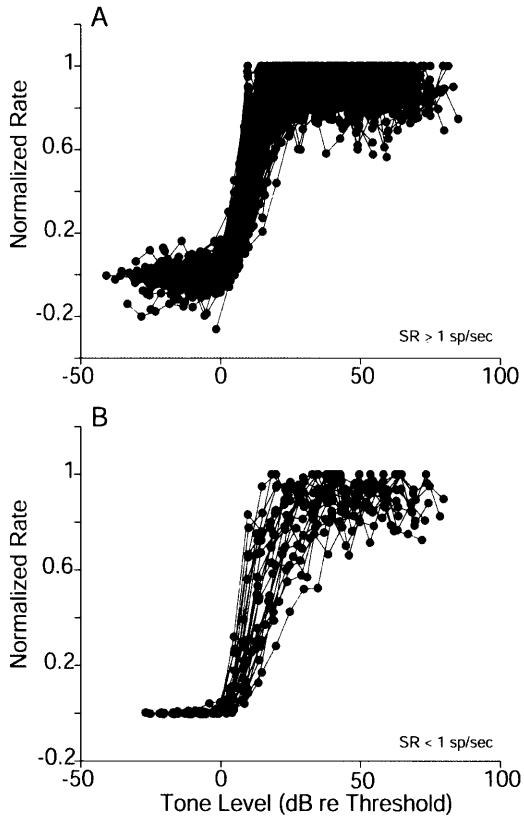

Figure 3.5: Superimposed rate-level functions segregated according to SR: SR $\geq$ 1 sp/sec (**Panel: A**) and SR < 1 sp/sec (**Panel: B**). Functions were normalized by: 1) dividing the vertical axis by the maximum driven rate, and 2) shifting along the horizontal axis according to model-fit thresholds.

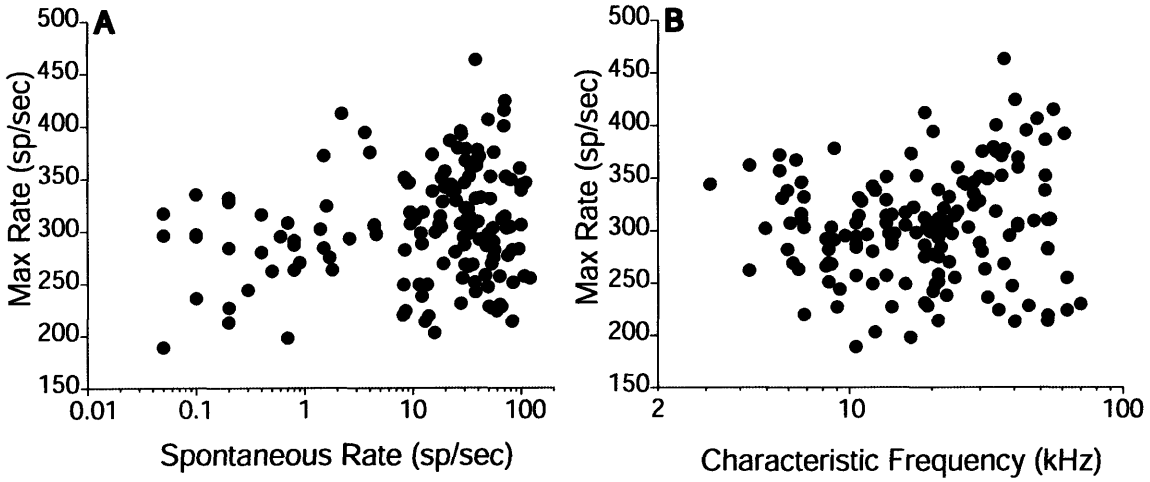

Figure 3.6: Relation between maximum rate and SR (**Panel A**) or characteristic frequency (**Panel B**). Maximum rate was obtained from the model-fit functions as described in Chapter 2.

"hard saturating", "sloping saturating", and "straight". In the CBA/CaJ AN, nearly all high-SR fibers (SR $\geq$ 1 sp/sec) had hard-saturating rate-level functions (Figure 3.5A). On the other hand, low-SR fibers were more heterogeneous in that all three level-function categories could be found among them (Figure 3.5B).

Among AN fibers in CBA/CaJ, there was a tendency for fibers with low-SR (< 1 sp/sec) to show lower maximum discharge rates than those with SR $\geq$ 1 sp/sec (Figure 3.6A): group mean differences were statistically significant (P = 0.005, Student's *t*-test). There did not appear to be

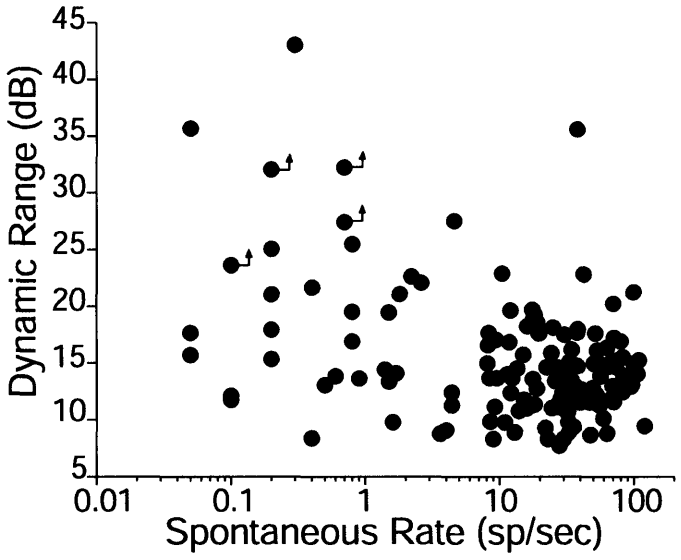

Figure 3.7: Relation between SR and dynamic range. Dynamic ranges were extracted from the model-fit data as described in Chapter 2.

any relation between maximum discharge rate and CF (Figure 3.6B).

Dynamic ranges of most AN fibers were less than 15 dB (Figure 3.7): as is typically done in AN studies, dynamic range was defined as the dB range between the 10 and 90% rate points). However, larger dynamic ranges were sometimes seen among fibers with SR < 1 sp/sec. Furthermore, dynamic ranges were more heterogeneous for this low SR group, ranging between 8.4 and 43.0 dB. In contrast, for high SR (≥ 1 sp/sec) fibers, the largest dynamic range was 35 dB.

3.2.5 Response Synchrony

When AN fibers respond to low-frequency tones, there is a correlation between the stimulus periodicity and the timing of spikes (Johnson 1980), as illustrated by the post-zero crossing histogram in the inset of Figure 3.8C. In cat, where it has been most systematically studied, this phase-locking, or synchrony, falls off dramatically as stimulus frequency approaches 4 kHz (Johnson 1980). In the mouse AN, there are relatively few fibers with rate threshold < 60 dB SPL at frequencies ≤ 4 kHz (e.g. Figure 3.1). Thus, given that high SPL tones elicit large cochlear microphonic potentials that can produce artifactual synchrony when picked up by the microelectrode, response synchrony could only be studied systematically in a few fibers. A model developed by Johnson (Johnson 1978) was used to compute a synchrony noise floor for each recording (based on the ratio of microphonic size to spike size) to prevent pollution of data by these microphonic-based artifacts (See chapter 2).

Although the sample size is limited by the general lack of low-frequency responsiveness in the mouse AN, the fundamental features of response synchronization are similar to those reported in other mammalian species. Data from one of the lowest-CF fibers in the present study

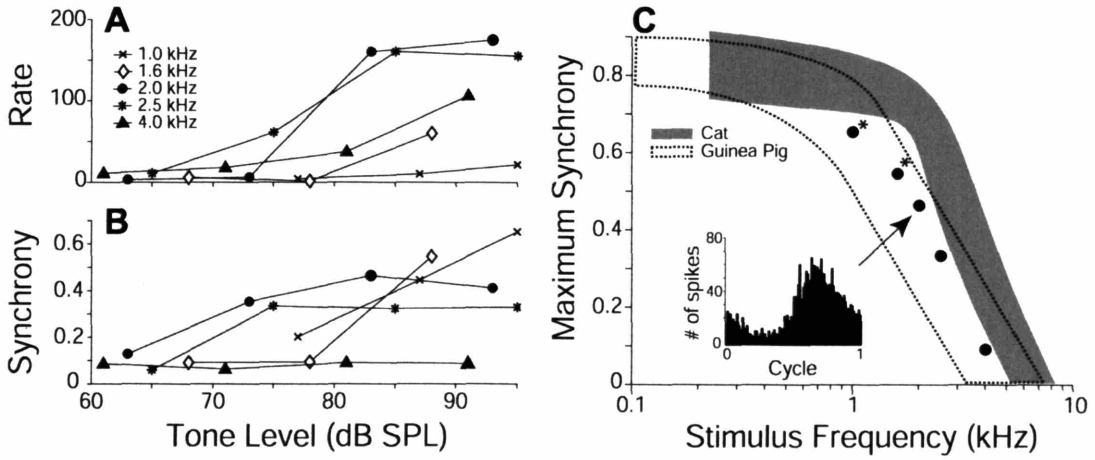

Figure 3.8: Phase-locking in mouse AN fibers. **Panels A and B** show data from one well-studied fiber (CF = 3.1 kHz, SR = 22.4 sp/sec). Synchrony (**Panel B**) and rate (**Panel A**) measures were extracted from post-zero-crossing histograms obtained from 15-sec continuous tones. The synchronization index (panel B) was calculated as described by Johnson (1980). **Panel C:** Comparison of maximum synchrony vs. tone frequency for mouse data from panel B compared to published cat data (shaded area (Johnson 1980)) and guinea pig data (Palmer and Russell 1986)), excluding an outlier at 1.68 kHz. Synchrony values marked by asterisks are underestimates of the maximum, since synchrony-level functions had not saturated at the highest sound level presented.

illustrate the main trends of the synchrony data from mouse AN (Figure 3.8A,B). For this fiber (CF= 3.1 kHz), rate and synchrony data were obtained for stimulus-level functions at 5 frequencies from 1 to 4 kHz. No synchrony was demonstrable in the response to 4 kHz, and maximum synchrony increased systematically as stimulus frequency decreased towards 1 kHz (Figure 3.8B,C). As reported in other species, the AN discharge can synchronize to the stimulus period at lower SPLs than those at which the average rate increase (e.g. data at 1 or 2 kHz), although this is not always the case (e.g. 1.6 kHz). Note that the maximum synchronization index seen across all mouse AN fibers studied was lower than the values reported for similar stimulus frequencies in the cat (gray region in Figure 3.8C) but similar to guinea pig (dotted region in Figure 3.8C), another rodent species.

3.3 Discussion

3.3.1 Relevance to other data on auditory function in mouse

Two previous studies, Finck and Berlin (1965) and Ehret and Moffat (1984), describe recordings from mouse AN fibers, using the CBA/J strain and the (outbred) NMRI strain, respectively. In both studies, electrode tracks traversed the CN to access the AN, thus the possibility for unit mis-classification exists. This possibility was acknowledged, but not addressed, by Finck and Berlin; Ehret and Moffat developed a classification scheme based on average FSL. Thus, as in the present study, their database may include a small population of globular bushy cells in addition to the majority population representing AN response.

Aspects of AN physiology characterized in these previous studies included: response areas (i.e., tuning curves), thresholds at CF, masked thresholds to tone bursts in noise, and critical ratio bands. Since the present study did not examine noise masking, and previous studies did not directly quantify the sharpness of tuning curves, the only point of comparison among the three studies concerns the distribution of thresholds at CF. Threshold data from the three studies are compared in Figure 3.9A, where curves representing the minimum thresholds at CF for AN fibers sampled in the present study (filled circles) are compared to AN data from CBA/J (open diamonds) and NMRI strains (open circles). Minimum thresholds for the NMRI strain are lower at most CF regions than those seen in the present study. However, data from the present study do not show the precipitous loss of sensitivity for CFs > 30 kHz (see below). Minimum threshold envelopes for the CBA/J data and the present CBA/CaJ data are similar for CFs < 30 kHz. For higher CF regions, CBA/CaJ maintains low minimum thresholds out to the high-frequency limits of our acoustic system (~70 kHz); whereas, the CBA/J data show steeply sloping loss of threshold sensitivity. It is not clear whether these differences in high-frequency behavior reflect true inter-strain differences in high-frequency sensitivity, differences in acoustic calibration procedure or artifactual loss of sensitivity in the CBA/J due, for example, to cochlear cooling in the anesthetized preparation (Brown et al. 1983).

Comparisons of single-fiber thresholds from the present study with behavioral thresholds for a number of mouse strains are also shown in Figure 3.9B. With the exception of an extremely low value for 1-kHz behavioral threshold in the NMRI mouse, all behavioral threshold functions agree reasonably well with the minimum single-fiber thresholds measured in CBA/CaJ in the present study. Note that none of the behavioral curves show the precipitous threshold elevation for frequencies > 30 kHz seen in the CBA/J single-fiber study (Birch et al. 1968).

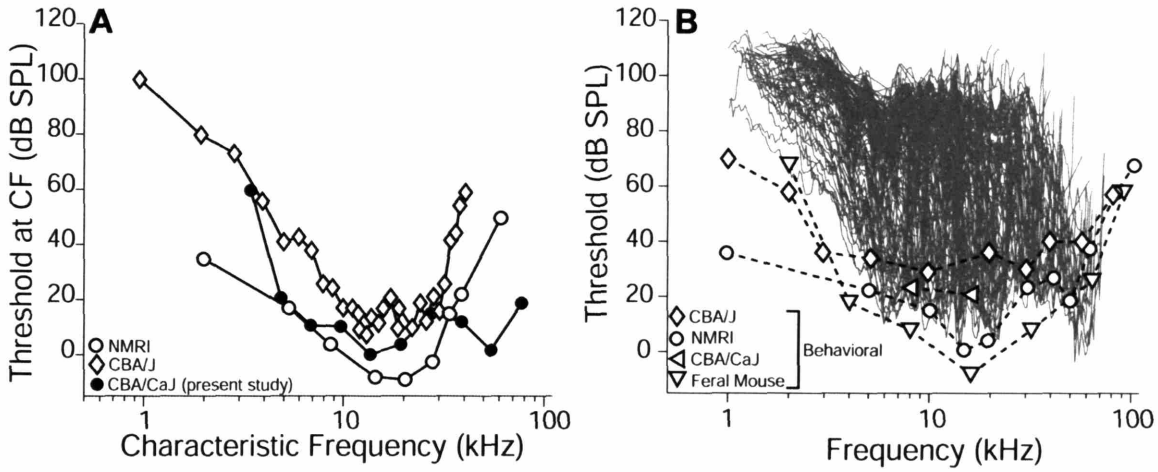

Figure 3.9: Minimum thresholds as a function of characteristic frequency for all CBA/CaJ AN fibers recorded in the present study compared to minimum thresholds from other mouse studies (**Panel A**). Data from CBA/CaJ strain was binned according to CF (half-octave bins), and the minimum fiber threshold for each bin was found. **Panel B:** Superimposed tuning curves from all CBA/CaJ fibers in the present study (gray) compared to behavioral threshold data from other mouse studies. Behavioral data are from the following sources: CBA/CaJ mouse (Prosen et al. 2003), CBA/J mouse (Birch et al. 1968), feral house mouse (Heffner and Masterton 1980), NMRI mouse (Ehret 1974) and C57BL/6 (Mikaelian et al. 1974). AN data are from the following sources: NMRI mouse (Ehret and Moffat 1984), CBA/J (Finck and Berlin 1965), and CBA/CaJ (present study).

3.3.2 Comparison to data from other mammals

3.3.2.1 Tuning-curve tips vs. tails and rate vs. synchrony coding

Tuning curves recorded from the mouse AN were qualitatively similar to those recorded in other mammalian species. They showed sharply tuned "tips" near the characteristic frequency and broadly tuned low-frequency "tails" (Figure 3.1). As in other mammals, mouse AN fibers showed increasing sharpness of tuning with increasing CF (Figure 3.2B). A more quantitative comparison of mean Q_{10dB} values obtained from several mammalian species is shown in Figure 3.10. The combined data suggest a common relationship between Q_{10dB} and CF, with similar sharpness of tuning seen across several mammalian species, where CF regions overlap.

A more quantitative comparison of tuning-curve "tails" shows that low-frequency thresholds are significantly elevated in mouse compared to other mammalian species (e.g., cat (Liberman 1978), guinea pig (Evans 1972), chinchilla (Dallos and Harris 1978), and gerbil (Ohlemiller and Echteler 1990)). For example, a direct comparison of mouse and cat tuning curves for fibers with CF near 15 kHz (Figure 3.11) shows that, whereas thresholds in mouse increase monotonically for frequencies below CF and rise above 90 dB for frequencies < 4 kHz, thresholds in cat show a second minimum at low frequencies and do not rise above 90 dB SPL until frequencies fall below ~0.2 kHz.

In mammals with better low-frequency hearing than mouse, significant information is carried in the fine timing of AN discharge, in addition to the information carried by changes in average rate. Maximum response synchrony in cat AN is constant for frequencies < 1 kHz, rolls off

dramatically above 1 kHz and is essentially absent for stimulus frequencies > 4 kHz (Johnson 1980). Thus, in cat or guinea pig, and probably humans, low-frequency sensitivity is such that AN fibers spanning many octaves of CF will show phase-locked response to a moderate-level (80 dB), low-frequency (e.g. 1 kHz) tone. In mouse AN, by contrast, there would be almost no fibers responding to such a stimulus (See Figure 3.9B). This raises the question as to whether this mammalian ear specialized for high-frequency hearing has also developed specializations to shift the frequency range of AN phase-locking. Data in the present study suggest that this is not the case: the relation between maximum synchronization index and stimulus frequency appears to be fundamentally similar to that seen in other mammals (Figure 3.8). Indeed, if anything, the high-frequency limit of synchronization occurs at a lower frequency than in cat. Thus, the data further suggest that phase-locking of AN response is not a particularly important component of mouse hearing.

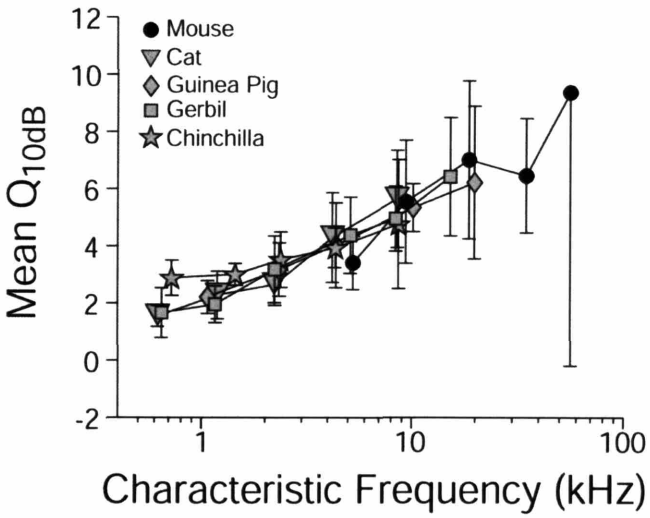

Figure 3.10: Mean Q_{10dB} as a function of CF for AN tuning curves in five mammalian species (see key). Data from each species were segregated into groups according to characteristic frequency (octave bins), and the average Q_{10dB} for each bin was placed at the mean fiber CF. Data are only shown for frequency bins containing at least 5 data points. Data for mouse (present study), cat (Liberman 1978), guinea pig (Tsuji and Liberman 1997) and chinchilla (Liberman, unpublished) are all from our laboratory; thus the methods for data aquisition and analysis are identical. Data for gerbil are from other investigators (Ohlemiller and Echteler 1990).

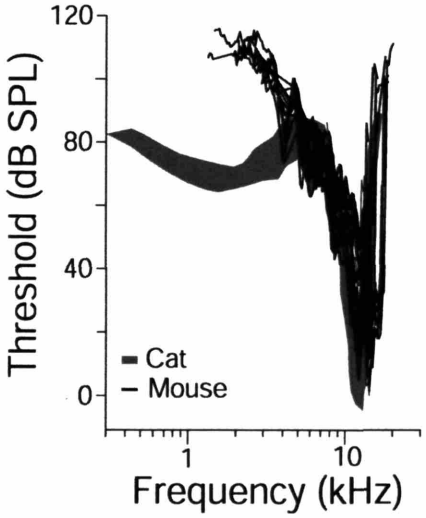

Figure 3.11: Comparison of tuning curves from cat and mouse AN fibers in a similar CF range (11 - 16 kHz) illustrates the difference in low-frequency sensitivity. The cat tuning curves were obtained in a previous study (Liberman, 1978).

3.3.2.2 Spontaneous Discharge and SR groups

In cat and guinea pig, where it has been most exhaustively studied, differences in SR are strongly correlated with differences in other response properties such as threshold sensitivity (Liberman 1978), adaptation (Rhode and Smith 1985), susceptibility to forward masking (Relkin and Doucet 1991) and dynamic range (Winter et al. 1990), among others.

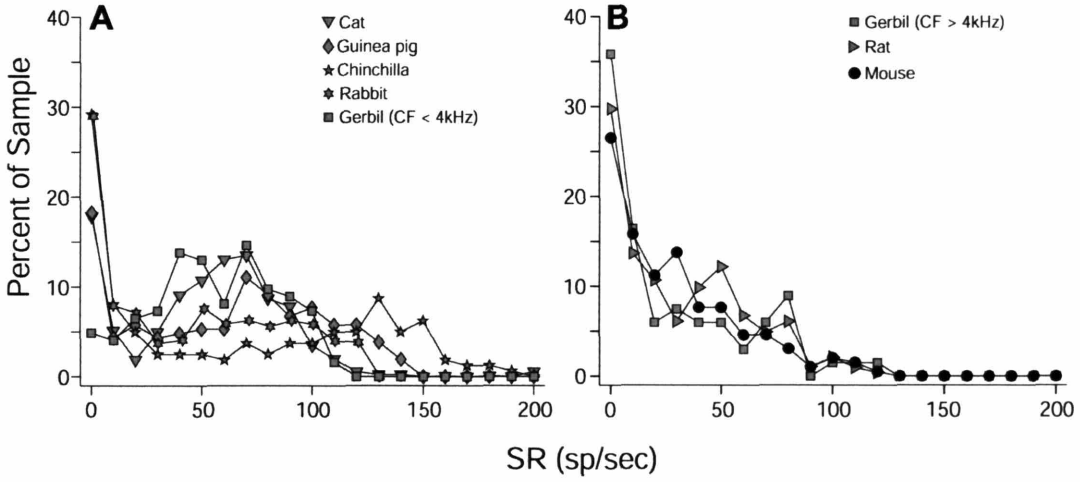

Figure 3.12: Comparison of SR distributions for AN fibers recorded from a number of different mammalian species. Bimodal distributions are grouped in **Panel A**: cat (Liberman 1978), guinea pig (Liberman ,unpublished), rabbit (Borg et al. 1988), chinchilla (Liberman, unpublished), and the low-CF region of the gerbil cochlea (Ohlemiller and Echteler 1990). Non-bimodal distributions are grouped in **Panel B**: mouse (present study), rat (el Barbary 1991) and the high-CF region of the gerbil (Ohlemiller and Echteler 1990).

In cat, where data from hundreds of fibers can be obtained from individual animals under highly stable recording conditions, analysis of the relation between SR and threshold sensitivity suggested that three SR groups could be defined: high-, medium and low, with SR ranges of >18, 0.5 to 18 and < 0.5 sp/sec respectively (Liberman, 1978). Subsequent structure-function correlations using intracellular injection of neuronal tracers revealed that there are systematic differences among these three groups, in 1) locus of peripheral terminal on the IHC circumference (Liberman 1982b), 2) size and complexity of the synaptic apparatus within the IHC (Merchan-Perez and Liberman 1996), 3) degree of branching of the central axon (Fekete et al. 1984) and 4) the CN subdivisions to which they project (Liberman 1991, 1980). Many of the same structure-function relationships have been corroborated in the guinea pig, suggesting that the subdivision of AN fibers into SR-based groups is part of the fundamental mammalian plan (Tsuji and Liberman 1997).

In cat, guinea pig, chinchilla and rabbit (Figure 3.12A) the SR distribution is fundamentally bimodal, and fibers from the lower peak in the SR distribution have higher thresholds than those from the high rate peak (Tsuji and Liberman 1997). Although the SR distribution in the mouse is not as clearly bimodal as in these other species, the general relation between SR and threshold sensitivity is maintained (although the evidence for discrete SR groups rather than a continuum of response is not clear). Recent ultrastructural work in mouse suggests that, in this species, as previously reported in cat and guinea pig, the AN terminals contacting the modiolar side of the

IHC are lower in mitochondrial content than those on the pillar side (Francis et al. 2004). In cat, these mitochondrion-poor afferents have been definitively identified as corresponding to the high-threshold low-SR group. Thus, the same anatomical differences may underlie the observed SR-based heterogeneity of response in mouse.

With respect to the shape of the SR distribution, mouse is similar to rat (el Barbary 1991), another high-frequency animal, and to high-CF AN fibers in gerbil (Ohlemiller and Echteler 1990), where the SR distribution varies dramatically with CF. As can be seen in Figure 3.12B, for rat, mouse and the basal turn of gerbils, the SR distribution is not clearly bimodal and is shifted towards lower spontaneous rates. This association between a compressed SR distribution and high-frequency hearing is interesting given that robust background discharge may be most useful at frequencies < 4kHz, where response synchronization occurs, and where synchrony rises at lower SPLs than average rate (Figure 3.8A,B).

As for cat (Rhode and Smith 1985) and guinea pig (Muller and Robertson 1991), response adaptation in mouse AN is related to fiber SR (Figure 3.4A) and CF (Figure 3.4B). In both cat and guinea pig, response adaptation for fibers with CF < 4 kHz was smaller than response adaptation in fibers of higher CF (Muller and Robertson 1991; Rhode and Smith 1985). Given that phase locking occurs for frequencies < 4 kHz (Johnson 1980), Rhode and Smith (Rhode and Smith 1985) hypothesized that the lower peak rates observed in cat low CF fibers were due to an interaction between phase locking and rapid adaptation. In mouse, there was a difference in response adaptation between fibers with CF below vs. above 20 kHz (Figure 3.4B). This CF-related difference clearly cannot be correlated with presence or absence of synchrony; rather, it likely arises from CF-related changes in the kinetics of synaptic transmission.

3.3.2.3 Dynamic range in the auditory periphery

Rate-vs.-level functions for AN responses to CF tone bursts have been best studied in cat (Sachs et al. 1989), guinea pig (Winter et al. 1990) and gerbil (Ohlemiller et al. 1991). In all

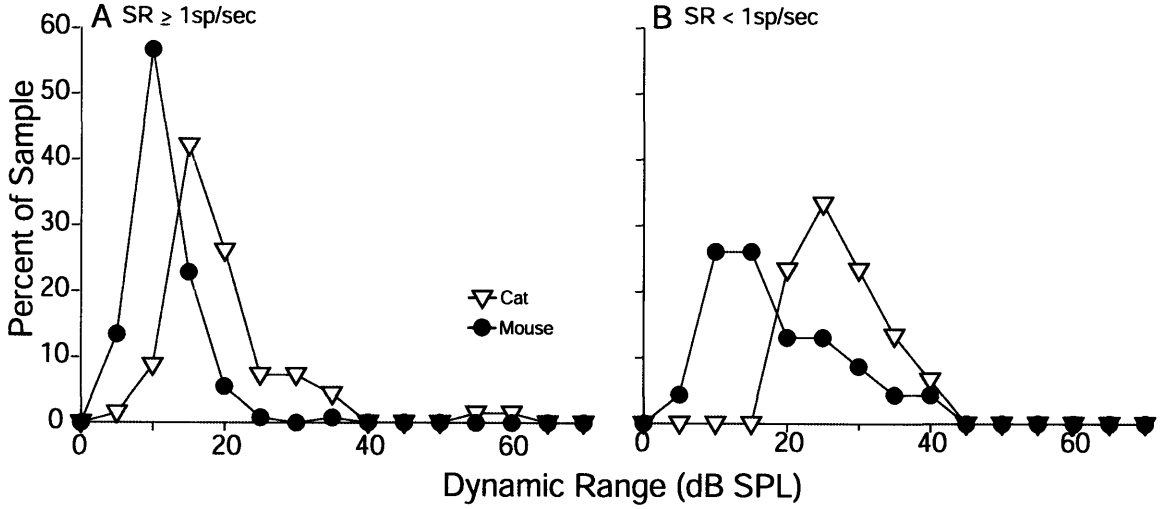

Figure 3.13: Comparison of dynamic ranges for cat and mouse AN fibers, separated into high and low SR groups (Panels A and B respectively). Mouse data are from the present study. Cat data are from a previous study (Guinan and Stankovic 1996) using an identical data acquisition paradigm, i.e. 50 msec tone bursts at CF presented in random order.

three of these mammals, dynamic ranges depend strongly on SR: low-threshold, high-SR fibers show hard rate-saturation and small dynamic ranges; whereas high-threshold, low-SR fibers show sloping saturation or non-saturating rate-vs.-level functions with significantly larger dynamic ranges. Data in the present study show that the mouse AN has fundamentally the same behavior (Figure 3.7); thus these SR-related differences in dynamic range also appear to be part of a general mammalian plan.

A striking difference between AN properties in mouse vs. other mammals is the small dynamic range of the low-threshold, high-SR fibers. For example, figure 3.13 compares dynamic ranges for high-and low-SR AN fibers from the present study to data from cat (Guinan and Stankovic 1996) which were derived according to exactly the same stimulation and analysis protocols. The great majority (> 90%) of high-SR fibers in the mouse had dynamic range values less than 18 dB, while the majority (>70%) of high-SR fibers in cat showed dynamic ranges greater than 18 dB. Gerbil high-SR fibers (Ohlemiller et al. 1991) have been shown to have even higher dynamic range values (25-40 dB). Quantitative data for guinea pig are not available, however visual inspection of rate-level functions shown by Winter et al. (Winter et al. 1990) suggest that dynamic ranges in this species for high-SR fibers are comparable to those in cat.

The small dynamic ranges seen among mouse AN fibers, compared to those measured in other mammalian ears, may be related to the fact that the mouse ear is specialized for high frequencies: most of the hearing range is above stimulus frequencies at which response phase-locking can be used to carry information. In the gerbil AN, there is a CF-dependence to dynamic range (Ohlemiller et al. 1991): high-frequency fibers, with CFs above the limits of phase locking, show a smaller mean dynamic range (~25 dB) than low-CF fibers (~35 dB). The existence of steeper rate-vs.-level functions in mouse high-SR fibers might be expected to subserve an enhanced ability to detect small changes in stimulus intensity at levels near threshold. However, existing measurement of intensity difference limens in mouse do not suggest any extraordinary abilities compared to other mammalian species investigated (Fay 1988).

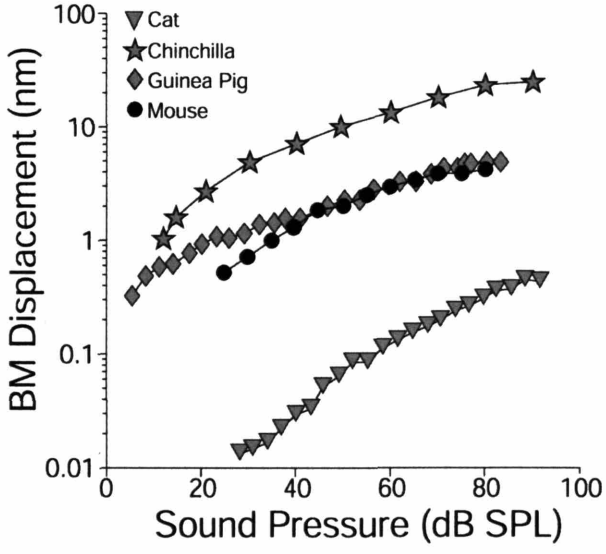

Figure 3.14: Comparison of basilar membrane responses to CF tones recorded in cat, chinchilla, guinea pig, and mouse at locations in the basal turn. Data for the cat, chinchilla and guinea pig were replotted from Robles and Ruggero (2001). The mouse data were re-plotted from Legan et. al. (2000).

The steepness of rate-vs.-level functions in mouse could arise at several stages in cochlear processing. Comparison of basilar membrane displacement-vs.-level functions for tones at CF near the base of the cochlea in mouse (Legan et al. 2000) compared to other mammals (Robles

and Ruggero 2001) do not suggest striking differences in slope (Figure 3.14). Thus, the basis for the observed differences in dynamic range must arise within the inner hair cell, the auditory nerve, or the synaptic transmission between the two.

3.4 Summary

This study provides the first systematic description of spontaneous and sound-evoked discharge properties of AN fibers in mouse, specifically in CBA/CaJ. Mouse AN fibers showed similar responses to other mammals: sharpness of tuning increased with characteristic frequency, phase-locking falls off for frequencies > 2kHz, and low SR (< 1 sp sec) fibers had higher thresholds and wider dynamic ranges than fibers with high SR. Mouse AN responses differed from other mammals in that dynamic ranges for mouse high-SR fibers were smaller (< 20 dB) than those seen in other mammals. In general, results from the present study indicate mouse auditory responses fall within the general mammalian plan and as such, may serve as a good model to study the genetic basis for auditory health and disease in mammals.

Chapter 4

Comparison of Auditory Nerve Fiber Responses in CBA/CaJ, C57BL/6 and 129/SvJ

4.1 Introduction

The availability of transgenic and mutant lines with interesting auditory phenotypes makes the mouse a valuable model for the study of the auditory system; and recording from single auditory nerve (AN) fibers provides a powerful tool for assessing the cochlear phenotype associated with any genetic manipulation. However, the interpretation of hearing results from mutant mouse lines is often complicated by the fact that these lines are created or maintained in several different inbred mouse strains (e.g., C57BL/6 and 129/SvJ). There can be clearcut interstrain differences in threshold sensitivity, as well as age-related, progressive degenerative changes at high frequencies, that complicate the interpretation of the mutant phenotype.

In this chapter, the spontaneous and sound-evoked discharge properties of AN fibers recorded from the CBA/CaJ strains are compared to recordings in wildtype animals from the C57BL/6 and 129/SvJ strains, two common strains used to create transgenic mice (Mullen and Ryan 2001) and the background strains for the knockout mice discussed in Chapters 5 and 6 respectively. Since the data collected from the C57BL/6 and 129/SvJ mice were obtained with the explicit purpose of being used as control data, they are of ages appropriate for the knockout studies. It will be shown that, ignoring responses from the high-frequency regions, where early-onset pathological changes have appeared, most aspects of AN fiber responses are qualitatively similar among the three strains tested.

4.2 Data Set

Fiber responses shown in this chapter were classified as AN fiber responses based on the criteria described in Chapter 2 and were obtained under cochlear conditions in which the threshold shifts for the distortion product otoacoustic emissions (DPOAEs) were $\leq$ 10dB for the C57BL/6 and 129/SvJ mice, and $\leq$ 5 dB for the CBA/CaJ mice. A larger DPOAE threshold shift criterion was used for the C57BL/6 and 129/SvJ mice, since their data pool was relatively small compared to the CBA/CaJ due to the limited number of animals available for study. In all, results from 196 AN fiber recordings from 28 CBA/CaJ mice aged 8-17 weeks, 72 fiber recordings from 13 C57BL/6 mice aged 16-17 weeks, and 52 fiber recordings from 7 129/SvJ mice aged 7-17 weeks, are presented in this chapter.

4.3 Results

4.3.1. Cochlear Sensitivity

Changes in DPOAE detection thresholds were used to monitor cochlear condition throughout each experiment. DPOAEs can be used to assess cochlear function since the normal cochlea is a

non-linear system that produces DPOAEs when two pure tones (f_1,f_2) are presented simultaneously (Mountain 1980). The generation of DPOAEs is significantly dependent on the condition of the outer hair cells (OHCs) (Mountain 1980; Schrott et al. 1991; Siegel and Kim 1982). Therefore, a decline in cochlear condition which affects OHC function would be reflected in lower amplitude DPOAEs or a rise in DPOAE detection thresholds.

Figure 4.1 shows mean DPOAE thresholds obtained in CBA/CaJ (stars), C57BL/6 (triangles) and 129/SvJ (circles) mice at the start of each experiment. As seen in previous studies where the relationship between DPOAE amplitudes in aged C57BL/6 mice (i.e., > 3 months) and CBA/CaJ mice are compared (e.g., (Jimenez et al. 1999)), mean DPOAE thresholds were similar at low frequencies (i.e., $f_2 \leq 16$ kHz) but significantly different at high-frequencies, where C57BL/6 mice showed higher DPOAE thresholds. The high-frequency disparity in DPOAE amplitudes between the two strains is likely due to basal-turn OHC loss, which is characteristic of C57BL/6 mice as they age (Hequembourg and Liberman 2001; Spongr et al. 1997). The 129/SvJ mice showed average mean DPOAE thresholds that were higher than CBA/CaJ at all test frequencies and higher than the C57BL/6 at all test frequencies except for $f_2 \geq 32$ kHz, where neither strain showed significant DPOAE responses.

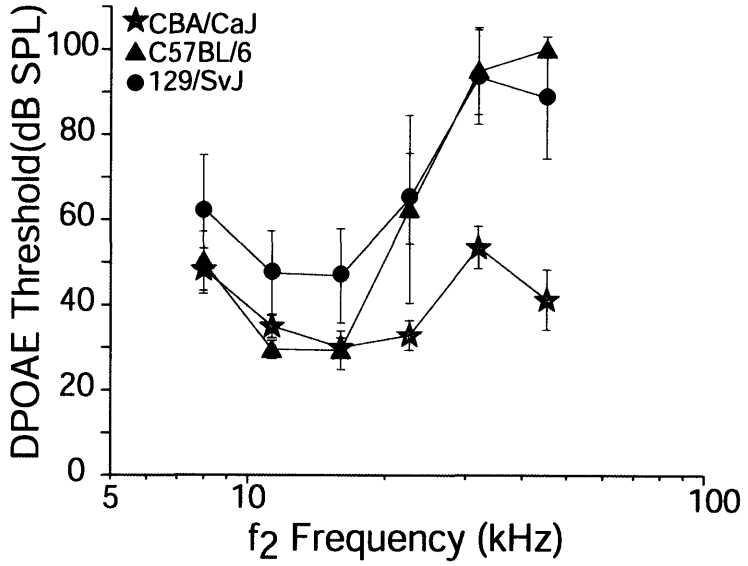

Figure 4.1: Mean thresholds for distortion product otoacoustic emissions (DPOAEs) recorded from animals of the three strains (see key) at the start of each experiment. DPOAE thresholds were determined as described in Chapter 2. A DPOAE threshold of 100dB was assigned in cases in which DPOAE amplitude failed to meet criterion even at the highest SPLs presented (80 dB).

As described in Chapter 3, a fundamental property of AN fibers is their frequency selectivity, which is often quantified via "threshold" tuning curves which track iso-response contours in the frequency-intensity plane. AN tuning curves show sharply tuned "tips", defining the characteristic frequency (CF: frequency of maximum sensitivity) of the fiber, and broadly tuned low-frequency "tails". Tuning curves were obtained for all AN fibers presented in this study. AN fibers with CF < 15 kHz showed similar tuning characteristics among the three strains

studied. On the other hand, AN fibers with CF $\geq$ 15 kHz in C57BL/6 and 129/SvJ mice had more heterogeneous tuning curve characteristics: some similar and others different from those observed in AN fibers in CBA/CaJ mice. Differences in tuning-curve characteristics found in C57BL/6 and 129/SvJ mice include (1) tuning curves with sharp tips but elevated thresholds and hyposensitive tails (Figure 4.2 B,F); (2) curves with broad tips, elevated thresholds and hypersensitive tails (Figure 4.2 C,G); and (3) curves with broad tips, elevated thresholds and normal tail sensitivity (Figure 4.2 D,H).

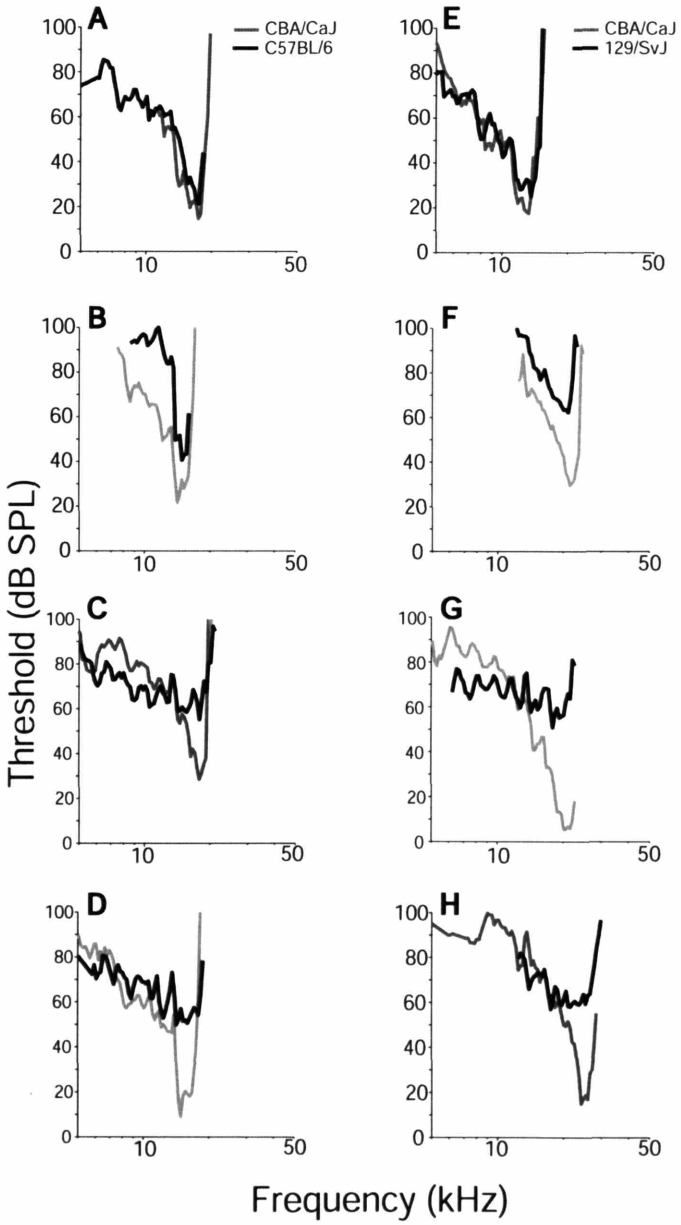

Figure 4.2: Comparison of tuning curve shapes for AN fibers from CBA/CaJ (gray) vs, C57BL/6 (left column) and 129/SvJ (right column). **Panel A, E:** sample tuning curve for each strain that are similar to CBA/CaJ (gray). **Panel B, F:** tuning curves with sharp tips but elevated thresholds and hyposensitive tails. **Panel C, G:** tuning curves with broad tips, elevated thresholds and hypersensitive tails. **Panel D, H:** Tuning curves with broad tips, elevated thresholds and normal tail sensitivity.

Plotting thresholds at CF provides an overview of the sensitivity and frequency range of the peripheral auditory system in these strains. In this study, CFs ranged from 3.1 – 69.8 kHz for fibers obtained in CBA/CaJ animals, from 2.5 – 22.1 kHz for C57BL/6, and from 2.4 kHz – 25.4 kHz for 129/SvJ (Figure 4.3A).

The highest CFs obtained for C57BL/6 mice and 129/SvJ were significantly lower than that seen in the CBA/CaJ. Given the clear trend in C57BL/6 and 129/SvJ for threshold elevations at CFs > 15 kHz, this truncated CF range likely represents the effects of basal-turn hair cell loss in these strains. In general, mean AN thresholds in C57BL/6 were higher than CBA/CaJ for fibers with CF $\geq$ 15 kHz, while mean thresholds from 129/SvJ were higher across all CFs (except for CFs < 4 kHz) than those in either CBA/CaJ or C57BL/6 strains (Figure 4.3B). These results correlate well with the differences in the DPOAE thresholds observed among the three strains (Figure 4.1).

Although the low-CF limit of fibers sampled from the three strains was comparable (3.1, 2.5 and 2.4 kHz for CBACa/J, C57BL/6 and 129/SvJ, respectively), it seemed particularly difficult to find low-CF fibers in the C57BL/6 animals. Despite explicit attempts to place the micropipets in regions of the nerve where low-CF fibers would be expected, the yield of low-CF fibers (CF<10 kHz) in C57BL/6 was significantly lower (19%) than that in CBA/CaJ (36%) or 129/SvJ (38%).

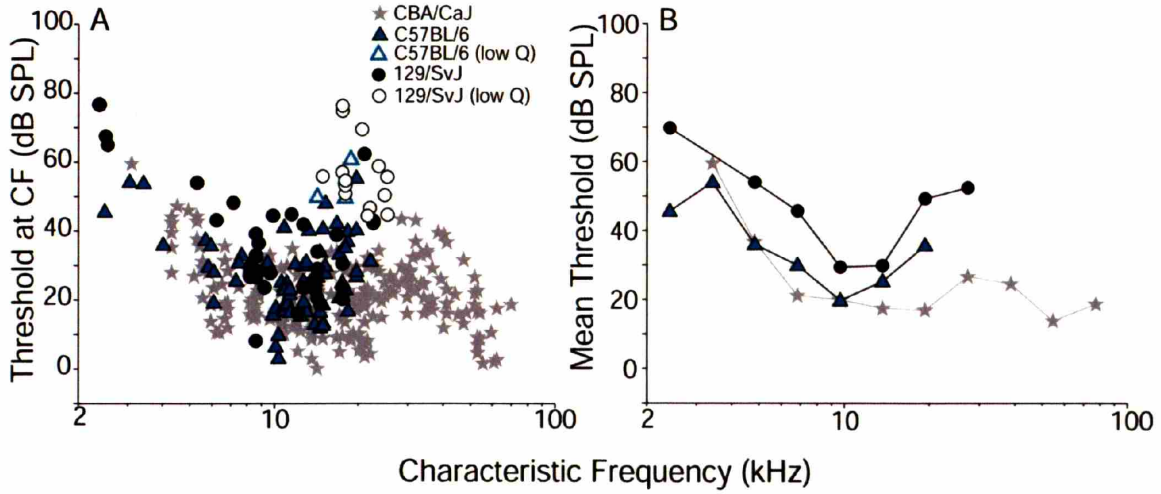

Figure 4.3: Panel A: Thresholds at CF for 196 AN fiber in 28 CBA/CaJ mice, 72 AN fibers in 13 C57BL/6 mice, and 52 AN fibers in 7 129/SvJ mice. Open symbols are from fibers with broad tuning curves (low Q). **Panel B:** Mean thresholds as a function of CF. Data from each strain binned according to CF (half-octave bins), and the average threshold for each bin was calculated.

The relationship between sharpness of tuning (Q_{10dB}: ratio of CF to bandwidth at 10 dB above threshold at CF) and CF was similar in all strains, except for CFs > 15 kHz where some fibers in C57BL/6 and 129/SvJ mice displayed broader tuning than that in CBA/CaJ (Figure 4.4, open symbols). These fibers also had higher thresholds than most CBA/CaJ fibers of similar CF (Figure 4.3A open symbols). The presence of a broad tuning curve tip in these fibers implies outer hair cell pathology and raises the possibility that the CF values shown may be inaccurate; thus, these fibers will be represented by open symbols in all subsequent figures in this chapter.

4.3.2 First Spike Latency

The first spike latency (FSL) was measured in each fiber encountered from the responses to CF tone bursts presented at 30 dB above threshold. These data were obtained primarily to aid in distinguishing AN fibers from cochlear nucleus cells (See Chapter 2), however, they also proved to provide insight into the nature of the phenotype in one of the knockout strains studied (See Chapter 6). As shown in Figure 4.5, the relation between CF and FSL, in all three strains, showed a monotonic decrease with increasing CF, reflecting, in large part, the decreasing traveling wave delay in the basal turn. There did not appear to be any anomalies in the FSLs of fibers with exceptionally low Q (open symbols).

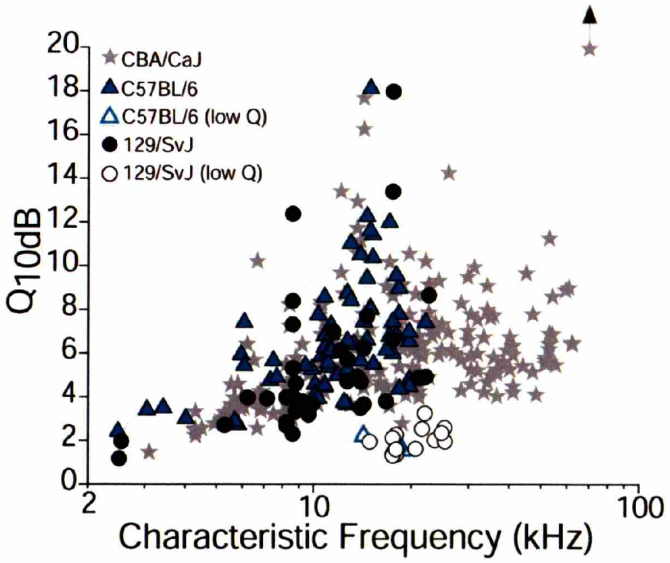

Figure 4.4: Sharpness of tuning as a function of CF for 196 AN fiber in CBA/CaJ mice, 72 AN fibers in C57BL/6 mice, and 51 AN fibers 129/SvJ mice. The CFs of fibers with broad tuning curves (low Q) is difficult to determine accurately and are shown as open symbols.

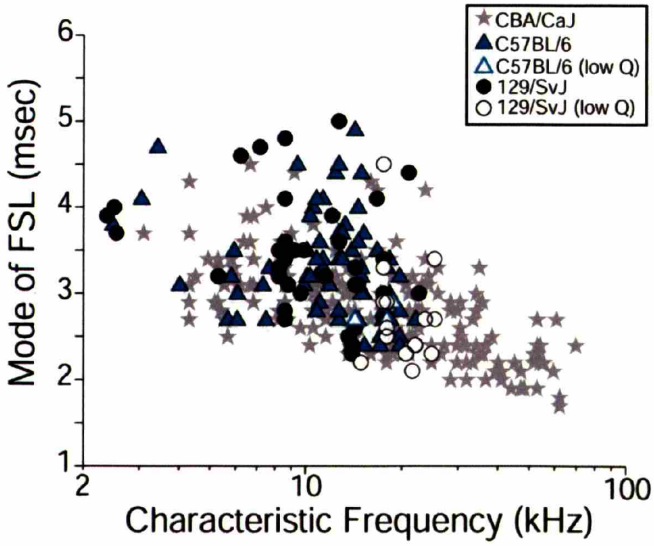

Figure 4.5: Mode of the first spike latency (FSL) as a function of CF for AN fibers in CBA/CaJ, C57BL/6, and 129/SvJ. Fibers with low Q are shown as open symbols.

4.3.3 Spontaneous Rate

As seen in Figure 4.6, the spontaneous rate (SR) distributions for fibers sampled from the three strains showed differences: compared to CBA/CaJ, populations appeared shifted towards low-SR fibers in C57BL/6 and towards high-SR fibers in 129/SvJ. SRs ranged from 0 - 120 sp/sec in CBA/CaJ and C57BL/6, and from 0 - 155 sp/sec in 129/SvJ, with 49% (CBA/CaJ), 67% (C57BL/6) and 29% (129/SvJ) of fibers with SRs < 20 sp/sec. The SR distribution in 129/SvJ was biased towards higher SRs compared to both CBA/CaJ and C57BL/6; mean SRs in 129/SvJ mice were significantly higher than CBA/CaJ and C57BL/6 mice ($P << 0.0001$ Student's *t*-test).

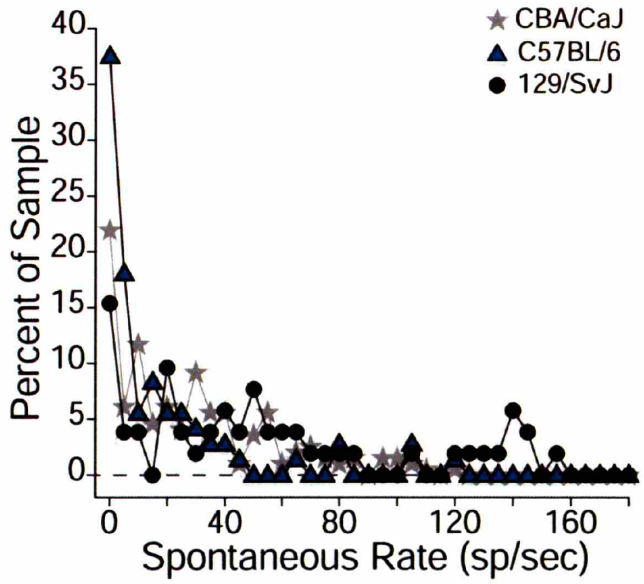

Figure 4.6: Spontaneous rate distributions for fibers sampled from the three strains. Data from low-Q fibers are included in the samples.

While there is no clear relationship between fiber SR and CF in either the CBA/CaJ or the 129/SvJ data, there is a curious lack of high-SR fibers among the low-CF fibers sampled in C57BL/6 animals (Figure 4.7): only 3/14 fibers with CF < 10 kHz showed SR > 10 sp/sec.

In all mammalian ears evaluated to date, there is a clear relationship between fiber threshold and SR (Liberman 1978; Tsuji and Liberman 1997). As seen for CBA/CaJ, fibers with the lowest relative thresholds (with respect to mean thresholds of high-SR fibers of similar CF) tended to have the highest SRs (Figure 4.8). However, the high-threshold, broadly tuned fibers in both C57BL/6 and 129/SvJ (open symbols) tended to have high SRs. Their presence added noise to the relationship between SR and relative threshold. Such an added spread in relative threshold would be expected among high-SR fibers in the presence of outer hair cell pathology, since damage to the outer hair cells should raise thresholds without affecting SR (Liberman and Dodds 1984a).

The fact that, at all CF regions, mean thresholds in the 129/SvJ AN fibers were high relative to both C57BL/6 and CBA/CaJ (see Figure 4.3), suggests that there could be a sampling bias against high-threshold, low-SR fibers in 129/SvJ: the spectral energy of the search stimulus used to find fibers when advancing the electrodes may not have been sufficient in 129/SvJ to excite some of the low-SR fibers. Therefore, the SR distribution obtained in 129/SvJ may be less

representative of the true underlying distribution than that seen for the CBA/CaJ and C57BL/6 strains.

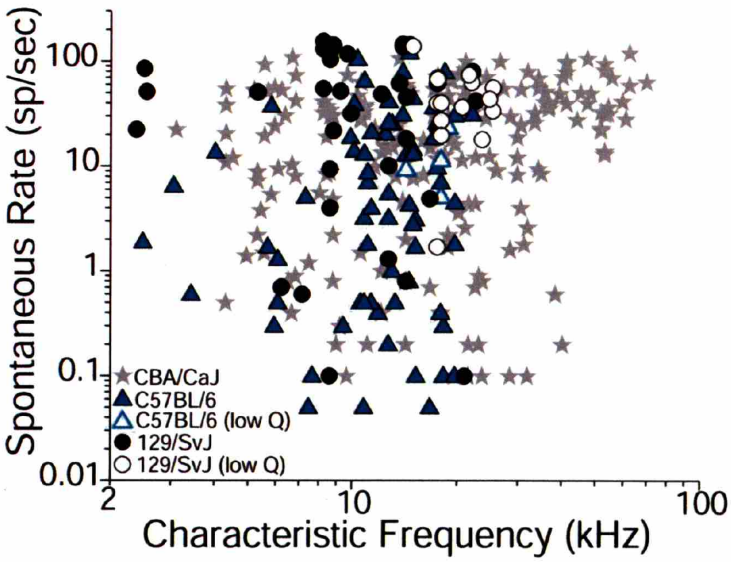

Figure 4.7: Spontaneous rate as a function of CF for AN fibers from the three strains. In this and all subsequent figures, SR values of 0 are plotted as 0.05 sp/sec.

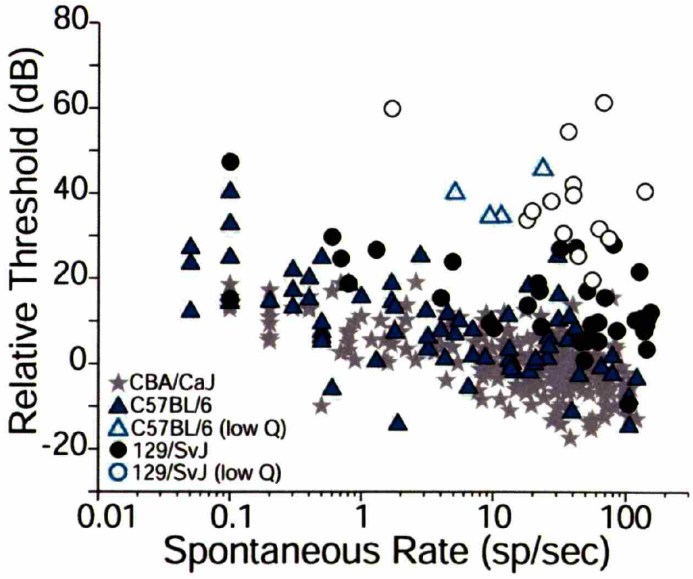

Figure 4.8: Relation between spontaneous rate and threshold sensitivity for AN fibers from the three strains. Relative threshold is defined by referring the threshold at CF of each fiber to the mean threshold of high-SR fibers (SR>1 sp/sec) of similar CF from CBA/CaJ.

4.3.4 Response adaptation

PST histograms of AN fibers show a peak in discharge rate at tone-burst onset, which decays to a steady-state response (Kiang et al. 1965; Smith 1977). The ratio of peak to steady-state rate is one measure of response adaptation. As will be discussed in later Chapters, the onset rate is important, because it is a key determinant of the amplitude of commonly obtained gross cochlear potentials such as ABR and CAP.

In the present study, adaptation of AN responses was studied using PST histograms of responses to CF tone bursts at 30 dB above threshold. The histograms were normalized by the number of tone burst presentations and the histogram bin width (0.5 msec), to give the instantaneous discharge rate. Example histograms from AN fibers with CFs < 20 kHz from CBA/CaJ, C57BL/6 and 129/SvJ mice are shown in Figure 4.9.

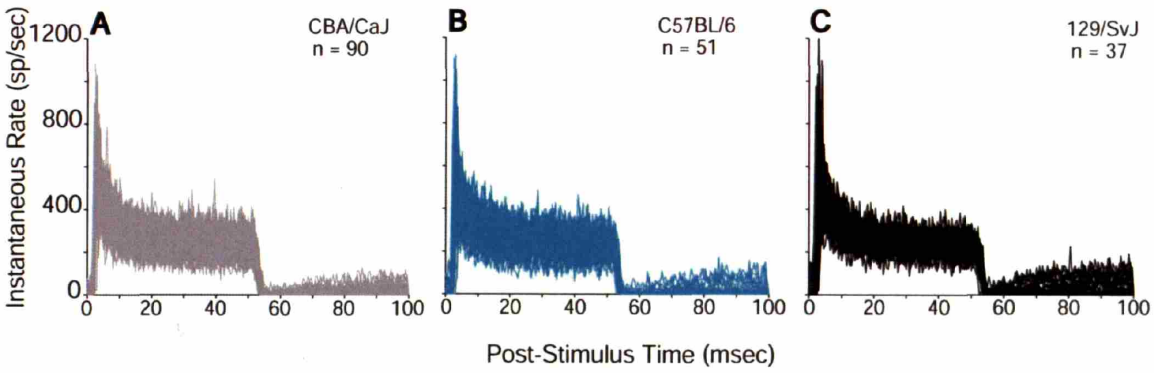

Figure 4.9: Superimposed PST histograms from AN fibers in CBA/CaJ (**Panel A**), C57BL/6 (**Panel B**), and 129/SvJ (**Panel C**). Each histogram shows data from all fibers sampled in each strain with CF < 20 kHz and SR > 1 sp/sec. Histograms are divided by the number of stimulus presentations and bin width (0.5 msec) to give instantaneous discharge rate.

Response adaptation is a function of CF and SR in the mouse AN. Peak-to-steady-state ratios for AN fibers in CBA/CaJ increase with CF, especially for CF > 20 kHz (Figure 4.10). A great majority of AN fibers recorded from C57BL/6 (99%) and 129/SvJ (81%) in this study had CFs < 20kHz and accordingly, an increase in peak-to-steady state ratio with fiber CF was not observed (Figure 4.10). For fibers of all CFs, a strong determinant of adaptation for all three strains was SR; high-SR (≥ 1 sp/sec) fibers generally had larger peak-to-steady-state ratios than low-SR fibers (Figure 4.11).

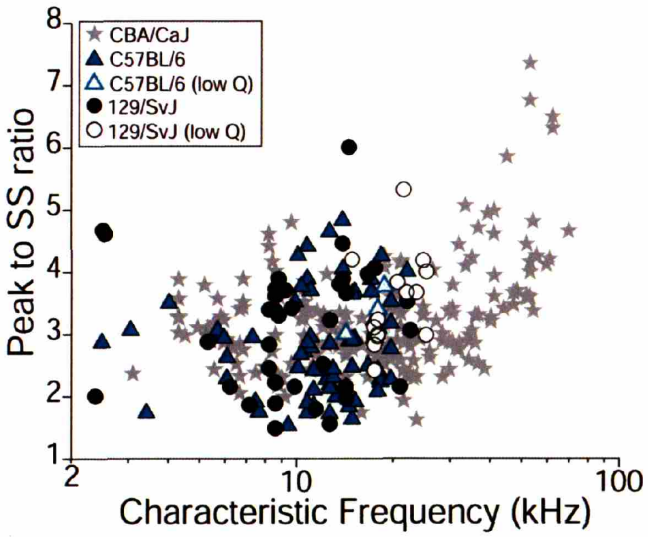

Figure 4.10: Response adaptation as a function of CF. Adaptation was derived from PST histograms based on CF tone bursts, 30 dB above threshold. Peak to steady state (SS) ratio was obtained by dividing the maximum rate by the average rate during the last 15 ms of the burst response.

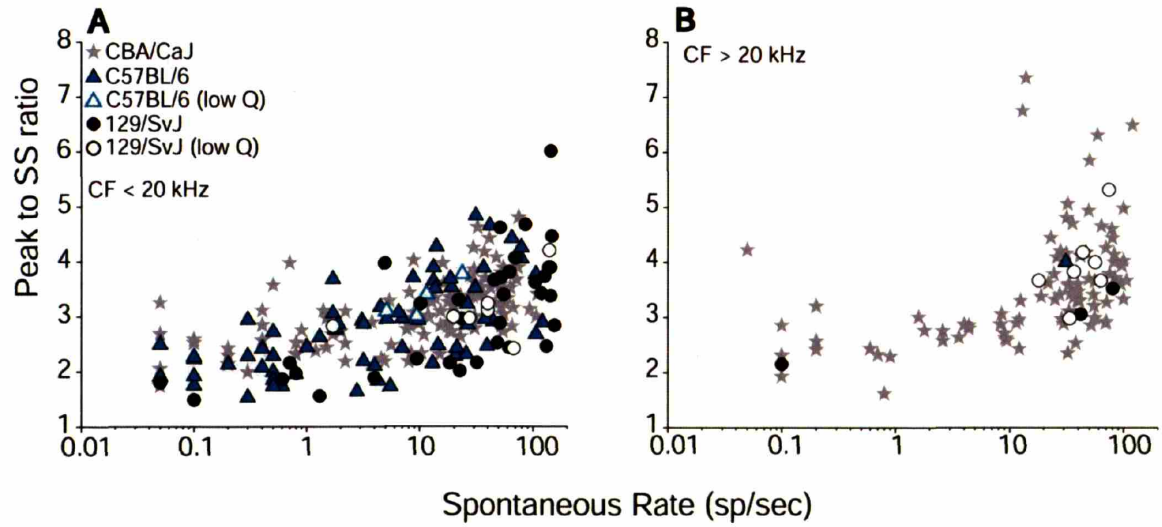

Figure 4.11: Response adaptation as a function of spontaneous rate. Adaptation was derived from PST histograms based on CF tone bursts, 30 dB above threshold. Peak to steady state (SS) ratio was obtained by dividing the maximum rate by the average rate during the last 15 ms of the tone bursts. **Panel A:** Fibers with CF < 20 kHz. **Panel B**: Fibers with CF > 20 kHz. Symbol key on Panel A also applies to Panel B.

4.3.5 Rate-level functions and dynamic range

Maximum discharge rates and dynamic ranges of AN fibers in C57BL/6 and 129/SvJ mice were investigated by measuring discharge rate vs. sound level for tone bursts at CF. Each level function was fit by a modified version of an existing model (Sachs et al. 1989) in order to better estimate the dynamic range (see chapter 2).

In data from guinea pig AN (Winter et al. 1990), rate-level functions have been categorized as "hard saturating", "sloping saturating", and "straight". As seen in data from CBA/CaJ AN, nearly all high-SR fibers (SR ≥ 1sp/sec) in C57BL/6 and 129/SvJ mice had hard-saturating rate-level functions (Figure 4.12A,C,E). Note that all broadly tuned (low-Q) fibers for which a level-function was obtained had SR > 1 sp/sec. Low-SR fibers in CBA/CaJ and C57BL/6 were more heterogeneous than high-SR fibers in that all three level-function shapes could be found among them (Figure 4.12 B,D). Low-SR fibers in 129/SvJ were more homogenous: none showed hard-saturating level functions and several had straight level functions (Figure 4.12 F).

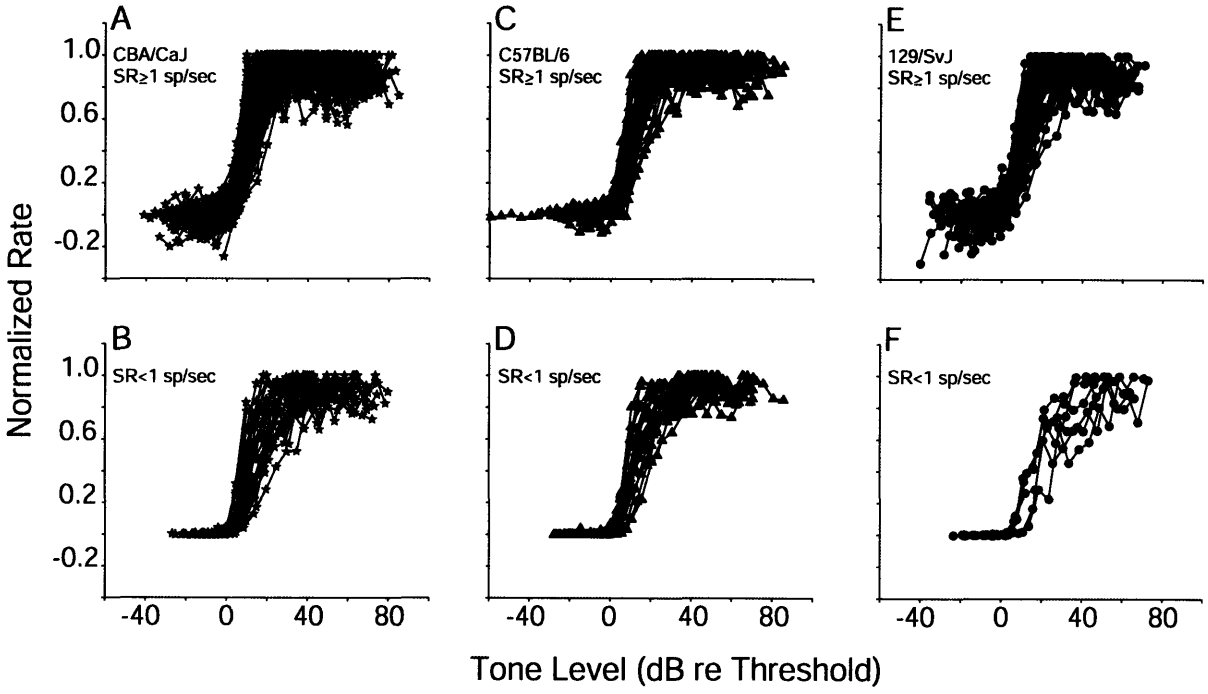

Figure 4.12: Shapes of rate-level functions obtained from CBA/CaJ, C57BL/6, and 129/SvJ fibers, divided into those with SR ≥ 1 sp/sec (Panels: A,C,E) and SR < 1 sp/sec (Panels: B,D,F). Data for CBA/CaJ are shown in the first column, for C57BL/6 in the second column, and for 129/SvJ in the third column. All functions were normalized by: 1) dividing the vertical axis by the maximum driven rate, and 2) shifting along the horizontal axis according to model-fit thresholds.

There was a tendency for AN fibers with low SR (< 1 sp/sec) to show lower maximum discharge rates than those with high SR (Figure 4.13A) in the three strains studied. Group mean differences in maximum discharge rates between high- and low-SR fibers were highly significant (P = 0.00003, Student's *t*-test) when data from the three strains were pooled. There did not appear to be any relation between maximum discharge rate and CF (Figure 4.13B) in any of the three strains. The high-CF fibers with broad tuning curves showed no obvious difference in maximum discharge rate compared with fibers of normal Q of similar CF.

More than 55% of AN fibers in the three strains had dynamic range less than 15 dB (Figure 4.14: dynamic range was defined as the dB range between the points corresponding to 10 and

90% of the (model fit) maximum driven rate). However, there was a larger percentage of fibers with SR ≥ 10 sp/sec with dynamic range > 20 dB in C57BL/6 (17%) and 129/SvJ (21%) than in CBA/CaJ (5%) mice. In all three strains, low-SR fibers showed larger dynamic ranges than high-SR fibers.

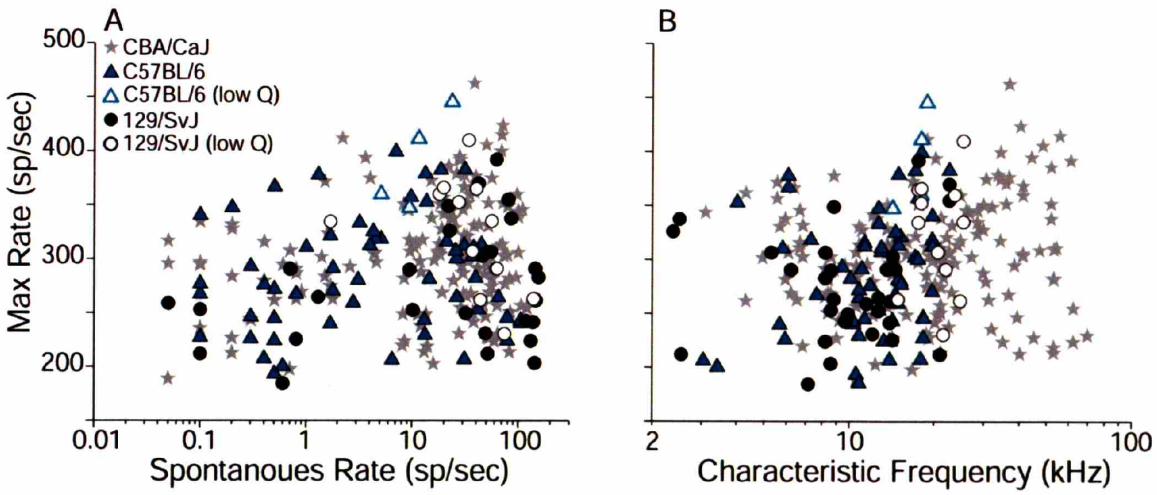

Figure 4.13: Relation between maximum discharge rate and spontaneous rate (**Panel A**) or characteristic frequency (**Panel B**). Data are shown for all fibers in CBA/CaJ, C57BL/6, and 129/SvJ from which a rate-level function was obtained. Symbol key in Panel A applies to Panel B.

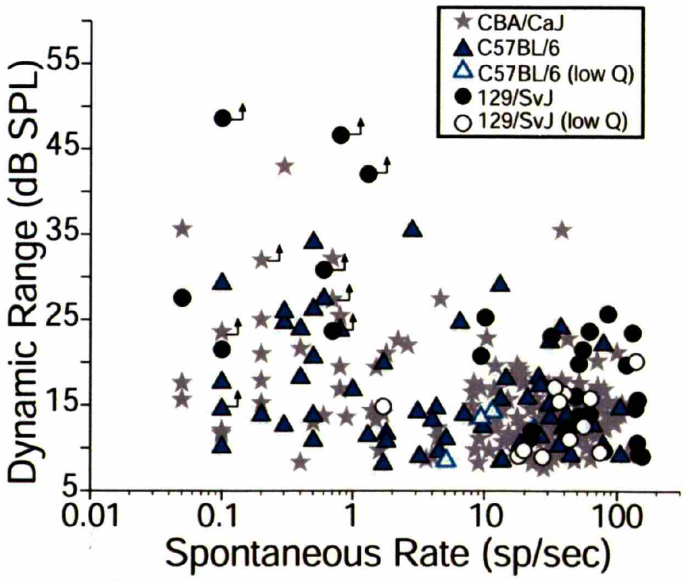

Figure 4.14: Dynamic range as a function of spontaneous rate for all fibers in CBA/CaJ, C57BL/6, and 129/SvJ for which a rate-level function was obtained. Upward arrows indicate rate-level functions which had not saturated at the highest SPLs presented.

4.3.6 Response synchrony

Although the sample size is limited by the general lack of low-frequency responsiveness in the mouse AN (see Chapter 3), the fundamental features of response synchronization were similar among CBA/CaJ, C57BL/6, and 129/SvJ fibers. Rate and synchrony data were obtained, whenever possible, for stimulus-level functions at 5 frequencies from 1 to 4 kHz for CBA/CaJ and C57BL/6 mice and at 2 kHz for 129/SvJ mice. Synchrony results using a 2 kHz stimulus are shown in Figure 4.15. It can be seen that AN fibers in all three strains (1) can synchronize to the stimulus period at lower SPLs than those at which the average rate increase, and (2) have similar maximum synchronization indices. Comparing maximum synchronization indices obtained across test frequencies from AN fibers in CBA/CaJ and C57BL/6 mice (Figure 4.16C), it is clear that, for both strains, there is a sharp roll off for frequencies > 2 kHz.

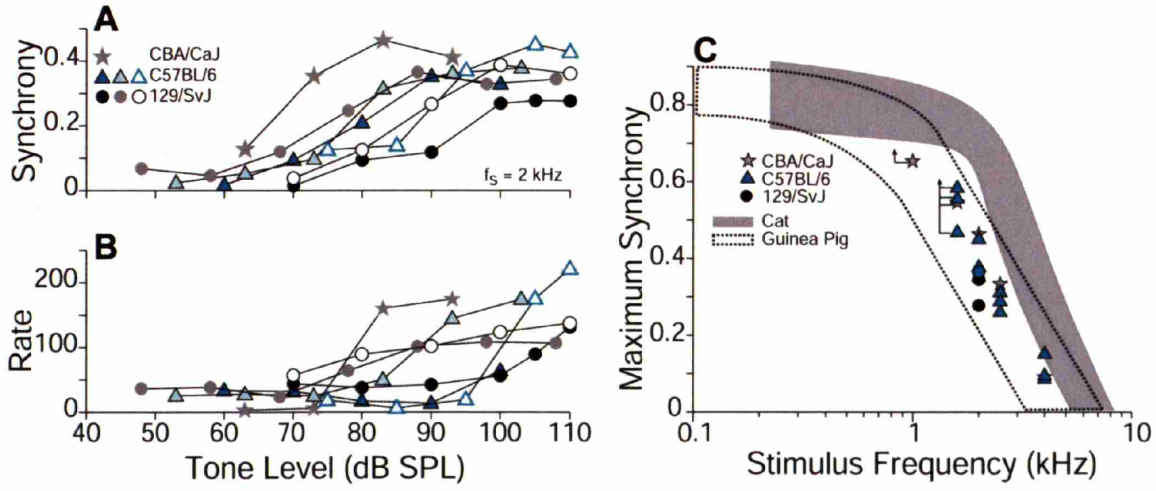

Figure 4.15: Phase-locking in AN fibers from CBA/CaJ, C57BL/6, and 129/SvJ. **Panel A and B**: data from one CBA/CaJ fiber (CF = 3.1 kHz, SR = 22.4 sp/sec), three C57BL/6 fibers (CF = 7.66 kHz, SR = 74.6 sp/sec, dark triangle; CF = 5.81 kHz, SR = 37.5, gray triangles; CF = 15 kHz, SR = 13, open triangles), and three 129/SvJ fibers (CF = 8.21 kHz, SR = 55 sp/sec, dark circles; CF = 2.54 kHz, SR = 51.3 sp/sec, gray circles; CF = 9.21 kHz, SR = 52 sp/sec). Synchrony (**panel A**) and rate (**panel B**) were extracted from post-zero-crossing histograms obtained from 12-s continuous tones. Synchronization index (SI: **panel A**) was calculated as described by Johnson (1980). **Panel C**: comparison of maximum SI vs. tone frequency for data obtained in CBA/CaJ, C57BL/6 and 129/SvJ fibers. Published data from cat (shaded area; (Johnson 1980)) and guinea pig (dotted area;(Palmer and Russell 1986)) are shown as references to maximum synchrony values obtained in other mammals. SI values shown for test frequencies 1 kHz and 1.6 kHz are underestimates of the maximum SI because the SI vs. level function had not saturated at the highest sound level presented. Data shown in **Panel C** are all above the calculated synchrony noise floor (see Chapter 2).

4.4 Discussion

4.4.1 Comparisons to other data on auditory function in C57BL/6 and 129/SvJ mice

As discussed in Chapter 3, all neural input to the central nervous system available for processing auditory stimuli comes through the ~20,000 fibers of the AN. Thus, the minimum envelope of tuning curves obtained from mouse AN should relate in a relatively simple way to behavioral measures of threshold sensitivity in this species. Figure 4.16 shows an overlay of AN tuning curves obtained in C57BL/6. Given the progressive high-frequency hearing loss in this strain, it is critical that animals of the same ages be compared. The data from the present study were taken from animals aged 16-17 weeks. We found one behavioral study in the literature of behavioral thresholds in C57BL/6 for which the age was appropriate: 16 weeks. The minimum envelope of our single-fiber data is consistent with behavioral thresholds for C57BL/6 mice, at least for frequencies below 20 kHz. The reason for the discrepancy at high-frequency between the behavioral thresholds and the neural data is not clear. In neurophysiological studies such as this one, incomplete sampling is a possible source of discrepancy. However, incomplete sampling is probably not an issue in the present study: the steep rise in thresholds as CF approaches 20 kHz in our data sample (Figure 4.3) strongly suggests that we have effectively sampled fiber responses right up to the edge of the progressively extending cochlear lesion in this strain (Hequembourg and Liberman, 2001). Comparisons between single-fiber and behavioral thresholds could not be made for 129/SvJ mice, because behavioral measures of auditory function in this strain were not available in the literature.

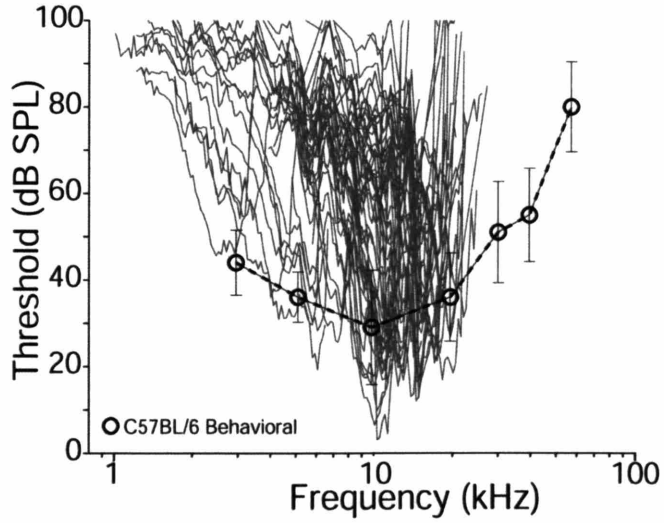

Figure 4.16: Superimposed tuning curves from all C57BL/6 fibers in the present study (gray) compared to behavioral threshold data from another study, (Mikaelian et al. 1974)). Error bars represent one standard deviation.

Compound action potentials (CAPs) and auditory brainstem responses (ABRs) are additional measures that have been used to assess the hearing sensitivity of C57BL/6 and 129/SvJ (Hequembourg and Liberman 2001; Lang et al. 2002; Yoshida and Liberman 2000; Zheng et al. 1999a). CAPs recorded from the round window represent the synchronous firing of AN fibers. Wave 1 of the ABR also represents the summed activity of AN fibers; however ABR can be measured in a more non-invasive way. Since CAP and ABR amplitudes depend upon the activity of AN fibers, they can be used to assess overall cochlear sensitivity. A common finding in C57BL/6 is an elevation of CAP and ABR thresholds that progresses from high to low

frequencies as the animals age (Hequembourg and Liberman 2001; Lang et al. 2002). However, the extent of threshold shift is highly variable across identically aged animals from the same strain, even between the two ears of a single animal (Francis et al. 2003). This pathology and its variability add to the complexity of using C57BL/6 and 129S mice as background strains for gene mutation studies.

Comparisons between CAP and ABR thresholds from C57BL/6 (Hequembourg and Liberman 2001; Lang et al. 2002) or 129S (Hequembourg and Liberman 2001; Yoshida and Liberman 2000) and superimposed AN tuning curves from this study (Figure 4.17A,B) show reasonably good agreement in overall pattern of threshold vs. frequency. The absolute values of "threshold" in any study of gross or single-fiber responses, will depend critically on the criterion used to define "threshold". This is particularly important in studies of gross potentials, since the "threshold" value will decrease significantly as increasing numbers of responses are averaged. Another source of uncertainty is the inter-laboratory differences in techniques for calibrating sound pressure at these high frequencies. Given these considerations, the most informative comparisons to be made are those between the 4-month single-fiber thresholds and the ABR thresholds at 3 and 7 months, since these data sets were all obtained in the same laboratory using very similar acoustic systems and calibration procedures. For frequencies at and below 20 kHz, there is remarkably close agreement in absolute thresholds between ABR and single fiber thresholds, for both 3-month and 7-month ABR data sets. At the highest ABR frequency (32 kHz), the 7-month ABR thresholds track the 4-month AN thresholds more closely than the 3-month ABR data. The fact that the single-fiber data do not fall intermediately between the two ABR data sets (as their relative ages would predict) may arise from subtle genetic differences between the sets of animals used in the two experiments: though nominally of the same strain, the animals used in the ABR study were from a colony maintained by Jackson laboratories, whereas the animals in the present study were from a colony maintained by Vanderbilt

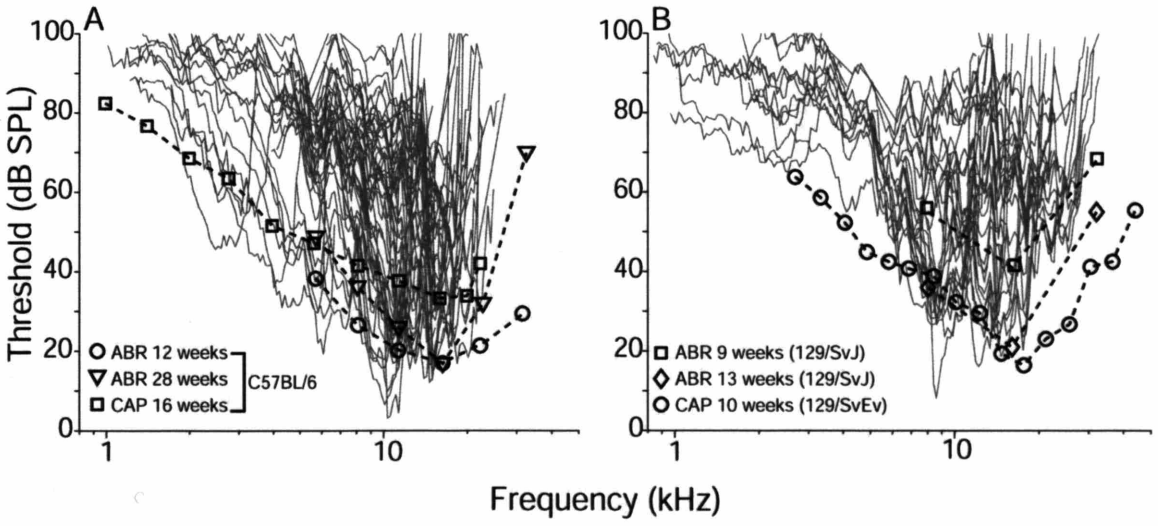

Figure 4.17: Superimposed tuning curves from all C57BL/6 (**Panel A**) or 129/SvJ (**Panel B**) fibers in the present study (gray) compared to ABR and CAP data from other mouse studies. CAP data are from the following sources: C57BL/6 (Lang et al. 2002) and 129/SvEv (Yoshida and Liberman 2000). ABR data are from the following sources: C57BL/6 (Hequembourg and Liberman 2001) and 129/SvJ (Zheng et al. 1999a).

University, that was derived by backcrossing, for 10 generations, a targeted mutation in another strain into C57BL/6. Thus, it is unlikely that the two sets of animals were truly identical genetically.

With respect to the 129/SvJ mice, data available for comparison include 1) CAP thresholds obtained in our laboratory, but for mice from a different 129 substrain: 10-11 week old 129/SvEv mice (Yoshida and Liberman 2000), and 2) ABR thresholds from the same substrain, but obtained in a different laboratory (Zheng et al. 1999a). The CAP data from 129/SvEv track single-fiber thresholds well for frequencies below 30 kHz (Figure 4.17B). The discrepancy at high-frequencies may arise from differences in the progression of age-related hearing loss between the 129 substrains. The published ABR data for 129/SvJ, the same substrain used in this study, show an internal inconsistency: thresholds from one cohort at 13 wks are better than thresholds from another cohort at 9 wks (Figure 4.17B). If we assume this discrepancy arises from natural variability in the age-related progress of cochlear degeneration (see above), and average the two ABR data sets, there is good agreement between the ABR data and the single-fiber thresholds at all three ABR frequencies. In summary, although detailed quantitative comparisons between threshold values is difficult for a variety of reasons, published CAP and ABR response thresholds obtained from C57BL/6 and 129S mice, of comparable ages to the ones used in this study, generally follow the minimum threshold envelope of single-fiber responses.

4.4.2 CF limits and cochlear frequency maps

Knowing the range of single-fiber CF present in the mouse AN is key to constructing an accurate cochlear frequency map, and cochlear frequency maps are critical in any attempt to carefully correlate structural and functional changes in the mouse ear (See for example, Section 4.4.3).

CFs encountered in our combined sample of AN fibers in this thesis ranged from 1.92 kHz to 69.8 kHz (Figure 4.3A, Figure 6.2A). We have already discussed the idea that the high-frequency CF limit in C57BL/6 and 129/S is imposed by the apically progressing, early-onset degeneration in the cochleas of these strains. In Chapter 3, we pointed out that the high-frequency limit for CBA/CaJ was artificially imposed, because the probe-tube microphone response was too attenuated at high frequencies to justify calibration above 70 kHz. In contrast, the low-frequency CF limit of 1.92 kHz is subject only to sampling errors: i.e. low-CF fibers were rare, and the true low-CF limit may be somewhat lower. However, the data in this thesis, from a total of 447 AN fibers from three strains, must provide a reasonably good estimate of the lowest CF in the mouse cochlea.

It is instructive to consider how dramatically the value chosen for apicalmost CF affects the nature of these maps. A low-frequency CF limit of 1.92 kHz is significantly higher than the value predicted by two older cochlear frequency maps for mouse (Ehret 1975; Ou et al. 2000), however, it is ~1 octave lower than that suggested by the most recent map (Mueller et al., 2004). The oldest map (Ehret 1975) was derived by choosing values for the upper and lower limit of mouse hearing from behavioral measures, and then fitting a power function of the type inferred for the human cochlear map based on psychophysically derived critical bands (Greenwood 1961). The lower limit chosen for mouse hearing was 0.8 kHz. As shown in Figure 4.17, our data suggest that the perception of frequencies < 1.92 kHz is mediated by excitation of the "tails" of the apical-most AN fibers, not by fibers with CFs of 0.8 kHz.

A second cochlear map for mouse was derived by comparing the patterns of noise-induced hair cell lesions to patterns of threshold shift seen in ABR responses (Ou et al. 2000). The data set did not include any frequency points below ~6 kHz, but the best-fit logarithmic function extrapolated to a value of 1.5 kHz for the apical-most CF in mouse. According to the present results, this value may also be too low by ~1 octave. A similar discrepancy between the cat cochlear map inferred by correlating lesion site to cochlear sensitivity changes was detected when a definitive map was derived by intracellular labeling of single physiologically characterized nerve fibers (Liberman 1982a).

Recently, a mouse map was more directly derived by injecting HRP extracellularly into the CN after recording neuronal responses and correlating CF with the locations of labeled terminals in the cochlea (Mueller et al. 2004). Although there were no data points for the apical cochlea (lowest CF was ~7 kHz); the best-fit logarithmic function extrapolated to a minimum CF value of 4.8 kHz. The present study shows that tuning in the cochlear apex extends to at least 1.92 kHz. Thus, the simple log-frequency-to-linear-distance relation suggested Mueller et al. (2004) should be modified to a function of the Greenwood type, such that frequency representation in the apical turn changes more slowly with distance, as is the case in cat (Liberman 1982a). The modified equation suggested by the data in the present study is:

$$f(kHz) = 9.8 \cdot \left(10^{d*0.92} - 0.68\right) \qquad (1)$$

where f is frequency and d is normalized distance from the cochlear apex (0-1).

.

4.4.3 Age-related cochlear pathology in C57BL/6 and 129/SvJ

C57BL/6 mice are commonly used as animal models of age-related hearing loss. Published ABR studies show that at ages < 3 months, cochlear sensitivity in C57BL/6 is comparable to CBA/CaJ; whereas, at later ages, severe threshold shifts set in at high frequencies and progress to low frequencies (Hequembourg and Liberman 2001). Mice from the 129/SvJ strain also display significant age-related hearing loss, as well as relatively poor thresholds even at 2 months of age, when their ABR thresholds are higher than those in both CBA/CaJ and C57BL/6 (Zheng et al. 1999a).

Studies on the morphological correlates of age-related hearing loss in C57BL/6 describe a base-to-apex degeneration of cells in the spiral ligament (e.g. type-IV fibrocytes), as well as hair cells, with outer hair cell degeneration extending more apically than inner hair cell degeneration. In the basal turn, there is a secondary degeneration of AN fibers in regions of significant inner hair cells loss. In addition, there are signs of primary neural degeneration in the apical turn: spiral ganglion cells aggregate into large clumps of tens of cell bodies, in which individual cells appear to have lost their myelin sheaths. Furthermore, spiral ganglion cell counts show a loss of 40% in the apical turn of 7-month old animals in the absence of significant inner hair cell loss (Hequembourg and Liberman 2001; Spongr et al. 1997).

Morphological studies of age-related hearing loss have not been published for 129/SvJ, but data are available for 129/SvEv, a related 129 substrain that also displays age-related hearing loss (Ohlemiller and Gagnon 2004a). Morphological correlates of aging in this strain also suggest differing pathologies in the apical and basal turns. In the base, there is loss of OHCs and type-IV fibrocytes as well as supporting cell pathology. In the apical turn, there is pathology of

the fibrocytes in the spiral limbus, and only rare signs of neuronal degeneration (Ohlemiller and Gagnon 2004a).

The loss of spiral ganglion cells in the apical half of the C57BL/6 cochlea, which may not be present in 129 substrains (see above), may explain why it was particularly difficult to find low-CF fibers in C57BL/6 mice. Despite explicit attempts in all strains to place recording electrodes in regions of the nerve where low-CF fibers were expected, our yields of low-CF fibers (CF < 10 kHz) in C57BL/6 was significantly lower (19%) than that in CBA/CaJ (36%) or 129/SvJ (38%) mice.

Fibrocytes in the spiral ligament may participate in K^+ recycling from the organ of Corti to the scala media, and thus in maintenance of the endocochlear potential (EP) (Hequembourg and Liberman 2001). A drop in EP will elevate thresholds and decrease SRs in all AN fibers (Sewell 1984a, b). Although both C57BL/6 and 129/SvEv display age-related type-IV degeneration, EP does not decrease with age in these strains (Lang et al. 2002; Ohlemiller and Gagnon 2004b). Therefore, major anomalies would not be predicted in the SR distribution seen in recordings from AN fibers in either C57BL/6 or 129 strains: and, indeed, no major anomalies were observed (Figure 4.6). The apparent increase in percentage of low-SR fibers seen in the fiber sample from C57BL/6J is not the pattern of change that would be expected from a decrease in EP, for which the mean SR for high-SR fibers would be also be decreased. Alternatively, this apparent increase in the fraction of low-SR fibers in C57BL/6J could be related to the unique spiral ganglion cell pathology observed in the apical half of the cochlea in this strain (Hequembourg and Liberman, 2001). As shown in Figure 4.7, the fraction of low-SR fibers was particularly high among the low-CF fibers sampled in this strain (43% of fibers with CF < 10 kHz), and only 3/14 fibers with CF < 10 kHz showed SR > 10 sp/sec.

Analysis of the changes in tuning curve shapes (Liberman and Dodds, 1984) in C57BL/6 and 129/SvJ can provide further insight into the nature of the functionally important structural changes underlying the threshold shifts in these early-onset progressive pathologies. Fibers with CF > 15 kHz in C57BL/6 and 129/SvJ mice typically showed threshold elevations consistent with the base-to-apex progression of some cochlear pathologies in these strains (Figure 4.3). Tuning curve shapes from these high-threshold fibers in C57BL/6 and 129/SvJ included many with elevation of "tip" threshold and hypersensitivity of the tuning-curve "tail" (Figure 4.2). This type of tuning curve anomaly is consistent with selective damage to outer hair cells, as has been seen in cats with exposure to acoustic injury or ototoxic drugs (Liberman and Dodds 1984b). The presence of hypersensitive tails effectively rules out changes in EP, as a decrease in EP will lead to elevations of threshold on both tips and tails of tuning curves (Sewell 1984a). The further observation that these low-Q fibers had high SRs is also consistent with selective OHC damage, as previous studies have suggested that selective damage to the outer hair cells does not result in a SR decrease (Liberman and Dodds, 1984b), and is further evidence against changes in EP in these animals. Existing histological analyses of hair cell loss patterns in aging C57BL/6 mice concluded that frank loss of outer hair cells did not extend far enough apically to account for the border of the region of hearing loss (Hequembourg and Liberman, 2001). The above analysis of tuning curve shapes suggests that a transition zone of damaged outer hair cells may extend further apically from the edge of the region of hair cell degeneration.

Loss of OHCs leads to loss of compression in the basilar membrane response (Ruggero and Rich 1991) that might increase the steepness (i.e. decrease the dynamic range) of rate-level functions for some AN fibers. As has been argued by Heinz and Young (2004), low-threshold, high-SR fibers should not be affected by loss of basilar membrane compression, since their

response range spans only the lowest SPLs, at which the normal basilar membrane response is linear. In contrast, high-threshold, low-SR fibers, with dynamic ranges spanning SPLs for which normal basilar membrane responses are compressive, normally show "sloping" saturation; correspondingly, their dynamic ranges might decrease after outer hair cell damage. In mouse, sloping rate-level functions were normally seen only for fibers with SR < 1sp/sec (Figure 4.12). Unfortunately, the sample of low-Q fibers recorded from 129/SvJ or C57BL/6 strains did not include any with low SR, presumably because their thresholds were so elevated by the outer hair cell loss that they were not stimulated by our search stimulus and therefore not identified as the electrode was advanced.

Results from AN studies in acoustically traumatized cats suggest that tuning curves with elevated tips and hyposensitive tails, such as those shown in Figure 4.2B,F can arise if there is damage to, or loss of stereocilia on inner hair cells in regions where outer hair cell function remains (Liberman and Dodds, 1984). To date, there has been no analysis of systematic stereocilia condition in either C57BL/6 or 129/SvJ; present results suggest that such an analysis might reveal another aspect of the functionally important histopathology in these strains.

4.5 Conclusion

The availability of transgenic and mutant lines with interesting auditory phenotypes makes the mouse a valuable model for the study of the auditory system. However, the interpretation of hearing results from mutant mouse lines is often complicated by the fact that these lines are created or maintained in several different inbred mouse strains, and there can be clearcut interstrain differences in threshold sensitivity that complicate the interpretation of the mutant phenotype. In this chapter, the spontaneous and sound-evoked discharge properties of AN fibers recorded from the CBA/CaJ strains were compared to recordings in animals from the C57BL/6 and 129/SvJ strains, two common strains used to create transgenic mice (Mullen and Ryan 2001). It was found that despite the presence of high-CF fibers with pathological tuning, due to age-related cochlear pathology in C57BL/6 and 129/SvJ mice, a number of basic response properties of AN fibers were not significantly altered, including first spike latencies, maximum discharge rates, onset rates, response adaptation, and the dynamic ranges of AN fibers, i.e. the range of sound pressure levels over which suprathreshold discharge rate changes from spontaneous to saturated rate. Many fibers with CF > 15 kHz in C57BL/6 and 129/SvJ mice displayed pathological tuning curve shapes that resemble those found in animals with outer hair cell loss due to acoustic injury or ototoxicity. This finding, along with the observation that outer hair cell loss in aging C57BL/6 mice does not extend far enough apically to account for the border region of hearing loss in these animals (Hequembourg and Liberman, 2001), suggests that the transition zone of damaged hair cells may extend further apically from the edge of the region of hair cell degeneration. One possibility is that hair cells just apical to the region of hair cell loss may display stereocilia damage which affects function. Indeed there are fibers that with tuning curves that displayed elevated "tips" and hyposensitive tails, which is characteristic of damage to inner hair cell stereocila (Liberman and Dodds 1984b). Therefore, future studies on age-related hearing loss in C57BL/6 and 129/SvJ mice should look for stereocilia damage as another aspect of the histopathology of age-related hearing loss.

Chapter 5

Auditory Nerve Recordings in Mice with Targeted Deletion of Calcitonin-Gene Related Peptide (CGRP)

5.1 Introduction

There are two subdivisions of the olivocochlear efferent system that innervate the mammalian cochlea: lateral and medial. The lateral olivocochlear (LOC) efferents are thin unmyelinated neurons with cell bodies in or near the lateral superior olive. Their axons project primarily to the ipsilateral cochlea, where they form axodendritic synapses with auditory afferent fibers and more sparsely, with inner hair cells (IHCs) (Guinan et al. 1983; Liberman et al. 1990). The medial olivocochlear (MOC) efferents are large, myelinated neurons with cell bodies medial to the medial superior olive. Their axons project to the contralateral cochlea and synapse with outer hair cells (OHCs) (Guinan et al. 1983). Although much is known concerning the physiology of MOC neurons (Cody and Johnstone 1982; Liberman and Brown 1986; Robertson and Gummer 1985), little is known concerning the physiology or function of LOC neurons, since it is difficult to selectively record from and electrically stimulate these unmyelinated neurons.

The LOC system is neurochemically heterogeneous and may play a number of different roles in hearing. There are several putative neurotransmitters/neuromodulators that have been immunolocalized within LOC efferent terminals and cell bodies: Acetylcholine, GABA, CGRP, dopamine, enkaphalins, dynorphins, and urocortin (Abou-Madi et al. 1987; Eybalin et al. 1993; Vetter et al. 1991; Vetter et al. 2002). It has been hypothesized that the LOC system may play a role in the protection of primary afferent fibers from excitotoxicity. In support of this hypothesis are findings that intracochlear application of dopamine decreases auditory nerve activity without changing OHC function and that intracochlear application of the dopamine receptor blocker eticlopride, leads to dendritic swelling in some auditory nerve fibers, which is an early sign of excitotoxicity (Ruel et al. 2001). The LOC system may also be important for the normal development of OHCs given that urocortin-deficient mice display elevated distortion product otoacoustic emissions (DPOAEs) thresholds (Vetter et al. 2002), suggesting OHC dysfunction, and also show shortening of the OHCs, when compared to their wildtype littermates. Lastly, the LOC system may have a role in maintaining spontaneous rate distributions in auditory afferent fibers given that (1) in the lateral line organ of the a *Xenopus laevis*, a non-mammalian hair cell system, CGRP increases spontaneous activity in afferent fibers (Adams et al. 1987; Bailey and Sewell 2000) and (2) in chronically de-efferentated mammals, afferent spontaneous discharge rate distributions are lower than normal (Liberman 1990; Zheng et al. 1999b).

CGRP is a 37 amino acid peptide. It has two isoforms that differ in mice by three amino acids and are derived from two different calcitonin genes: $CGRP_{\alpha}$ and $CGRP_{\beta}$. Two classes of G-coupled protein CGRP receptors have been pharmacologically characterized based on various binding studies: CGRP1 and CGRP2 (Juaneda et al. 2000). The activation of these receptors increases the production of cyclic-AMP which may lead to the activation of protein kinases. There are various biological effects that have been associated with CGRP release by pre-synaptic neurons: vasodilation (Brain et al. 1985), increased desensitization of nicotinic acetylcholine receptors (nAChRs) in mouse muscle fibers (Mulle et al. 1988), and changes in AChR

biosysnthesis in muscle fibers (Osterlund et al. 1989). Interestingly, the CGRP knockout mice display normal blood pressure and have normal neuromuscular development (Lu et al. 1999).

The $CGRP_{\alpha}$ knockout mouse is an interesting model to study LOC function and the role of CGRP in cochlear physiology and auditory processing. CGRP has been immunolocalized in the cochlea to LOC efferent terminals underneath IHCs, to efferent terminals underneath OHCs, and to the spiral modiolar artery (Carlisle et al. 1990; Maison et al. 2002; Sliwinska-Kowalska et al. 1989; Vetter et al. 1991; Ylikoski et al. 1989). An immunohistochemical study of $CGRP_{\alpha}$ knockout mice using antibodies that recognize both CGRP isoforms (i.e., $CGRP_{\alpha}$ and $CGRP_{\beta}$) showed that CGRP is absent in the cochleae of these mice (Maison et al. 2003). $CGRP_{\alpha}$ knockout mice display normal DPOAEs, normal suppressive effects when electrically stimulating the OC bundle at the floor of the IVth ventricle, but decreased suprathreshold amplitudes in wave 1 of the auditory brainstem response (ABR) (Maison et al. 2003). The normal DPOAEs and the apparent lack of effect of CGRP deletion on the classic MOC-mediated suppressive effects suggests that CGRP's role in the efferent terminals on outer hair cells is minimal. Given that LOC fibers are in a position to influence auditory nerve (AN) responses directly without influencing OHC function, and given that wave 1 of the ABR is a measure of the synchronous activity of AN fibers (Melcher and Kiang 1996). it is possible that the response phenotype observed in the knockout mice reflects changes in LOC neurotransmission.

This study uses recordings from single auditory nerve fibers to better understand the reduction in ABR wave 1 amplitude reported by Maison et. al. (2003), and more generally to understand the contributions of CGRP to the response processing in the cochlea. There are several mechanisms that could account for a reduction in wave 1 amplitude: larger variance in first spike latency (FSL) response, lower instantaneous rates, a change in the unitary potential, and a reduction in the number of fibers within the population. The first two mechanisms can be directly tested using AN fiber recordings. An additional hypothesis of the role of CGRP comes from the work of Bailey and Sewell (Bailey and Sewell 2000). Their study of the lateral line organ in *Xenopus laevis* showed that the application of CGRP caused an increase in afferent spontaneous activity and a decrease in response modulation and sensitivity. This result suggests that we should also look for differences in SR, sound-evoked discharge rates, and phase-locking between the CGRP knockout and wildtype mice.

5.2 Data Set

Fiber responses shown in this chapter were classified as AN responses based on the classification criterion described in Chapter 2. In this Chapter, results from 72 AN fibers from CGRP wildtype mice aged 16-17 weeks, and 70 fibers from CGRP knockout mice aged 16-17 weeks, are compared. Data from Chapter 3 summarizing responses of 196 AN fibers from CBA/CaJ mice aged 8-17 weeks are superimposed on most Figures for an additional point of comparison.

The decision to record from CGRP wildtype and knockout mice at 16-17 weeks of age was based on the observation from the previous gross-potential study that differences in auditory phenotype between wildtype and knockout animals was clearer at 16 weeks than at 8-10 weeks (Maison et al. 2003).

The CGRP deletion was initially engineered in a mouse line that involved hybridization of 129/SvJ for ES cells, C57BL/6 mice for the blastocysts, and Black Swiss mice for the back-crossing of chimeras to achieve homozygosity. Subsequently, the CGRP deletion was backcrossed into C57BL/6 for 10 generations, thus satisfying the commonly accepted criteria for

creation of a congenic strain, i.e. one in which the genetic background is "identical" to mice from other C57BL/6 colonies, except for the existence of a targeted mutation at the CGRP locus.

5.3 Results

5.3.1 DPOAE Data

Changes in DPOAE thresholds were used to monitor cochlear condition throughout each experiment. Figure 5.1 compares mean DPOAE thresholds obtained in the CGRP wildtype and CGRP knockout mice at the start of each experiment. Consistent with a previous study (Maison et al. 2003), wildtype and knockout mice had similar DPOAE thresholds at all test frequencies. Both genotypes of the CGRP line had mean DPOAE thresholds which were similar to CBA/CaJ at low frequencies (i.e., $f_2 \leq 16$ kHz) but significantly higher at high frequencies. The high-frequency disparity is likely due to age-related OHC damage that is characteristic of the C57BL/6 strain, the background strain for the CGRP line.

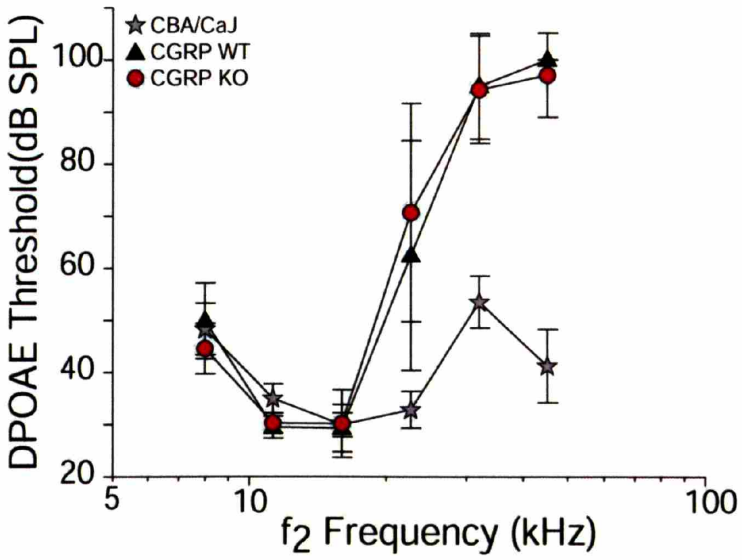

Figure 5.1: Mean distortion product otoacoustic emissions (DPOAEs) recorded at the start of each experiment for CBA/CaJ (stars), CGRP WT (triangles), and CGRP KO (circles) mice. DPOAE thresholds were determined as described in Chapter 2. A DPOAE threshold of 100dB was assigned when the DPOAE failed to reach criterion at the highest SPL presented (80) dB). Error bars represent one standard deviation.

5.3.2 Rate Threshold and Tuning

A fundamental property of AN fibers is their frequency selectivity, which is often quantified via "threshold" tuning curves which track iso-response contours in the frequency-intensity plane. AN tuning curves show sharply tuned "tips", defining the characteristic frequency (CF) and broadly tuned low-frequency "tails" (see Chapter 3). Tuning curves were obtained for all AN

fibers encountered. Plotting thresholds at CF provides an overview of the sensitivity and frequency range of the peripheral auditory system. CFs ranged between 2.5 kHz – 22.1 kHz for 72 fibers obtained in CGRP wildtype mice and between 2.6 kHz – 23.7 kHz for 70 fibers in CGRP knockout mice (Figure 5.2A).

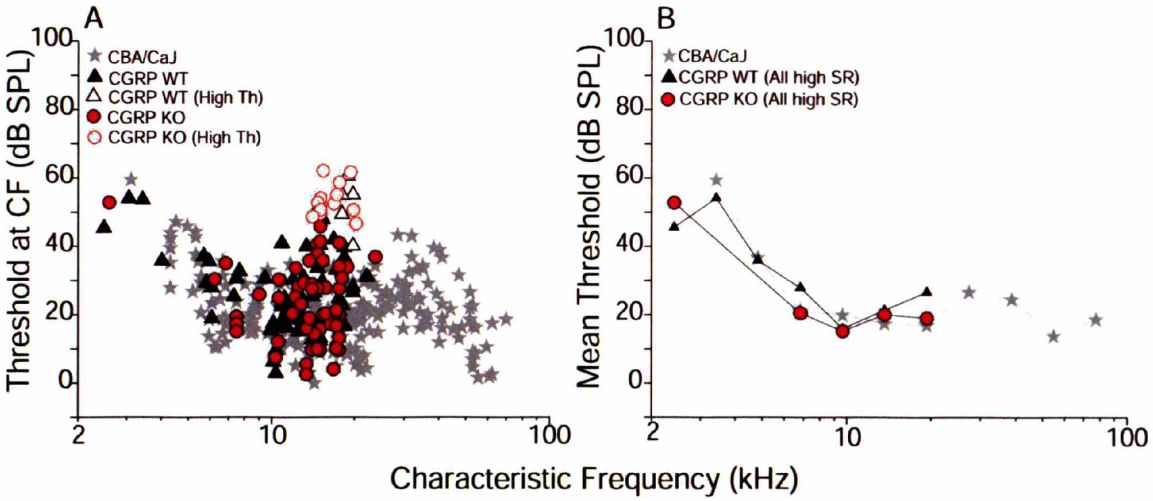

Figure 5.2: **Panel A:** Thresholds at CF for AN fibers in CBA/CaJ, CGRP wildtype mice, and CGRP knockout mice. Open symbols are from "pathological" fibers, defined as any high-SR fiber with threshold at CF > 30 dB higher than mean high-SR thresholds from CBA/CaJ fibers of similar CF or low-SR fibers with threshold at CF > 35 dB higher. **Panel B:** Mean thresholds as a function of CF. Data for high-SR fibers from each group (see key) were binned according to CF (half-octaves) and average threshold for each bin was calculated. Data from pathological units were not included in the means from the CGRP lines.

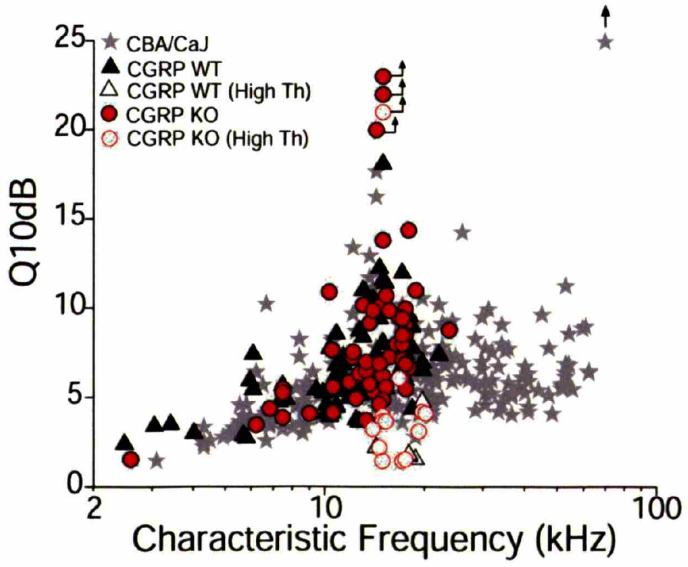

Figure 5.3: Sharpness of tuning as a function of CF for AN fibers in CGRP knockouts vs wildtypes, compared with data from CBA/CaJ. CF of pathological fibers with low Qs is difficult to determine accurately (open symbols).

Because the CGRP line is in a background strain (C57BL/6) that displays early-onset cochlear degeneration (Hequembourg and Liberman, 2001), some of the AN fibers recorded in CGRP mice of either genotype may show pathology, especially at high CF, that is due to the background rather than the loss of CGRP (see Chapter 4). In the present study, "pathological" fibers were defined based on their relative threshold compared to high-SR (SR>1 sp/sec) fibers of similar CF from CBA/CaJ (Chapter 3): the cutoff values for relative threshold to segregate out pathological fibers were 30 dB for high-SR fibers and 35 dB for low-SR fibers. These pathological fibers will be identified by unfilled symbols in all subsequent Figures

Although no significant difference was found between wildtype and knockout mice in mean thresholds for high-SR fibers Figure 5.2B, the percentage of pathological fibers found in knockouts (18%) was greater than that in wildtypes (7%).

No significant differences were also found in sharpness of tuning (Q_{10dB}: ratio of CF to bandwidth at 10 dB above threshold at CF) between CGRP knockout and wildtype AN fibers (Figure 5.3). This finding is consistent with chronic de-efferentation studies, that show that the presence of an efferent system is not required for AN fibers to retain their sharpness of tuning (Liberman 1990). Note that the Q_{10dB} values for fibers defined as pathological were almost all lower than those seen in nonpathological fibers (Figure 5.3). This finding is consistent with the presence of outer hair cell dysfunction at the edge of the apically progressing lesion in the C57BL/6 background strain (See Chapter 4).

5.3.3 Spontaneous Rate

The LOC system may play a role in modulating spontaneous rates in AN fibers given that (1) CGRP increases spontaneous activity in afferent fibers in the lateral line of *Xenopus laevis*, a non-mammalian hair cell system, (Adams et al. 1987; Bailey and Sewell 2000) and (2) in chronically de-efferentated mammals, AN spontaneous rate (SR) distributions are lower than normal (Liberman 1990; Zheng et al. 1999b). These findings suggest that the SR distribution in CGRP knockout mice might be biased towards low SRs as compared to wildtype mice.

Figure 5.4 shows the SR distribution of AN fibers sampled in CGRP wildtype and CGRP knockout mice, compared to similar data from CBA/CaJ. As discussed in Chapter 4, there is a statistically significant difference between the SR distribution in the C57BL/6 animals (i.e. CGRP wildtypes) and the CBA/CaJ animals: there is a higher proportion of low SR units in the former group. The CGRP knockouts also show a significantly higher proportion of low-SR units than was seen in CBA/CaJ. Interestingly, the CGRP knockout showed an even higher proportion of low-SR fibers than the CGRP wildtype; however, that inter-genotype difference did not reach statistical significance ($p= 0.13$, bootstrap method with replacement).

Comparing CGRP wildtype and knockouts, there were no significant differences in the relationship between SR and CF (Figure 5.5A) or between SR and relative threshold (defined with respect to the mean threshold of high-SR fibers of similar CF in CBA/CaJ mice) (Figure 5.5B). Note furthermore, that pathological fibers in both CGRP genotypes included a wide range of SRs (Figure 5.5A); and that, by definition, pathological fibers have high relative thresholds (Figure 5.5B).

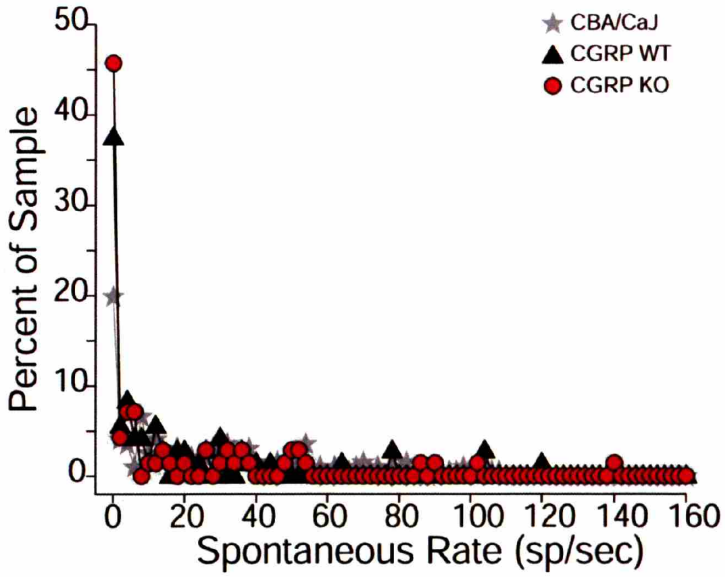

Figure 5.4: Spontaneous rate distributions for fibers from CGRP knockouts and CGRP wildtypes compared with CBA/CaJ. Data from CGRP lines includes pathological fibers. Bin width = 2 sp/sec.

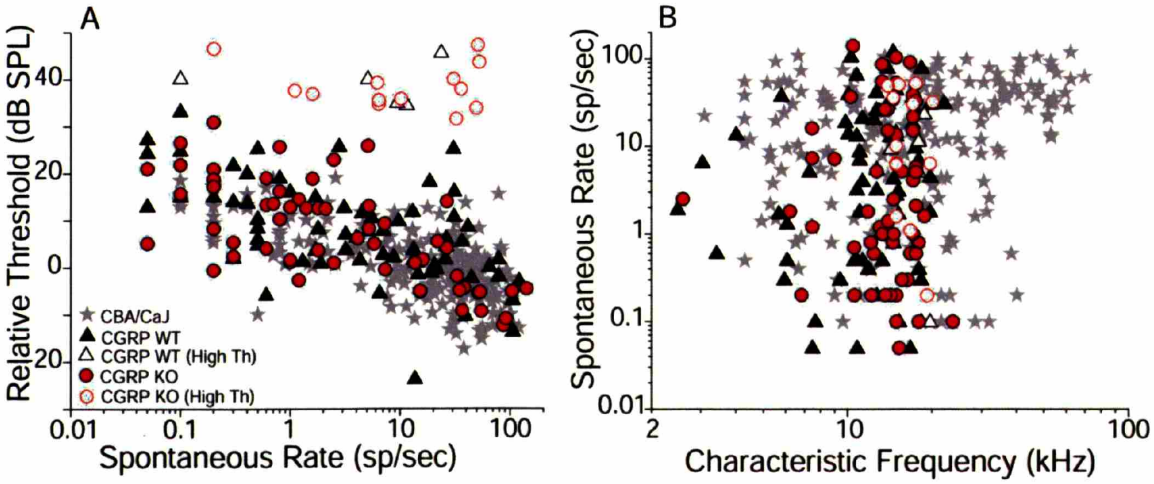

Figure 5.5: Relationship between spontaneous rate and relative threshold (**Panel A**) and between spontaneous rate and CF (**Panel B**). Relative threshold is defined by referring the threshold at CF of each fiber to the mean threshold of high-SR fibers (SR>1 sp/sec) of similar CF in CBA/CaJ mice. In this and all subsequent figures, SR values of 0 are plotted as 0.05 sp/sec.

5.3.4 First Spike Latency (FSL) and FSL Variance

Auditory gross potentials such as ABR are evoked by short tone pips, thus the amplitudes of these ABR waveforms depend critically on the synchronous firing of auditory neurons (Melcher and Kiang 1996). Thus, in addition to considering the average discharge rates (see Section 5.3.5) of AN fibers in CGRP knockout vs wildtype mice, it is important to consider measures of variability in spike timing. One useful measure is the variance in AN first spike latency (FSL) seen in response to supra-threshold tone levels. Since histograms of FSLs (from 150 CF tone bursts at 30 dB above threshold) were used to aid in differentiating AN fibers from cochlear nucleus neurons, these data were available for all fibers. Analysis of the mode of the FSL and the variance reveals no significant differences in FSL response between CGRP knockout mice and CGRP wildtype or CBA/CaJ mice (Figure 5.6AB). Note however, that in both the CGRP lines and the data from CBA/CaJ mice, there is a monotonic decrease in FSL variance as SR increases. As discussed further in Chapter 6, this SR-related effect on spike synchronization is intimately tied up with the monotonic increase in instantaneous onset rates as SR increases. Therefore, an increase in the percentage of low-SR fibers in CGRP knockout mice could theoretically lead to a decrease in ABR amplitudes (See Discussion).

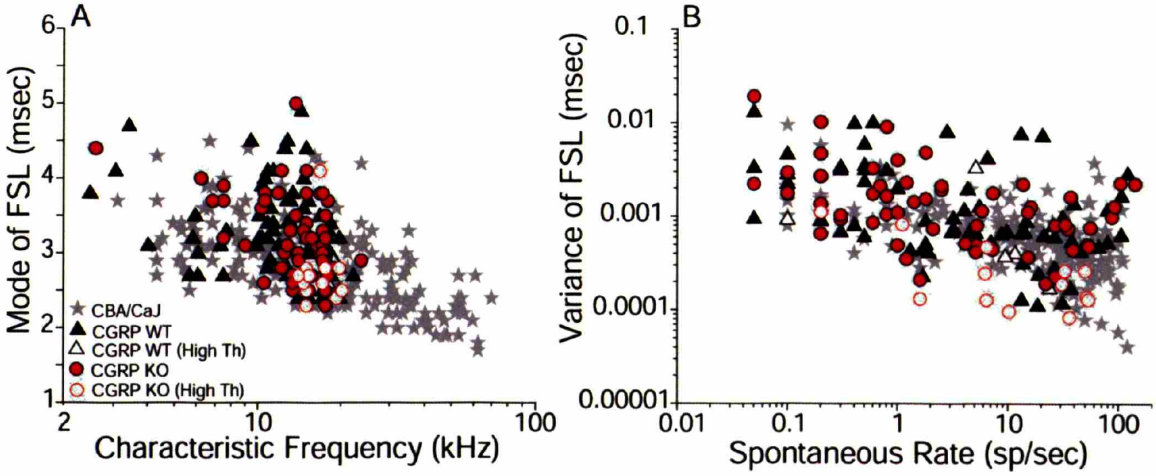

Figure 5.6: Mode of the first spike latency (FSL) as a function of CF (**Panel A**), and variance of the first spike latency as a function of SR (**Panel B**) for AN fibers from CBA/CaJ (stars), CGRP wildtypes (triangles), and CGRP knockouts (circles). Open symbols are from pathological fibers (see text).

5.3.5 Rate-level functions and dynamic range

Maximum discharge rates and dynamic range of AN fibers in CGRP wildtype and knockouts were investigated by measuring discharge rate-level for tone bursts at CF. Each level function was fit by a modified version of an existing model (Sachs et al. 1989) in order to get better estimates of dynamic range (see Chapter 2).

As seen in AN data from CBA/CaJ and CGRP wildtypes (Figure 5.7A,C), nearly all high-SR fibers in CGRP knockouts had hard-saturating rate-level functions (Figure 5.8E). Low-SR fibers in the knockout were similar to low-SR fibers in CBA/CaJ and CGRP wildtype in that they showed a mixture of hard saturating and sloping-saturating rate-level functions (Figure

5.7B,D,F). However, two low-SR fibers in the CGRP knockout displayed unusually large dynamic ranges, with rate-level functions that did not saturate at the largest sound pressure levels used (Figure 5.7F).

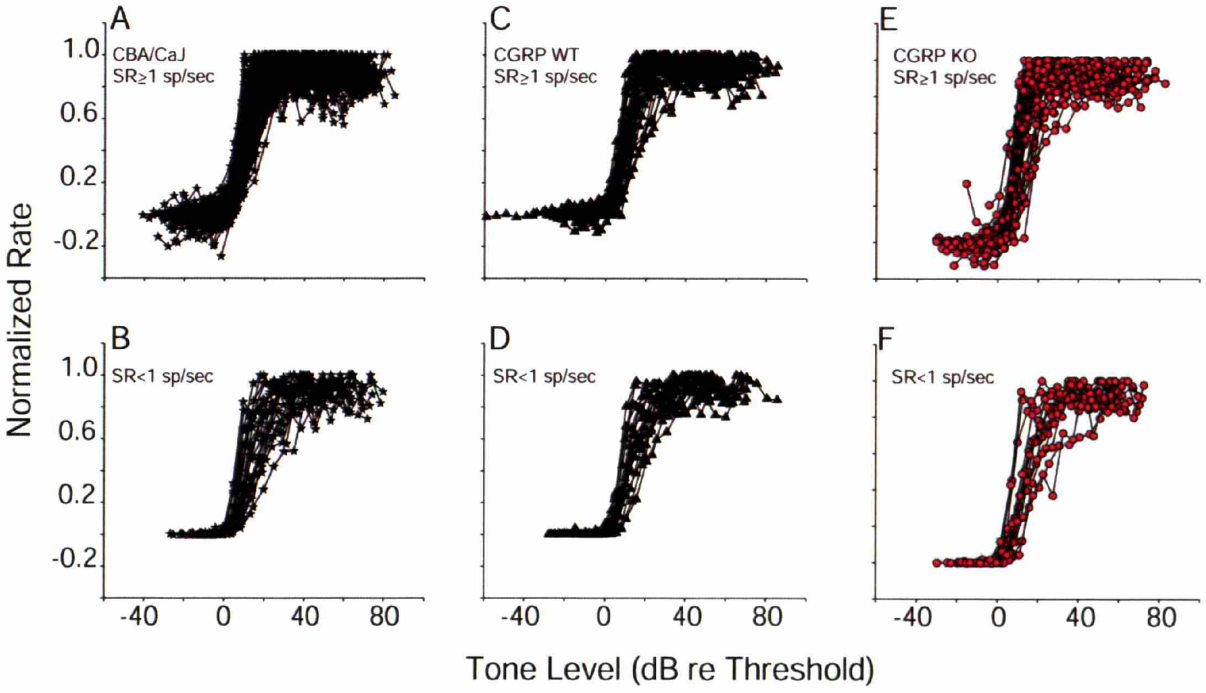

Figure 5.7: Superimposed rate-level functions from CGRP wildtype (WT: **Panels C and D**), CGRP knockout (KO; **Panels E and F**) and CBA/CaJ (**Panels A and B**) fibers, segregated according to SR: SR ≥ 1 sp/sec (**Panels: A, C, E**) and SR < 1 sp/sec (**Panels: B, D, F**). Functions were normalized by: 1) dividing the vertical axis by the maximum driven rate, and 2) shifting along the horizontal axis according to model-fit thresholds.

There was a tendency for AN fibers with low-SR (< 1 sp/sec) to show lower maximum discharge rates than those with high-SR in the three strains studied (Figure 5.8A). However, group mean differences in maximum discharge rates between high and low-SR fibers in CGRP knockout mice (P = 0.05, Student's *t*-test) were not as significant as in CGRP wildtype (P = 0.006, Student's *t*-test). With respect to the relation between CF and maximum rate, no significant differences were found between CGRP knockout and wildtype mice (Figure 5.8B). Note that for both KO and wildtypes, there was a tendency for pathological fibers to show higher maximum discharge rates than fibers of similar CF with threshold sensitivity closer to that seen in CBA/CaJ.

No significant differences were found between CGRP knockout and wildtype mice in the relationship between dynamic range and SR (Figure 5.9). This result, along with the others

presented in this section, suggests that release of CGRP by LOC fibers does not significantly influence rate-level responses in AN fibers.

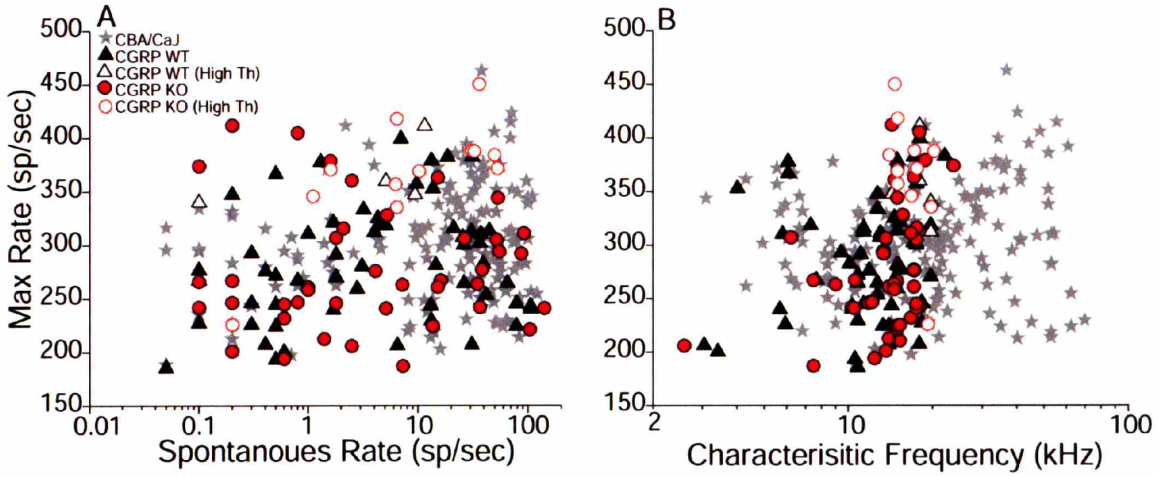

Figure 5.8: Relation between maximum discharge rate and spontaneous rate (**Panel A**) or characteristic frequency (**Panel B**). Data are shown for all fibers in CBA/CaJ, CGRP wildtype (WT), and CGRP knockout (KO) from which a rate-level function was obtained.

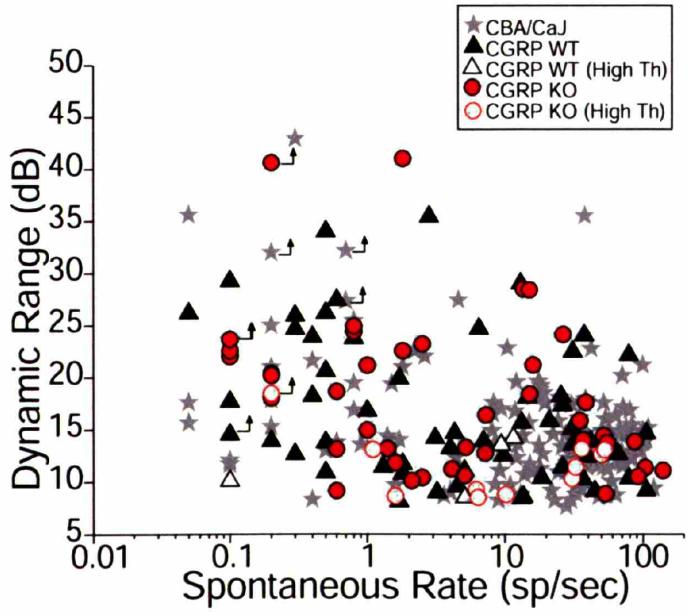

Figure 5.9: The relation between dynamic range and spontaneous rate for fibers from CBA/CaJ, CGRP wildtype (WT), and CGRP knockout (KO) mice. Dynamic range was extracted from the fitted curves and was defined as the difference between SPLs producing 10% and 90% of maximum driven rate.

5.3.6 Response Adaptation

Rate-level functions of the type considered in the Section 5.3.5 display discharge rates averaged over the entire tone-burst duration at each SPL. However, PST histograms of AN fiber response to the tone bursts used to construct such functions show a peak in discharge rate at tone-burst onset, which decays to a steady-state response that is significantly lower (Figure 5.10; (Kiang et al. 1965; Smith 1977)). ABR amplitude is dominated by the onset rate of auditory neurons, rather than by their steady-state rates (Melcher and Kiang 1996). Thus, in this section, we separately examine the onset rates and steady state rates of AN fibers in CGRP knockout vs wildtype mice.

PST histograms of AN responses to CF tone bursts at 30 dB above threshold were obtained from every fiber contacted. The histograms were normalized by the number of tone burst presentations and the histogram bin width (0.5 msec) to give the instantaneous discharge rate. In the three panels of Figure 5.10, we superimpose histograms from all high-SR fibers with CFs < 20 kHz obtained from CBA/CaJ, CGRP wildtype or CGRP knockout mice. Visual inspection of these superimposed data suggest that loss of CGRP leads to no significant differences in peak rates, steady-state rates, or the time constants of adaptation.

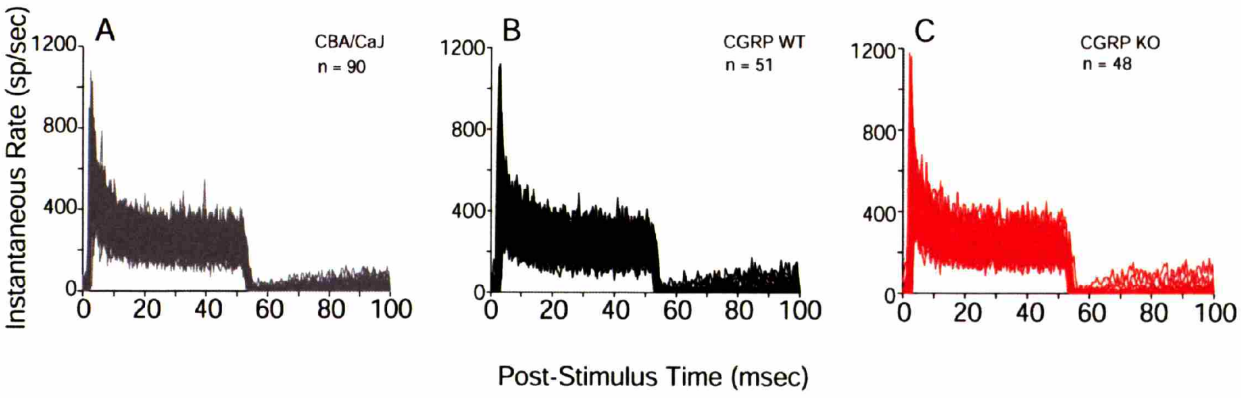

Figure 5.10: Superimposed PST histograms for responses to CF tone bursts at 30 dB above threshold for all low-CF (< 20 kHz), high-SR (> 1 sp/sec) fibers from CBA/CaJ (**Panel A**), CGRP wildtype (WT) (**Panel B**), and CGRP knockout (**Panel C**) mice. Numbers (n) of fibers in each panel are indicated. Histogram rates are divided by the number of stimulus presentations and bin width (0.5 msec) to give instantaneous discharge rate in spikes per second.

A more quantitative look at peak and steady-state rates is offered in Figures 5.11, where we plot these rate measures as a function of SR, because of the clear dependence of rates on SR in AN fibers (Chapter 3). No significant differences were found in peak rate (Figure 5.11A) or steady-state rates (Figure 5.11B) between knockouts and wildtype animals.

We attempted to measure adaptation time constants in the PST histograms by fitting of exponentials as described by Westerman and Smith (Westerman and Smith 1984). However, the PSTs from individual fibers were too noisy (i.e. had insufficient numbers of stimulus presentations) to produce meaningful fits. Thus, as an alternate measure of response adaptation,

we took the ratio of peak to steady-state response. As shown in Figure 5.12, this metric of adaptation did not differ between CGRP wildtypes and CGRP knockouts.

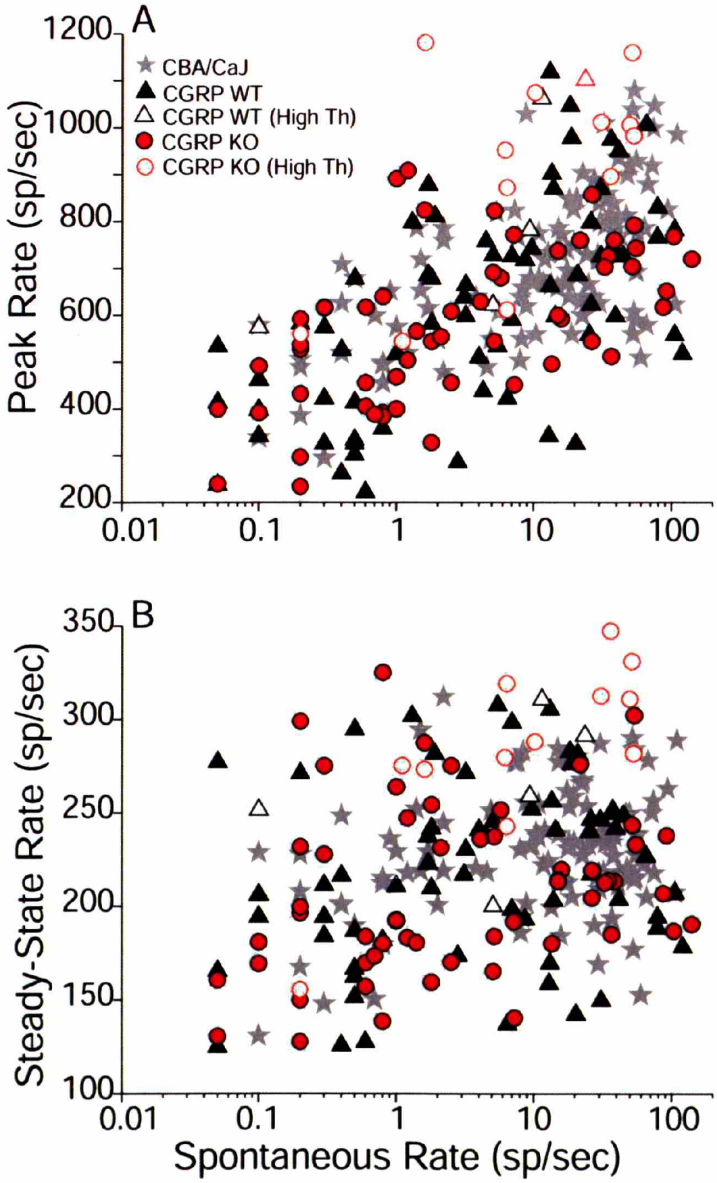

Figure 5.11: Peak instantaneous rates (**Panel A**) and steady-state rates (**Panel B**) as a function of SR. Peak rates were obtained from PST histograms such as those shown in Figure 5.10. Steady state rate was defined as the average rate during the last 15 ms of the tone bursts. Peak rate was defined as the maximum instantaneous rate.

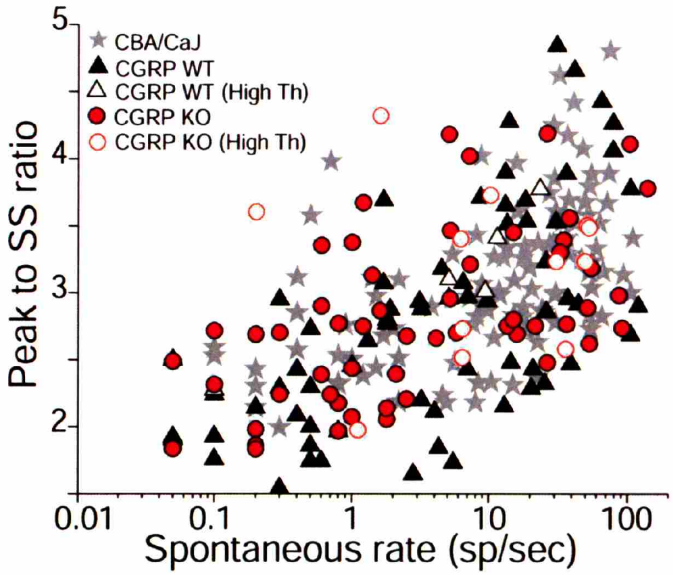

Figure 5.12: Response adaptation as a function of SR. Adaptation was derived from PST histograms of the type shown in Figure 5.10. Peak to steady state (SS) ratio was obtained by dividing the maximum rate by the average rate during the last 15 ms of the tone burst.

5.3.7 Response Synchrony

As shown in Chapters 3 and 4, mouse AN fibers show synchrony characteristics similar to those in other mammals (Johnson 1980), i.e. phase-locking falls off dramatically as stimulus frequency approaches 4 kHz. In the mouse AN, there are relatively few fibers with rate threshold < 60 dB SPL at frequencies ≤ 4 kHz (see Chapter 3). Thus, given that high SPL tones elicit large cochlear microphonic potentials that can produce artifactual synchrony when picked up by the microelectrode, response synchrony could only be studied systematically in a few fibers.

Although the sample size is limited by the general lack of low-frequency responsiveness in the mouse AN, response synchronization appears to be reduced in CGRP knockout AN fibers. Synchrony data were obtained for stimulus-level functions from three CGRP wildtype and three CGRP knockout AN fibers. Figure 5.13 shows synchrony-level functions for three test frequencies (f = 2 kHz, 2.5 kHz, and 4 kHz). In most cases, CGRP knockout ANFs synchrony level curves saturated at lower values than both the wildtype and CBA/CaJ mice.

Note , however, that the analysis is complicated by the fact that all four of the fibers sampled from CGRP knockout ears were "pathological", i.e. showed relative thresholds > 30 dB higher than those in CBA/CaJ. These pathological fibers tended to have hypersensitive tuning curve tails (See Chapter 4), which made them tempting subjects for study of low-frequency responses. Unfortunately, the lack of "normal" knockout fibers in the sample was not noted until after the experimental series was complete.

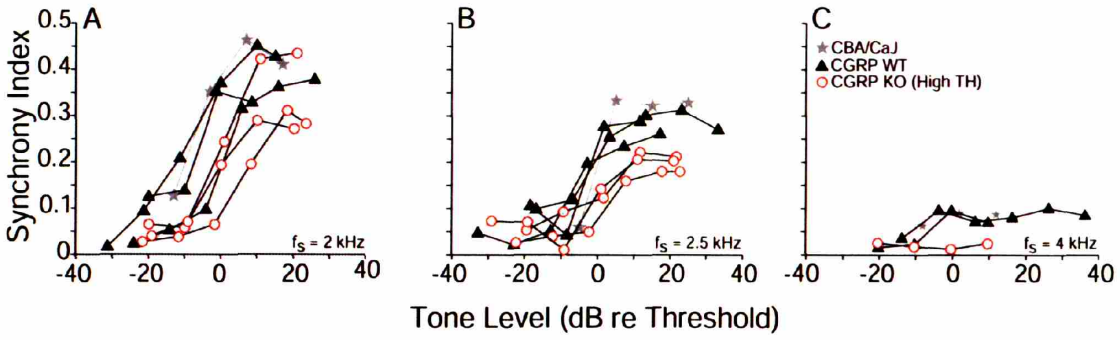

Figure 5.13: Synchrony vs. level functions for AN fibers from CBA/CaJ (1 fiber), CGRP wildtype (3 fibers), and CGRP knockouts (4 fibers), in response to continuous tones at 2 kHz (**Panel A**), 2.5 kHz (**Panel B**) or 4.0 kHz (**Panel C**). Data from the same fibers are shown in the different panels. Synchronization indices were extracted from post zero-crossing histograms obtained from 15-s continuous tones as described by Johnson (1980). Symbol key in Panel C applies to all Panels.

5.4 Discussion

5.4.1 Predicted Effects of CGRP Loss

In this study, recordings were made from single AN fibers in CGRP knockout mice to better understand the role played by CGRP in cochlear function. In mouse, CGRP has been immunolocalized to olivocochlear (OC) efferent terminals in the IHC and OHC area (Maison et al. 2002). In all these terminals, CGRP appears to be co-localized with the neurotransmitter acetylcholine (ACh).

In other cholinergic systems, including the adrenal medulla and the neuromuscular junction, CGRP has been implicated in the modulation of nicotonic acetylcholine receptor (nAChR) desensitization (Nistri and Angelantonio 2002) and the expression of nAChRs and acetylcholinesterase at the synapse (Fernandez et al. 1999). The mechanism by which CGRP is thought to modulate neurotransmission is via second messengers, occurring downstream to CGRP action on its G protein coupled receptor complex (Juaneda et al. 2000) or in some cases, via direct interactions with the nAChRs (Giniatullin et al. 1999).

MOC efferent suppressive effects on OHC function are thought to be mediated through the activation of nAChRs. Given that CGRP has been shown to modulate cholinergic neurotransmission and that CGRP is co-localized with ACh in MOC terminals, it is possible that loss of CGRP may change the magnitude or time course of classic MOC suppressive effects on cochlear function. However, the findings reported by Maison et. al. (2003) indicates that classic MOC effects and DPOAE thresholds remain unchanged in CGRP knockout mice. Consistent with the latter, results from the present study also show that DPOAE thresholds in knockout mice were comparable to wildtype mice (Figure 5.1). Together, these results suggest that CGRP does not play a major role in influencing OHC function via activation of MOC efferents.

A recent study has shown that activation of the lateral olivocochlear (LOC) system can cause long-lasting enhancement or suppression of AN response without affecting OHC function (Groff and Liberman 2003). This suggests that there might be at least two functional subsystems within the LOC. An interesting possibility is that release of CGRP by LOC fibers is responsible for the long-lasting excitation of AN responses, as discussed below.

The effects of CGRP on hair cell afferent responses have been best studied in the lateral line organ, where both afferent fibers and cholinergic CGRPergic efferent fibers contact hair cells (Bailey and Sewell 2000; Sewell and Starr 1991). Application of CGRP on the lateral line organ increases the frequency of excitatory post-synaptic potentials (EPSPs) and spontaneous discharge rates in afferent fibers (Sewell and Starr 1991). The site of action for CGRP is hypothesized to be the hair cell, given that application of cobalt, a drug that blocks calcium-dependent neurotransmitter release (Weakly 1973), blocks CGRP effects (Sewell and Starr 1991). Application of CGRP on the lateral line organ has also been shown to reduce phase-locking and decrease stimulus-evoked discharge rates in afferent fibers (Bailey and Sewell 2000). The general process by which CGRP has been hypothesized to both increase spontaneous activity and decrease response sensitivity in afferent fibers is as follows: CGRP released by efferent fibers activate G-protein-coupled receptors that increase intracellular calcium levels both near neurotransmitter release sites, thereby increasing the probability of spontaneous neurotransmitter release, and at sites near calcium-gated potassium channels that when activated, hyperpolarize the cell and decrease the amount of neurotransmitter release (Bailey and Sewell 2000).

Consistent with the hypothesis that release of CGRP by LOC fibers may play a role in AN fiber excitation is the finding in a previous study that there is a 20% reduction in ABR amplitudes at all sound pressure levels without changes in DPOAE thresholds (Maison et al. 2003) in CGRP knockout mice. Studies of chronic de-efferentation also suggests a role in AN excitation by the efferent system given that in chronically de-efferented animals, there is a decrease in the SR distribution seen among AN fibers (Liberman 1990; Zheng et al. 1999b) and in one study, a decrease in maximum discharge rates in AN fibers was also found (Zheng et al. 1999b). These findings suggest that AN fibers in knockout mice might have decreased SR and sound-evoked discharge rates and that other measures such as tuning, threshold sensitivity, or other aspects of AN response that are shaped largely by the OHCs, would be unchanged.

5.4.2 AN phenotype in CGRP knockout animals

The interpretation of auditory phenotypes in CGRP knockout mice is complicated by the pathologies that are associated with the background strain: for example, recordings from non-compromised fibers with CFs > ~15 kHz cannot be made. Putting aside this caveat, we found no statistically significant differences in most aspects of AN response in the knockout animals, including tuning, threshold sensitivity, dynamic ranges, peak or steady-state rates, the range of SRs encountered in the nerve, or the basic relation between SR and threshold.

According to results from the lateral line organ, AN fiber responses in CGRP knockout mice might be expected to show (1) lower spontaneous rates, (2) larger stimulus-evoked discharge rates, and (3) better phase-locking than wildtype AN fibers. However, in this study, there were no significant differences found in the SR distribution (Figure 5.4) or in sound-evoked discharge rates between knockout and wildtype mice (Figure 5.8). These discrepancies may be due to the different mechanisms of CGRP action in the mammalian cochlea versus the lateral line organ

since the primary target of LOC neurons are the dendrites of AN fibers while that of lateral line efferents is the hair cell itself.

We also noted a decrease in maximum synchrony in the CGRP knockouts (Figure 5.13). However, this observation is clouded by the fact that the sample of high-CF fibers in the knockout animal, by chance, happened to include only "pathological fibers". As discussed in Chapter 4, the dominant pathology at the apical border of the progressive lesion in this background strain appears to be OHC dysfunction. Outer hair cell dysfunction causes elevation of tips and hypersensitivity of tails (Liberman and Dodds 1984b). However, these mechanical effects would not be expected to have any effects on maximum synchrony. Effects on maximum synchrony suggest changes in synaptic transmission at the IHC, which could be due to CGRP. However, the direction of change is opposite to that expected from the results in the lateral line (Bailey and Sewell 2000).

In summary, the auditory phenotype in the CGRP knockout mouse is subtle, if there is any phenotype at all. When considering knockout animals with no obvious phenotype, one need not conclude that the eliminated molecule has no function, because there is often a redundancy built in, such that the missing function can be subserved by some remaining (related) element. In this case, the possibility that CGRPβ "replaces" α must be considered: however, immunological results showed no CGRP α or β staining in these knockout ears (Maison et al. 2003). Similarly, in contrast to receptor subunit knockouts, where a different subunit type could subserve many of the functions of the missing element, the knockout in this case is of the ligand. It seems unlikely that there are other endogenous ligands for the CGRP receptor that can compensate for the loss of CGRP.

5.4.3 Are AN results contradictory with previous ABR results ?

A 20% reduction in suprathreshold auditory brainstem response (ABR) wave 1 amplitude in CGRP knockouts compared to their wildtype littermates was reported by Maison et. al. (2003). ABRs were not measured in the present study for practical reasons – the kind of testing carried out previously requires about 1 hour of recording time. In a typical AN experiment, adding that amount of gross-potential recording time would decrease the time available for obtain single-fiber data by 25%.

Wave 1 amplitudes depend on (1) response synchronization in AN response to tone bursts, (2) number of fibers responding, (3) peak onset rates in response to tone bursts, and (4) the shape of the unitary potential, i.e. the contribution of a single spike generator to the waveform at the recording electrode (Melcher and Kiang 1996). The variance in first spike latency (FSL) is a good measure of response synchronization: it was unchanged by the loss of CGRP (Figure 5.6). Threshold sensitivity, a key determinant of the number of responding fibers, was also unchanged by the knockout (Figure 5.2); as were the magnitudes of the onset rates and the relation between onset rates and SR (Figure 5.11). We have no data on the shape of the unitary potential; thus a CGRP-related change in its amplitude remains a logical possibility.

Another important factor is the absolute numbers of responsive fibers. Information on absolute numbers is difficult to determine from a single-fiber study such as this one. Without explicit counts from histological analysis (which was not performed), the only indicator we have available is a sense of the inter-unit density in electrode tracks. Given the difficulties in making single-fiber recordings from mouse, specifically the frequency with which long stretches of

electrode penetration do not yield any fiber contacts whatsoever, it would be impossible to rule out a 20% decrease in the numbers of auditory nerve fibers in the knockout animals.

A final mechanism to consider for ABR amplitude reduction is a shift in the proportion of low- vs. high SR fibers, given that low-SR fibers have lower onset rates by almost a factor of two (492 vs 728 spikes/sec) (Figure 5.11). The slight increase in the proportion of low-SR fibers noted in the CGRP knockout (46 vs 38%; Figure 5.4) is in the right direction to decrease ABR amplitudes. However, the magnitude of the group shift is not large enough to explain a 20% decrease in Wave 1: all other things being equal, the proportion of low-SR fibers would have to increase from 38% to 93% to decrease the ABR by 20%.

In summary, given that all parameters that might contribute to ABR amplitudes could not be measured here, one cannot consider the results of the two studies to be irreconcilable. Nonetheless, there is no compelling explanation for such a reduction seen in the single-fiber data. It must be reiterated that, for practical reasons, ABRs were not measured in the present study, thus it cannot be stated with certainty that the animals studied here did indeed have an inter-genotype difference in ABR amplitudes. In addition to possible genetic differences in the background discussed below, it is also worth noting that the anesthetic used in the present study (urethane and xylazine) differed from that used in the previous study (xylazine and ketamine), thus providing another possible explanation for the failure to see a stronger AN phenotype.

5.4.4 Are the mice in this study genetically identical to those studied previously?

In the initial generation of typical knockout mouse, a 129/C57 hybrid genetic background is created because 1) the genetic recombination to eliminate the gene of interest is carried out in J1 stem cells (derived from a 129/SvJ strain), 2) the stem cells are implanted into a blastocyst derived from C57BL/6 and placed into the uterus of a C57BL/6 foster-mother and 3) the chimeric male offspring for which the gonads are stem-cell derived are crossed with C57BL/6 females and then 4) subsequent generations are produced by interbreeding among the hybrid offspring. The presence of this heterogenous genetic background, with multiple heterozygosities at multiple genetic loci, adds variability to behavior of wildtype animals. This is manifest in cochlear studies by a high degree of variance in cochlear thresholds, because both of the originating strains (C57BL/6 and 129/SvJ) have early-onset cochlear pathologies of different etiology (Hequembourg and Liberman 2001; Zheng et al. 1999a). For this reason, many investigators will try to create a knockout line which is "congenic" with one of the two originating strains, e.g. C57BL/6. A true C57BL/6 "congenic" animal is one in which all genetic loci are once again homozygous for the C57BL/6 allele and the only difference between any wildtype and mutant mouse is at the targeted locus. In practice, the creation of congenic line involves backcrossing the mutation for 10 generations back into the C57BL/6 line, and assuming, based on mathematical arguments, that > 99% of the loci have become homozygous for the original C57BL/6 alleles, except for the targeted mutation, which is assayed at each generation to identify the knockout animals.

The animals in the present study were said to be C57BL/6 congenics, and they were nominally the same as those studied by Maison et al. They were derived from knockout and wildtype breeding pairs obtained from the Emeson laboratory at Vanderbilt University (Lu et al. 1999), the same laboratory that originally supplied the mice to Maison and colleagues (Maison et al. 2003). Animals in the present study were genotyped here in our laboratory, and the results for all animals tested were consistent with expectations – i.e. there is no reason to doubt the

genotypic classifications presented here (See Chapter 2, Figure 2.4). The only obvious difference is that this study was initiated roughly 2 years later, thus, roughly 35 generations of interbreeding had elapsed between the two sets of experiments.

Comparison of DPOAEs obtained from CGRP knockout mice in this study to the ones obtained in Maison et. al. (2003), shows a significant difference in auditory phenotypes between the two sets of mice (Figure 5.14). Given that the DPOAE measures were obtained in the same laboratory, with the same equipment and same response metrics, from animals at the same ages, the striking differences strongly suggest that the genetic background for the two groups of animals was *not* identical. If the animals were still in a highly hybrid background, this would not be at all surprising, given the continued genetic intermixing that 2 years of colony maintenance involves. Thus, one way to interpret the present results is that the genetic heterogeneity had not been completely removed from the "congenic" line we were studying, and that the background of the animals in our study was systematically different from that in the previous study. That difference in background apparently affected the degree or time of expression of the gene(s) causing early-onset basal-turn cochlear pathology and may also have affected the way in which GCRP deletion affects auditory function.

Whether or not this is the correct interpretation, we are still left with the overarching conclusion that CGRP plays a minimal role in shaping the responses of the mammalian cochlea.

5.5 Conclusion

The LOC system is a neurochemically heterogeneous system whose function in audition is not clearly understood. CGRP is a neuropeptide that has been immunolocalized to LOC efferent terminals and cell bodies (Vetter et al. 1991). The $CGRP_{\alpha}$ knockout mouse is an interesting model to study LOC function because they display normal DPOAEs, while displaying decreased suprathreshold amplitudes in wave 1 of the ABR (Maison et al. 2003), suggesting a direct effect on AN fiber responses caused by changes in LOC neurotransmission. In this study recordings from single AN fibers were used to understand better the reduction in ABR wave 1 amplitude as reported in Maison et. al. (2003). However, results from this study were unable to explain why wave 1 amplitudes in CGRP knockout mice were reduced compared to wildtype mice. In fact, results from this study suggests that the presence of CGRP in the cochlea is not necessary for normal AN fiber responses. Comparison of DPOAEs obtained from CGRP knockout mice in this study to the ones obtained in Maison et. al. (2003), suggests that the knockout mice used in this study had a different auditory phenotype than the ones used by Maison et. al. (2003) (Figure 5.14). This finding highlights one complex issue of studying knockout mice: auditory phenotypes can vary significantly from individuals of different breeding pairs and generations (Gao et al. 2004).

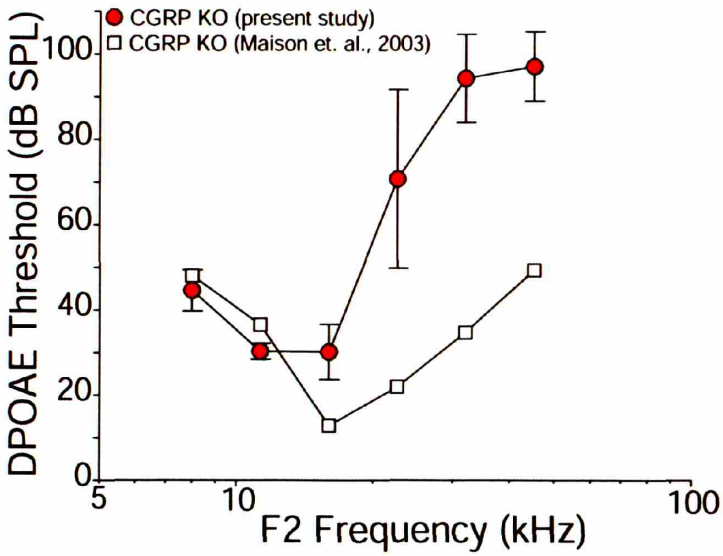

Figure 5.14: Mean thresholds for DPOAEs in the CGRP knockout mice recorded in this study compared to those reported by Maison et. al. (2003).

Chapter 6

Auditory Nerve Recordings in Mice with Targeted Deletion of the BK channel

6.1 Introduction

Large conductance voltage- and calcium-activated potassium (BK) channels are members of a sub-family of Ca^{+2}-gated potassium channels that display a high-unitary conductance (~250 pS (Vergara et al. 1998)), are activated by both intracellular calcium and membrane depolarization, and are blocked by the scorpion venoms charybdotoxin (ChTx) and iberiotoxin (IbTx) (Skinner et al. 2003). BK channels are composed of two subunits: α and β. The α subunit is a member of the *slo* family of potassium channels, which was originally identified in *Drosophila* (Ruttiger et al. 2004; Skinner et al. 2003; Vergara et al. 1998).

In hair cells of lower vertebrates, BK channels interact with voltage-gated Ca^{2+} channels to produce oscillatory voltage responses (Fettiplace and Fuchs 1999). This electrical resonance acts as an electrical filter maximizing the hair cell response at a particular sound frequency, the resonant frequency. The number of BK channels and their dynamic properties determines the resonant frequency of each cell (Fettiplace and Fuchs 1999). In the basilar papilla of the chick, it is thought that the differential distribution of splice variants of the α-subunit in BK channels, which influences the response dynamics of BK channels, is important for the generation of a tonotopic map in this organ (Navaratnam et al. 1997; Rosenblatt et al. 1997).

In contrast to lower vertebrates, little is known concerning the role of BK channels in mammalian hearing. In the mammalian cochlea, BK channels are found in inner hair cells (IHCs), outer hair cells (OHCs), efferent fibers under OHCs, the stria vascularis, the spiral ligament and spiral ganglion cells (Ruttiger et al. 2004; Shen et al. 2004; Skinner et al. 2003). Unlike lower vertebrates, mammalian hair cells do not show electrical resonance (Skinner et al. 2003). Their presence in IHCs is thought to lower membrane time constants allowing hair cell receptor potentials to synchronize to stimulus frequencies in the kilohertz range (Kros et al. 1998; Ruttiger et al. 2004). Pharmacological experiments performed in the guinea pig cochlea suggests that BK channels play a role in mammalian afferent neurotransmission, because blocking such channels with iberiotoxin or charybdotoxin significantly reduces compound action potential (CAP) amplitudes without significantly altering distortion product otoacoustic emissions (DPOAEs) (Skinner et al. 2003). The maintenance of DPOAEs suggests that these drugs must be acting "downstream" of the outer hair cell's contribution to cochlear mechanics. Because patch clamp recordings performed on individual inner hair cells (IHCs) show that blocking BK channels removes the fast outward current and increases the membrane time constant (Skinner et al. 2003), it is thought that the observed reduction in CAP amplitudes may in part be due to changes in IHC physiology. However, the exact mechanism by which such changes translate to a significant reduction in CAP amplitude is not understood.

To elucidate the role of BK channels in the development of normal mammalian hearing, a BK channel knockout mouse model was created by Ruttiger et. al. (2004) (Ruttiger et al. 2004) in which the gene encoding the α-subunit was deleted. In the first study of these mice, two *in vivo* physiological measures were used to assess cochlear function in knockout mice aged 4-17

weeks: click-evoked auditory brain stem responses (ABRs) and DPOAEs. The former measure provides information concerning the synchronous firing of nerve fiber populations along the auditory pathway and the latter measure provides information concerning OHC function because a reduction in OHC function leads to a reduction in DPOAE amplitude (Zurek et al. 1982). These BK α-subunit knockout mice showed elevated click-evoked ABR thresholds compared with their wildtype littermates, and they had no measurable DPOAEs at f_2 = 16 kHz, the only frequency tested. Histological analysis of the cochleae of α-subunit knockout mice reveal a base-to-apical progression of OHC degeneration with age that was coincident with increasing elevations in ABR thresholds. The stria vascularis, spiral ligament, and IHCs appeared normal, however their function was not directly assessed. These findings suggest that BK channels play a role in OHC survival.

More recently, the *in vitro* electrophysiology of IHCs from the BK knockout mouse was investigated by Dominik Oliver and colleagues (personal communication). Under whole cell voltage clamp, normal IHCs display fast and slow outward currents for voltage steps greater than -50 mV (Figure 6.1A). The fast component of the response is thought to be mediated through the activation of BK channels, since application of selective BK channel blockers on IHCs has been reported to remove this component (Skinner et al. 2003). Consistent with this prediction, in IHCs from the BK knockout mice, the fast component of the outward currents is absent (Figure 6.1B). To more closely mimic the *in vivo* situation, in which IHCs are activated by sound-evoked currents flowing through transduction channels, Oliver and colleagues measured the voltage responses of wildtype and knockout IHCs to a 2 kHz current waveform shaped by a saturating non-linearity meant to mimic the normal displacement-vs.current function for the IHC hair

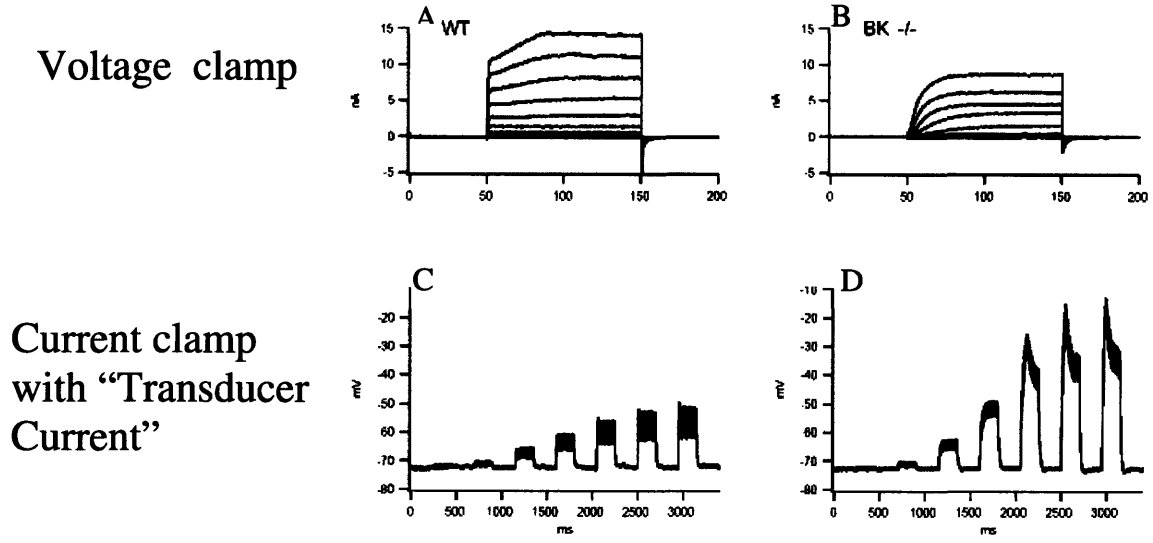

Figure 6.1: Voltage clamp (**Panels A,B**) and current clamp (**Panels C,D**) recordings from BK wildtype and knockout inner hair cells (IHCs) respectively. **Panels A,B**: Current families in response to voltage steps incremented by 10 mV (starting at -90 mV, holding potential was -80 mV). **Panels C,D**: The "transducer current" applied to the IHCs is a 2 kHz tone passed through a transfer function that mimics the saturating nonlinearity in the responses of IHC transduction channels to sinusoidal hair bundle deflections. The saturating current was 1 nA. Experimental data from Dominik Oliver, Ph.D. (personal communication).

bundle. In response to these 2-kHz "transducer currents", IHC voltage responses in the knockout (Figure 6.1D) displayed decreased AC responses and enhanced DC responses compared to wildtype (Figure 6.1C), presumably because the loss of BK channels increases the membrane time constant and increases the resistance of the cell, respectively.

The decreased AC and increased DC responses in IHCs *in vitro* suggest that AN responses, *in vivo*, in BK knockout mice might show (1) poorer phase-locking, and (2) smaller dynamic ranges because saturated rates would be reached more quickly as sound pressure was increased. The changes in onset time constant in IHC responses (Figure 6.1A,B) suggest that AN fiber responses in the knockout might show lower onset rates, due to a decreased synchronization of first-spike latencies to tone burst stimuli. Such onset time constant changes would not be expected to alter steady-state rates. The loss of a prominent K^+ channel might also result in a slight depolarization of the IHC's resting membrane potential. This, in turn, might be expected to lead to a slight increase in spontaneous discharge rates.

In this study, recordings were made from single auditory nerve (AN) fibers in BK knockout mice to describe the phenotype and compare the observations with the predictions made on the basis of the *in vitro* recordings from isolated IHCs in this same mutant line. The juxtaposition of data from isolated IHCs *in vitro* and individual AN fibers *in vivo*, in an animal model with such a dramatic change in IHC function, provides a unique opportunity to test current views of the way in which IHC voltage and current responses are converted into response patterns in their post-synaptic element, the afferent fibers of the auditory nerve.

6.2 Data Set

When possible, fiber responses shown in this Chapter were classified as AN fiber responses based on the classification criterion described in Chapter 2, which includes data on PST shape, coefficient of variance and first spike latency obtained from responses to tone bursts at CF delivered 30 dB above threshold. In cases where fiber threshold was within 30 dB of the maximum SPL deliverable by the acoustic system, PST histograms were derived from responses to tones at < 30 dB above threshold. Electrode depth was also used as a classification criterion; all fibers shown in this chapter were found at electrode depths > 1mm where AN fibers are expected to be found (see Chapter 2).

In total, recordings from 57 fiber recordings from 6 BK knockout (KO) mice aged 7-17 weeks and from 64 AN fibers in 7 wildtype (WT) mice aged 7-17 weeks are presented in this Chapter. For an additional point of reference, these data are compared to responses from AN fibers in CBA/CaJ mice aged 8-17 weeks, as presented in previous chapters. The wildtype and knockout mice are from the 129/SvJ strain.

6.3 Results

6.3.1 Overall Cochlear Sensitivity

DPOAE thresholds in BK wildtype and knockout mice are more variable and generally higher than average DPOAE thresholds from CBA/CaJ mice (Figure 6.2). This is not surprising, given that the background strain (129/SvJ) is known to have relatively poor hearing even at young ages (Zheng et al. 1999a). Consistent with the earlier study of ABR responses in this knockout line, BK knockout mice had higher DPOAE thresholds than their wildtype littermates across all test frequencies (Figure 6.2). There was, however, significant overlap in individual cases: some knockout ears were more sensitive than many wildtype ears.

As described in Chapter 2, DPOAE amplitude changes were typically used to monitor cochlear condition, because other common measures of cochlear function require either additional surgery (e.g., compound action potentials) or long recording periods (e.g., auditory brainstem responses). In the present experiments, 3 of 6 knockout animals had DPOAE thresholds, at the beginning of the experiment, that were close to system-distortion thresholds (i.e., > 70dB) for nearly all test frequencies. In these cases, DPOAE thresholds were not a useful monitor of acute changes in cochlear condition, because they could not rise significantly without reaching the threshold for system distortion. Thus, we could not apply a maximum DPOAE-shift criterion for database inclusion as was done in the other Chapters. For data in this Chapter, we rely more on the AN data from CBA/CaJ mice, as a point of additional comparison, for both the

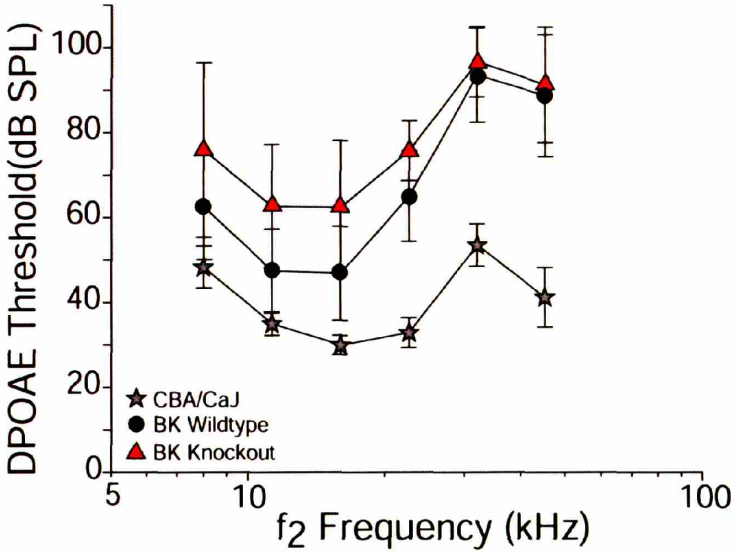

Figure 6.2: Mean thresholds for DPOAEs recorded at the start of each experiment for CBA/CaJ (stars), BK wildtype (circles), and BK knockout (triangles) mice. DPOAE thresholds were determined as described in Chapter 2. Error bars represent one standard deviation.

wildtype and knockout data. We will use relative thresholds, re CBA/CaJ mean data, as a metric of the degree of abnormality as we attempt to dissect out those response abnormalities that are due to the BK deletion and those that arise because of the background genetics in this mutant line.

6.3.2 Rate Threshold and Tuning

As described in Chapter 3, a fundamental property of AN fibers is their frequency selectivity, as quantified via "threshold" tuning curves which track iso-response contours in the frequency-intensity plane. AN tuning curves show sharply tuned "tips", defining the characteristic frequency (CF: frequency of maximum sensitivity) of the fiber, and broadly tuned low-frequency "tails". Tuning curves were obtained for all AN fibers in this study. Plotting thresholds at CF provides an overview of the sensitivity and frequency range of the peripheral auditory system. CFs ranged between 2.5 kHz and 25.4 kHz for fibers obtained in BK wildtypes and between 1.92 kHz and 20.1 kHz for fibers in BK knockouts (Figure 6.3A). Mean thresholds for high-SR

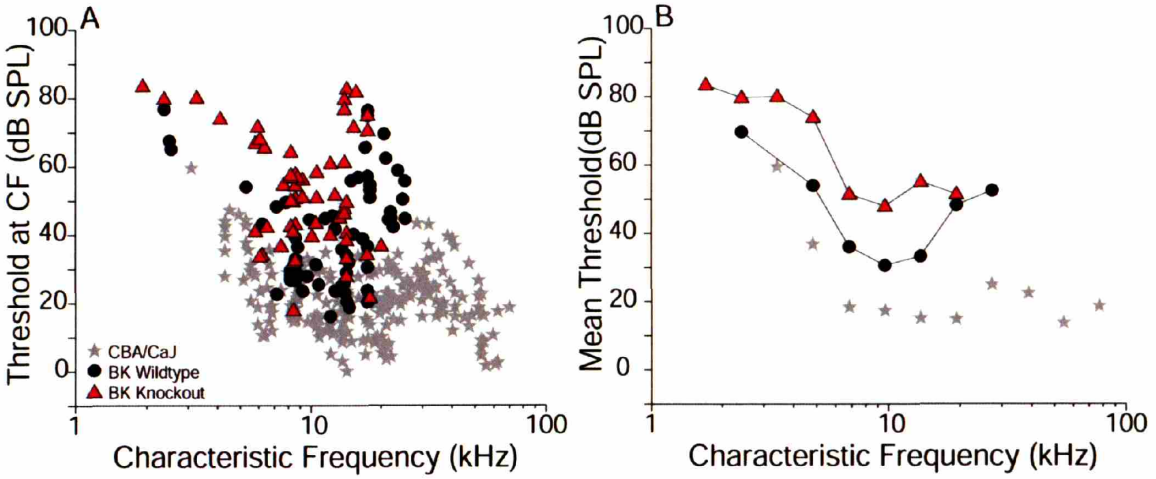

Figure 6.3: **Panel A:** Thresholds at CF for 64 AN fibers in 7 BK wildtype mice, and 57 AN fibers in 6 BK knockout mice compared to data from CBA/CaJ. **Panel B:** Mean thresholds at CF, as a function of CF. Data for high-SR fibers from each group were binned according to CF (half-octaves), and the average threshold for each bin was calculated.

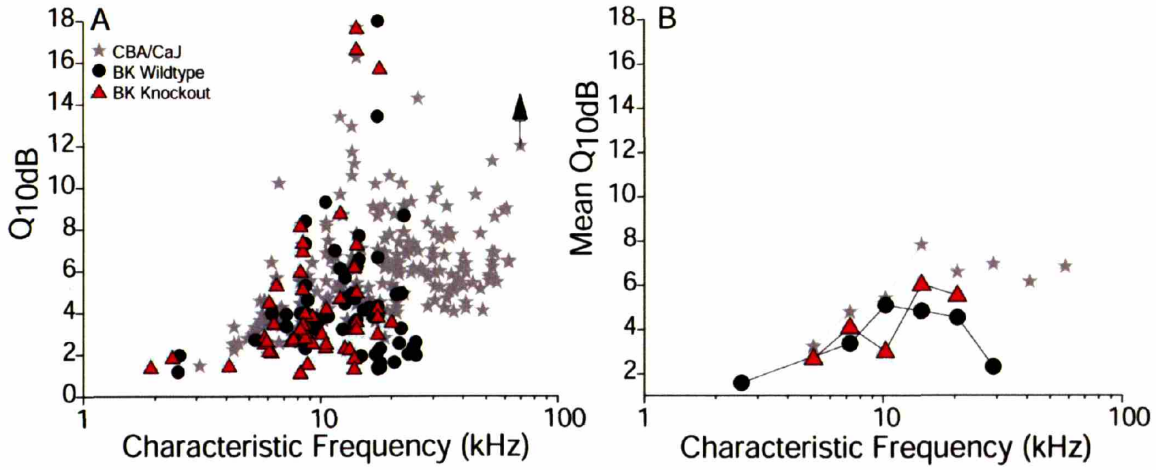

Figure 6.4: Sharpness of tuning (Q_{10dB}) (**Panel A**) and mean Q_{10dB} (**Panel B**) as a function of fiber CF. To calculate mean Q_{10dB} fibers were segregated into groups according to characteristic frequency (half-octave bins), and the average Q_{10dB} for each bin was placed in the middle of the bin. Data are only shown for frequency bins containing at least 2 data points.

fibers (SR $\geq$ 1 sp/sec) with CFs between 2 and 16 kHz in knockouts were higher than in wildtypes (Figure 6.3B). The sign and magnitude of the differences in mean single-fiber thresholds between the two genotypes (Figure 6.3B) are not dissimilar to the genotype differences in mean *initial* DPOAE thresholds (Figure 6.2), suggesting that the AN fiber database does not include disproportionate numbers of fibers with acute threshold shifts due to deterioration of cochlear condition during the recording sessions.

In lower vertebrates, BK channels are implicated in electrical tuning of hair cells (Fettiplace and Fuchs 1999). Although electrical resonance has not been found in mammalian IHCs

(Skinner et al. 2003), suggesting that this phenomenon is not critical for tuning in the mammalian cochlea, measurements of Q_{10dB} in BK knockout mice were made to verify the expected results. As expected, Q_{10dB} values in AN fibers from the BK knockout were comparable to those in wildtypes (Figure 6.4A), with the exception of a cluster of fibers with CFs near 10 kHz that showed Q-values that were lower than average (Figure 6.4B).

6.3.3 Spontaneous rates

AN fibers fire spontaneously in the absence of sound (Kiang et al. 1965), and this spontaneous discharge is highly random, having interspike intervals that display a poisson-like

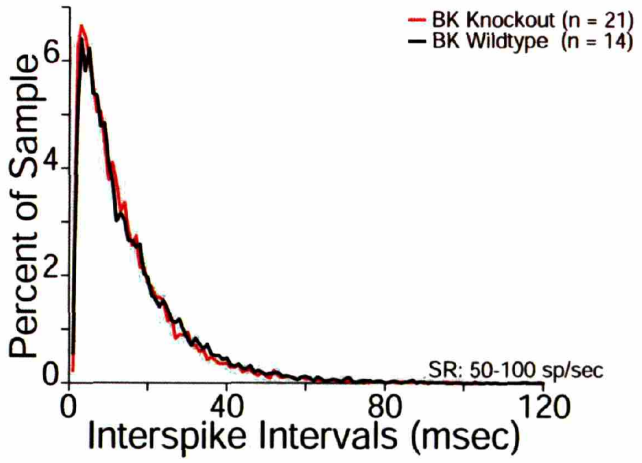

Figure 6.5: Mean histogram of the interspike intervals of spontaneous activity (SR: 50-100 sp/sec) in 21 BK knockout fibers and 14 BK wildtype fibers. Bin width is 1msec.

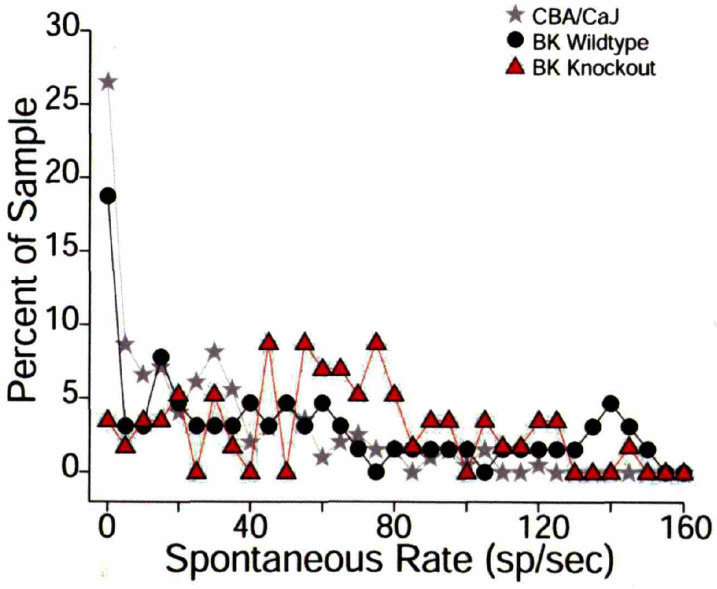

Figure 6.6: Spontaneous rate distributions for fibers from BK knockouts and BK wildtypes compared with CBA/CaJ. Bin width = 5 sp/sec.

distribution (Kiang et al. 1965). Mean interspike intervals of spontaneous activity (SR: 50-100 sp/sec) recorded in knockout AN fibers also show a poisson-like distribution, indistinguishable from that found in wildtype fibers (Figure 6.5).

The spontaneous discharge rate (SR) of each fiber is an important determinant of its threshold sensitivity, maximum discharge rate, dynamic range and other response attributes, as discussed in Chapters 3 and 4. As discussed in the Introduction, loss of BK channels in IHCs might be expected to slightly raise resting membrane potential, which, in turn, might lead to an overall increase in SRs in the knockout ears.

The changes in SR distribution for fibers sampled in the BK knockout vs wildtype ears were in the direction predicted (Figure 6.6); however the differences were either not statistically significant or a likely artifact of the threshold elevation in knockout ears (Figure 6.2). First, there was a decreased percentage of fibers with lower spontaneous rates: the histogram in Figure 6.6 (plotted with a bin width of 5 sp/sec) shows 4% of knockout fibers vs 18% of wildtype fibers are found in the first bin of this histogram. Both BK genotypes, in turn, show a lower percentage than that seen in CBA/CaJ (27%). However such differences could arise because (high-threshold) low-SR fibers are not excited by search stimuli as the electrode is advanced; this causes an undersampling of low-SR fibers that increases in direct proportion to the threshold elevation in the ear. Second, the mean SR value for high-SR fibers was slightly higher in knockout mice (65.4 sp/sec) than in wildtypes (60.6 sp/sec); however, statistical analysis suggested that the differences were not significant (P = 0.55, Student's *t*-test).

6.3.4 Response Synchrony

Phase-locking was studied in BK knockout AN fibers to determine if the reduction in AC response seen in the IHC *in vitro* data (Figure 6.1), was reflected in knockout mice *in vivo* as a decreased synchronization index for AN responses to low-frequency tones. As discussed in

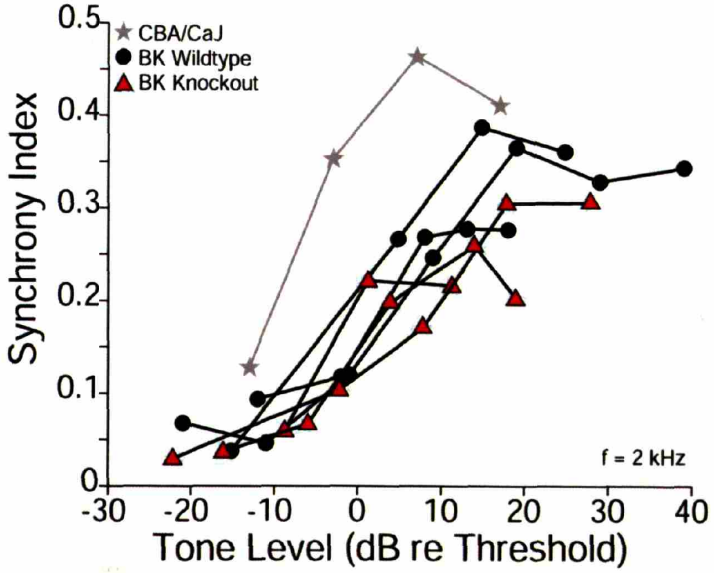

Figure 6.7: Synchrony-level functions for AN fibers from CBA/CaJ (1 fiber), BK wildtype (3 fibers), and BK knockout (3 fibers), in response to continuous tones at 2 kHz.

Chapters 3 and 4, phase-locking falls off dramatically as stimulus frequency approaches 4 kHz, and in the mouse AN, there are relatively few fibers with rate threshold < 60 dB SPL at frequencies ≤ 4 kHz (see Chapter 3). Therefore, response synchrony could only be studied systematically in a few fibers. Synchrony data was obtained for stimulus-level functions from three BK wildtype and three BK knockout AN fibers. The stimulus frequency chosen matches the frequency of the "transducer-like" current (i.e., 2 kHz) used in the patch clamp studies described in the Introduction (Figure 6.1). As shown in Figure 6.7, the limited data set we obtained in animals from the two genotypes are consistent with expectations from the *in vitro* data: synchrony-level functions in the knockout mice (average maximum synchrony = 0.2673) tended to be smaller than the wildtype mice (average maximum synchrony = 0.3432).

6.3.5 Rate-level functions and dynamic range

In vitro, IHCs from the knockout ears showed a faster rise in DC response with increasing "transducer current" steps (Figure 6.1D), consistent with increased IHC input resistance from loss of this large-conductance K^+ channel. *In vivo,* if sound-driven IHC DC potentials also increased more rapidly with increasing sound level, the dynamic ranges of AN fibers in the knockout ears might be decreased.

To assess this prediction, discharge-rate vs. sound-level functions for tone bursts at CF were measured in BK knockout vs. wildtype fibers. As illustrated in Figure 6.8A, the rate-vs.-level data were fit by a modified version of an existing model (Sachs et al. 1989) (see Chapter 2) to better estimate dynamic range than can be done with the raw data.

In fact, dynamic ranges in knockout fibers were not significantly different from those in wildtypes. As described in Chapters 3 and 4, and as illustrated in Figure 6.9, dynamic range in the mouse AN is a strong function of SR, with the largest dynamic ranges seen in fibers with the lowest SRs. If we consider only high-SR (SR >2 sp/sec) fibers, the mean dynamic range for knockout fibers was 14.1 dB (+/- 1.0 SEM); whereas the mean for wildtype was 14.8 dB (+/- 0.7 SEM). These differences were not significant (p=0.52 Students *t*-test).

The possibility must be considered that a difference between the two genotypes was obscured

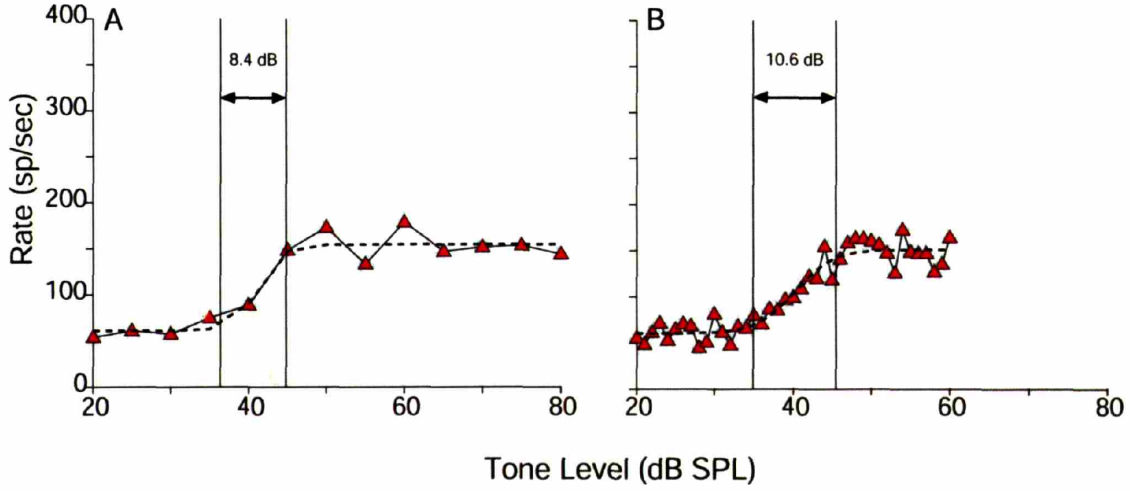

Figure 6.8: Discharge rate versus level functions obtained for a BK knockout AN fiber (CF=8.4 kHz; SR = 64 sp/sec) using a 5 dB resolution (**Panel A**) and a 1 dB resolution (**Panel B**).

by the fact that dynamic ranges in normal mice are small (10-15 dB for high-SR fibers) compared with the default step size (5 dB) in the present study. To assess this, whenever contact time permitted, functions obtained with 5 dB steps were compared with those from 1 dB steps. One example is shown in Figure 6.8, from a fiber with a particularly small dynamic range: the model-fit result for 5-dB steps was 8.4 dB; whereas that for 1-dB steps was 10.6 dB. In all, dynamic range comparisons for the two step sizes were available for 9 fibers. As shown in Figure 6.10, the average difference between dynamic range estimates using 5-dB steps versus 1-dB steps was 1.3 ± 4.6 dB, suggesting no systematic inaccuracy in the 5-dB measurements, once they have been put through the model-fit procedure. Thus, it appears unlikely that there are any changes in dynamic range in the knockout ears that went undetected due to the relatively large step size.

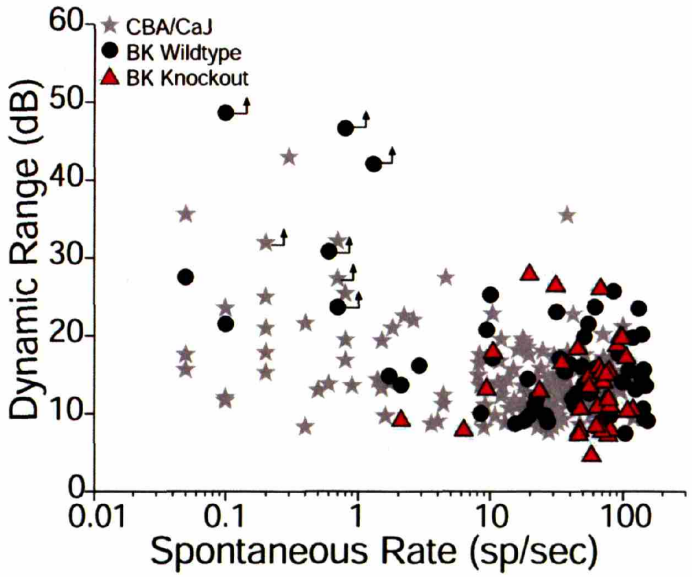

Figure 6.9: Relation between spontaneous rate and dynamic range for all fibers in CBA/CaJ, BK wildtype, and BK knockout fibers from which a rate-level function was obtained.

6.3.6 Maximum discharge rates: onset vs steady state

The most dramatic difference in AN response between KO and wildtype ears was in the maximum sound-evoked discharge rates. As discussed in Chapters 3 and 4, and as illustrated in Figure 6.6, virtually all high-SR fibers in mouse show hard-saturating rate-level functions, with a maximum discharge rate that is achieved within 10-15 dB above threshold levels. Superimposed rate-level functions for all high-SR fibers obtained from wildtype and knockout ears can be seen in Figures 6.11B and C, respectively, where they can be compared with similar data from CBA/CaJ (Figure 6.11A). The dashed line at 100 sp/sec is positioned such that virtually all saturated rates from the normal CBA/CaJ fibers as well as BK wildtypes fall above the line; by contrast, the majority of saturated rates in the knockout fibers fall below the line. Mean differences in maximum discharge rates between knockout and wildtype fibers was highly significant ($P << 0.0001$, Student's *t*-test). Data in Figure 6.8 are shown as driven rates, i.e. the

difference between sound-evoked and spontaneous rate. The same differences are seen in absolute maximum discharge rates, as seen in Figure 6.12A,B.

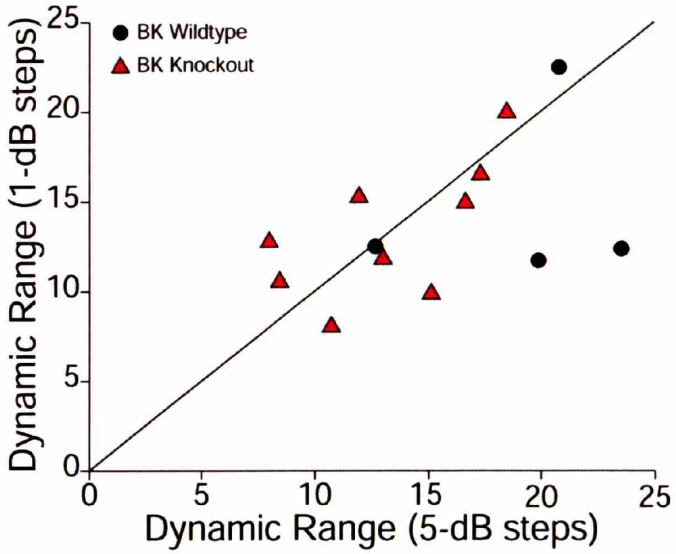

Figure 6.10: Dynamic range values obtained from rate-level functions with 1-dB resolution compared to those obtained using 5-dB resolution in 9 BK knockout and 4 BK wildtype AN fibers.

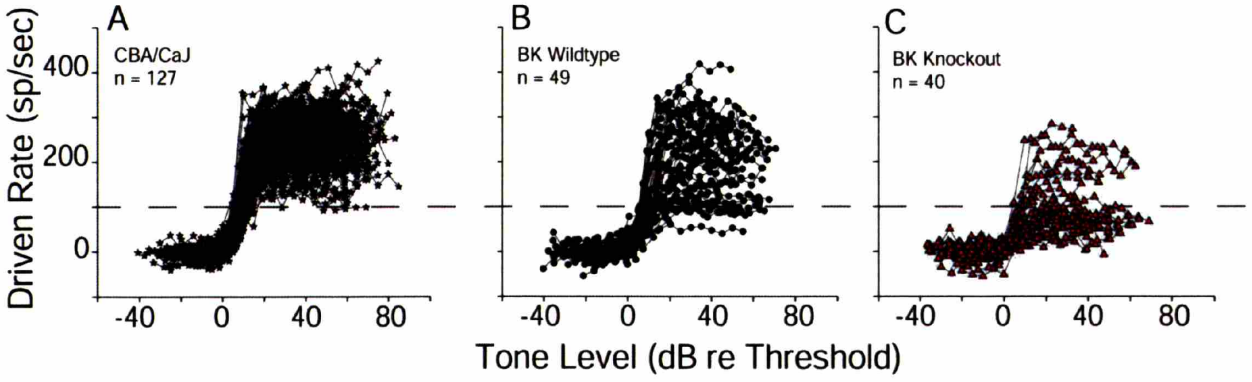

Figure 6.11: Superimposed rate-level functions for high-SR fibers from CBA/CaJ (**Panel A**), BK wildtype (**Panel B**) and BK knockout (**Panel C**) fibers. Functions were normalized by: 1) subtracting the SR from measured rate, and 2) shifting along the horizontal axis according to model-fit thresholds. See text for further details.

Given the slight but systematic difference in thresholds between the knockout ears and those of wildtype littermates (e.g. Figure 6.3), and given that some knockout ears have normal maximum rates (Figure 6.12A,B), the possibility has to be considered that difference in discharge rates is correlated with threshold shifts. To address this issue, maximum rates are plotted as a function of relative thresholds in Figure 6.12B. When the data are plotted this way, it

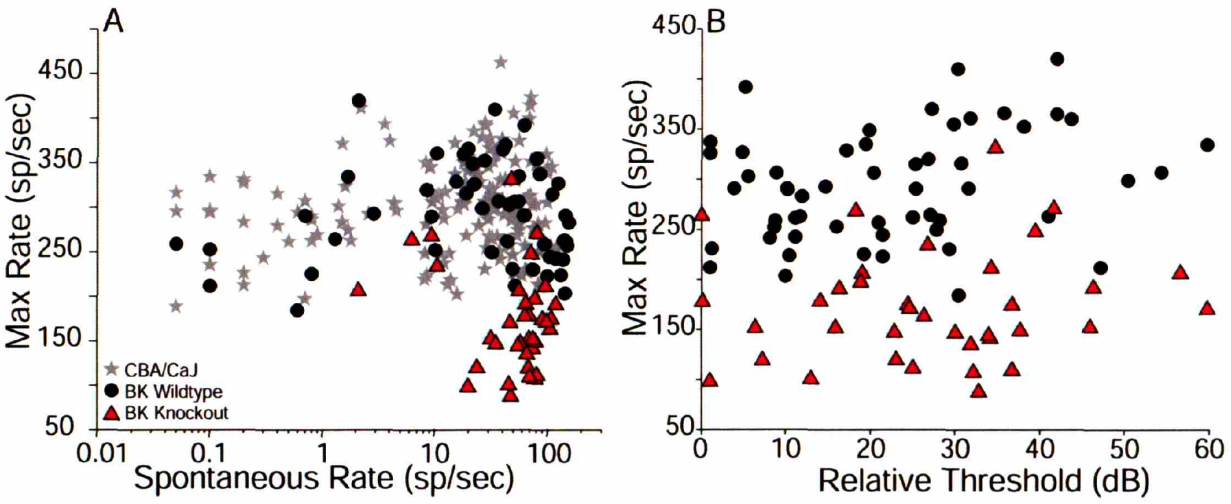

Figure 6.12: Relation between maximum rate and (Panel A) spontaneous rate or (Panel B) relative threshold. Data are shown for all fibers in CBA/CaJ, BK wildtype, and BK knockout from which a rate vs. level function was obtained. Relative threshold is defined by referring the threshold at CF of each fiber to the mean threshold of high-SR fibers (SR>1 sp/sec) of similar CF in CBA/CaJ mice.

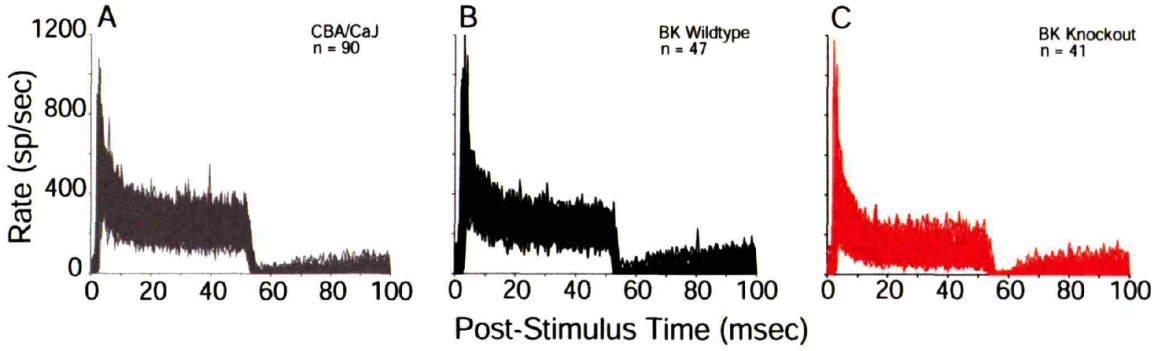

Figure 6.13: Superimposed PST histograms for responses to CF tone bursts at 30 dB above threshold for all low-CF (< 20 kHz), high-SR (> 1 sp/sec) fibers from CBA/CaJ (**Panel A**), BK wildtype (**Panel B**), and BK knockout (**Panel C**) mice. Numbers (n) of fibers in each panel are indicated. Histogram rates are divided by the number of stimulus presentations and bin width (0.5 msec) to give instantaneous discharge rate in spikes per second.

is clear that the two characteristics are independent: both low- and high-threshold knockout fibers showed abnormally low saturated discharge rates.

The analysis of rate-level functions concentrates on mean rates, averaged over the entire tone-burst on-time. As discussed in Chapters 3 and 4, there are striking differences between the onset rates and steady state rates in the response of AN fibers to tone bursts, and the ratio between onset and steady state provides an important metric of the degree of adaptation in the AN (Kiang et al. 1965; Smith 1977). The temporal dynamics of AN response in BK knockouts

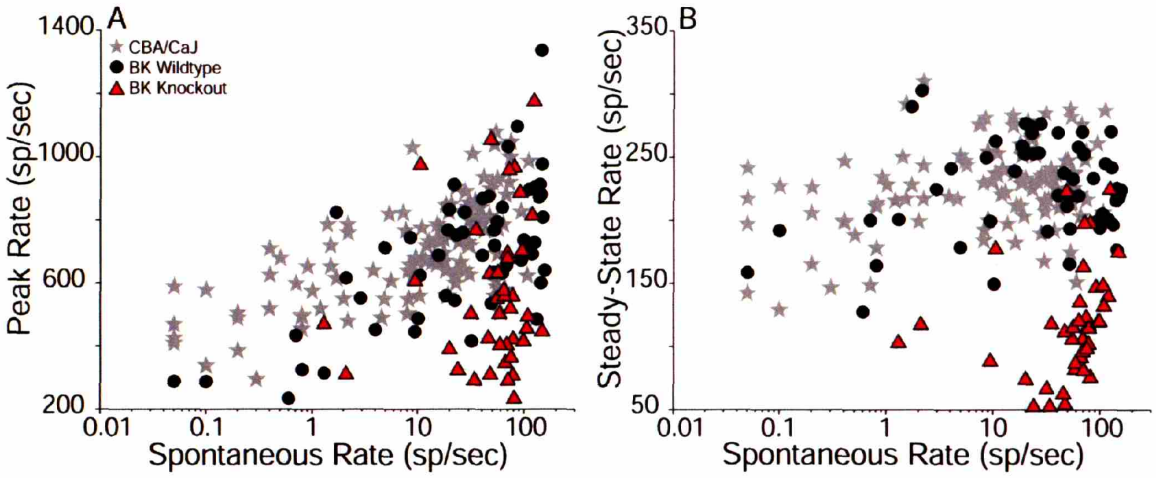

Figure 6.14: Peak instantaneous rates (**Panel A**) and steady-state rates (**Panel B**) as a function of SR. Peak rates were obtained from PST histograms such as those shown in Figure 6.13. Steady-state rate was defined as the average rate during the last 15 ms of the tone bursts. Peak rate was always seen in the first bin of the histogram. Fibers with SR=0 were assigned a value of 0.05 sp/sec.

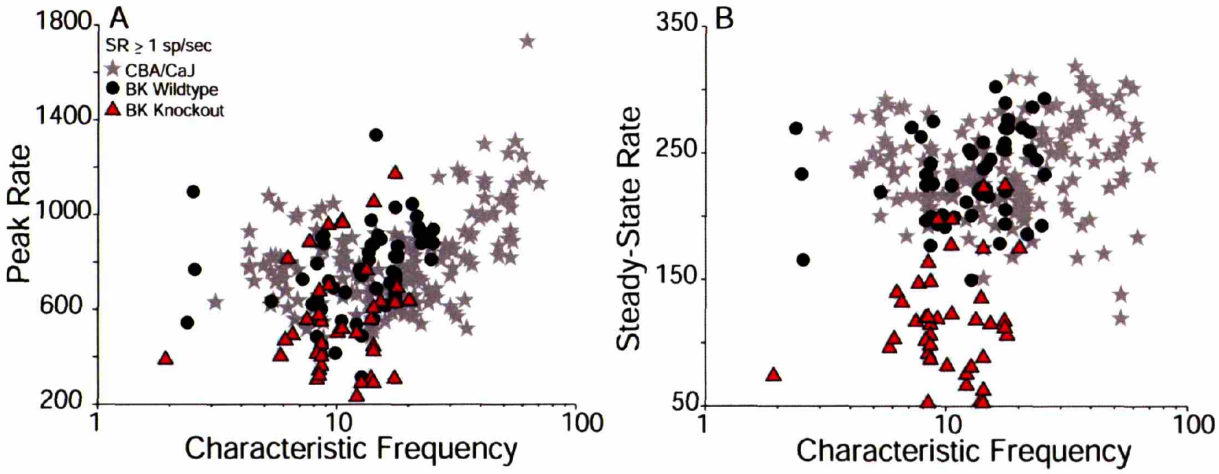

Figure 6.15: Peak instantaneous rates (**Panel A**) and steady-state rates (**Panel B**) as a function of CF. Peak rates were obtained from PST histograms such as those shown in Figure 6.13. Steady-state rate was defined as the average rate during the last 15 ms of the tone bursts. Peak rate was defined as the instantaneous rate from the first bin of the histogram. Fibers with SR=0 were assigned a value of 0.05 sp/sec.

were studied by constructing post-stimulus time (PST) histograms of responses to CF tone bursts at 30 dB above threshold. The histograms were normalized by the number of tone burst presentations and the histogram bin width (0.5 msec) to give the instantaneous discharge rate. Example histograms from AN fibers with CFs < 20 kHz and SR > 1 sp/sec in CBA/CaJ, BK wildtype and BK knockout mice are shown in Figure 6.13.

As seen in Figure 6.14 and 6.15, both onset and steady-steady state rates from BK knockouts tended to be lower than those seen in wildtypes. The differences were more dramatic with

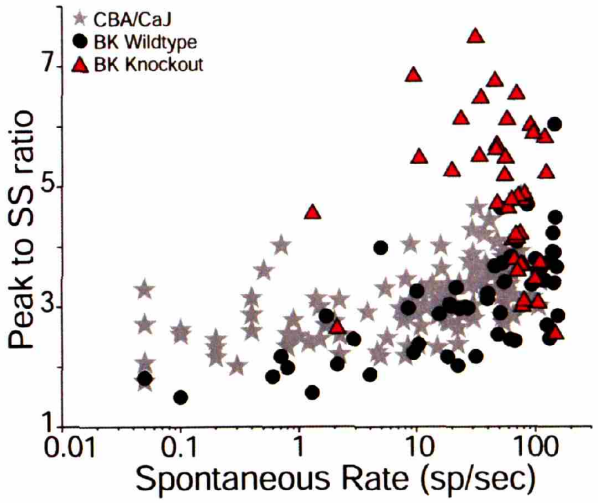

Figure 6.16: Response adaptation, measured as the ratio of onset to steady-state rate, as a function of SR. Adaptation was derived from PST histograms of the type shown in Figure 6.13. Peak to steady state (SS) ratio was obtained by dividing the maximum rate by the average rate during the last 15 ms of the tone burst.

respect to the steady state rates (6.14B, 6.15B), where the great majority of knockout fibers showed saturated rates below 150 sp/sec. The relatively small group of fibers from knockout ears which retained normal saturated rates (>150 sp/sec) was not concentrated in any particular CF region (Figure 6.15B), nor were they concentrated in particular animals: the percentage of low-rate fibers ranged from 50% (2/4) to 88% (7/8); thus every animal showed a mixture of normal and abnormal responses.

The fractional decrease in onset rate was smaller than the fractional decrease in steady-state rate such that the ratios of peak to steady-state rate tend to be higher in knockout fibers than in

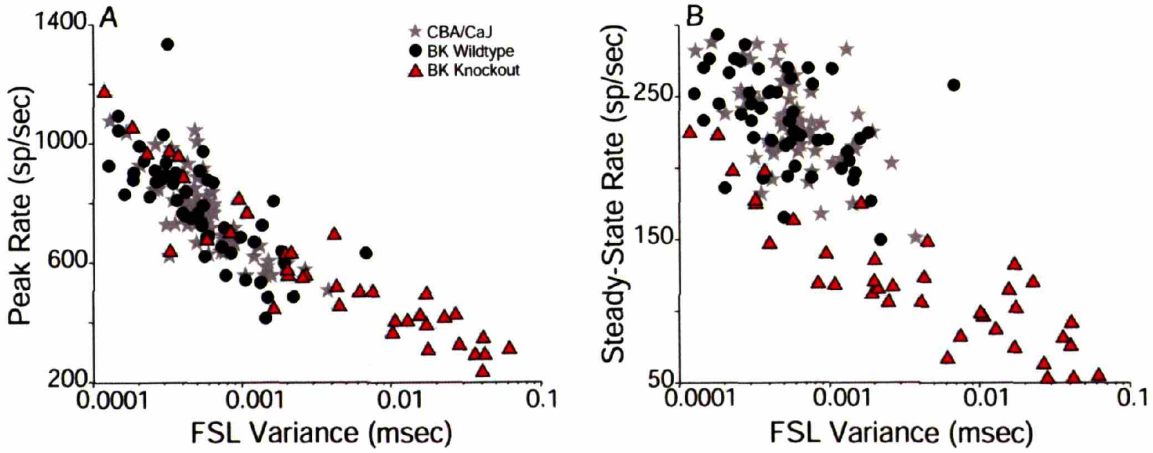

Figure 6.17: Peak instantaneous rates (**Panel A**) and steady-state rates (**Panel B**) as a function of the variance of the first spike latency (FSL). Data are shown for fibers with SR > 10 sp/sec and are extracted from the responses to 150 CF tone bursts presented at 30 dB above threshold.

wildtypes (Figure 6.16). Group mean differences were highly significant ($P << 0.0001$, Student's t-test). Put in other terms, the degree of post-onset adaptation in knockout fibers is greater than that in wildtypes. This trend can also be seen in the superimposed histograms of Figure 6.13.

The observation that IHCs from BK knockouts show slower current onsets to voltage steps *in vitro* (Figure 6.1A,B) might lead, *in vivo*, to decreased synchronization of action potentials at tone-burst onset, and consequently to the observed decreases in onset instantaneous rates (Figure 6.15A). An informative way to examine spike synchronization at tone-burst onset is by analysis of the variance of the first-spike latency (FSL) histograms. Recall from Chapter 2, that the *mode* of the FSL histogram (computed from responses to CF tone bursts) is one criterion used to differentiate AN fibers from cochlear nucleus cells. As shown in Figure 6.17A, there is a strict relationship between the *variance* of the FSL histogram and peak rates in normal ears (including CBA/CaJ and BK wildtypes): fibers with lower rates have larger variances. The data in Figure 6.17A also reveal several interesting aspects of AN responses in BK knockouts. First, as predicted, most BK knockout fibers show unusually large FSL variances, greater by two orders of magnitude than those from most normal fibers. Second, among the BK knockouts, fibers with normal peak rates also have FSL variances that are within the normal range.

In normal AN fibers, the correlation between FSL variance and steady-state rate (Figure 6.17B) is weaker than that between FSL variance and onset rates (Figure 6.17A). Note that those BK knockout fibers with normal FSL variances showed steady-state rates below the mean normal values, in contrast to the situation for peak rates, as described above. The latter observation suggests that an additional mechanism, beyond the slowing of IHC onset responses, must be invoked to explain the decreases in steady-state rates in BK knockout fibers.

6.4 Discussion

The present results show that, despite loss of the BK channel in the mouse cochlea, a number of basic response properties of AN fibers were not significantly altered, including 1) the normal stochastic pattern of discharge in AN fibers (spontaneous or sound-evoked), 2) the distribution of AN spontaneous rates, 3) the shapes of AN tuning curves, or 4) the dynamic ranges of AN fibers, i.e. the range of sound pressure levels over which suprathreshold discharge rate changes from spontaneous to saturated rate. The normality of tuning curve shapes in the knockout mouse strongly suggest that, in the mammalian ear, the BK channel does not play the same key role in establishing frequency selectivity in the inner ear as has been shown in non-mamalian vertebrates (Fettiplace and Fuchs 1999).

In contrast, the loss of BK channels did lead to the following alterations in cochlear responses: 1) a striking decrease in the synchronization of AN spikes at tone-burst onset, which was highly correlated with a decrease in the AN onset rates; 2) a striking decrease in saturated steady-state discharge rates of AN fibers; 3) a small but significant elevation in mean thresholds (seen in both AN fibers and DPOAE responses); and, possibly 4) a reduced degree of maximum phase locking of AN responses to continuous tones.

Studies with immunohistochemistry and/or in situ hybridization have presented evidence that BK channels in the mouse cochlea can be expressed in inner hair cells, outer hair cells, the lateral wall (i.e. spiral ligament or stria vascularis), and AN fibers themselves (Ruttiger et al. 2004; Shen et al. 2004; Skinner et al. 2003). In the following sections, we consider how the AN phenotype revealed in the present study is most parsimoniously explained based on current

understanding of the cellular distribution for BK channels, and their postulated roles in each of these cell types of the cochlear duct.

6.4.1 BK channels in outer hair cells and the lateral wall

A previous study of cochlear responses in the same BK line studied here showed that ABR thresholds were normal in knockout animals at age 4 weeks, but had deteriorated by 20–30 dB re wildtypes at age 8-17 weeks (Ruttiger et al. 2004). Although animals as young as 4 weeks were not studied here, this ABR threshold deterioration at 8-17 weeks is comparable to that observed in mean DPOAE thresholds in the present study for animals in a similar age range (Figure 6.2). This agreement between the magnitude of threshold shifts measured by DPOAEs and ABRs suggests that threshold elevation in the BK phenotype arises "upstream" of the inner hair cell (and its afferent synaptic transmission). That is to say, the data are consistent with the view that the threshold shifts in BK knockouts arise directly from outer hair cell dysfunction, or, even further upstream, in the magnitude of the endolymphatic potential, which is also necessary for the normal contribution of outer hair cells to the amplification of DPOAEs(Ruggero et al. 1997). The possibility that a decreased endolymphatic potential also contributed to threshold elevation in the BK knockout animals needs to be seriously considered, given that BK channels have been immunolocalized to cells in the stria vascularis (Skinner et al. 2003) and have been implicated in the function of spiral ligament fibrocytes using electrophysiological techniques and BK channel blockers (Shen et al. 2004; Skinner et al. 2003). Dysfunction in either of these cell types could lead to a decreased endolymphatic potential (Hibino et al. 1997; Takeuchi and Ando 1999) and therefore increased DPOAE and single fiber thresholds.

The previous study of cochlear function in BK knockouts (Ruttiger et al. 2004) concluded that outer hair cell dysfunction *per se* was responsible for the threshold elevation in the knockout animals. The authors based this conclusion on the demonstration that 1) outer hair cells immunostained for BK channels, especially in the region opposite the efferent synapses, 2) that ABR threshold deterioration was associated with a progressive base to apical loss of outer hair cells, 3) that this outer hair cell loss, in turn, was preceded chronologically by a decrease in outer hair cell immunostaining for a variety of markers including the potassium channel KNCQ4, and finally that, 4) in contrast, immunostaining of the lateral wall cells in the knockout ears revealed no change in expression of potassium channels (Kir4.1 and $K_v3.1$) thought to be important for EP generation (Hibino et al. 1997; So et al. 2001).

Data from the present study add to the evidence that threshold shifts in the knockouts do not arise secondary to a decrease in EP from strial (or spiral ligament) dysfunction. In addition to elevating thresholds, a reduction in EP would also decrease spontaneous rates in AN fibers (Sewell 1984a, b), presumably by reducing the resting current through inner hair cell transduction channels leading to an intracellular hyperpolarization. AN data from the present study show clearly that, if anything, spontaneous rates were increased in the knockout animals (Figure 6.6). This argues strongly against a decrease in the EP in the BK knockouts.

Damage to outer hair cells is expected to produce broad tuning in AN fibers innervating affected regions (Liberman and Dodds 1984b), as was observed in some fibers in the knockout animals (Figure 6.4). Outer hair cell loss is expected to cause a slight increase in AN SRs, as was observed as well (Figure 6.6). This slight SR increase, which has been observed in cases of OHC loss from other etiologies, may arise from a slight increase in EP due to decreased resting current across the reticular lamina. In contrast, outer hair cell loss would not be expected to affect

variance of the first spike latency, maximum discharge rates (either peak or steady state), or dynamic range of response (at least for high-SR fibers: see Chapter 4). Therefore, the mechanisms underlying these striking response abnormalities observed in the BK knockout mice must arise further "downstream" in the transduction cascade.

6.4.2 BK channels in IHCs

In mammalian inner hair cells (IHCs), two major K-currents are activated by depolarization: one fast (Ik,f), the other slow (Ik,s). The large conductance and fast kinetics of Ik,f imply a role in shaping IHC voltage responses, especially at high frequencies. The pharmacological profile suggests that Ik,f is carried by BK channels, e.g. this fast response can be blocked by iberiotoxin or charybdotoxin in IHCs isolated from adult guinea pigs (Skinner et al. 2003). Indeed, the changes in responses to current steps in IHCs induced by application of BK-channel blockers are very similar to the differences seen between wildtype and knockout IHCs from the mouse BK line, illustrated in Figure 6.1. These comparison, coupled with the immunocytochemical data showing an IHC expression of BK channels (Ruttiger et al., 2004) presents compelling evidence for the importance of this channel in shaping the rapid voltage responses of mammalian IHCs in both neonatal and adult cochleas.

In the present study, two aspects of AN response were evaluated that ought to be exquisitely sensitive to the loss of rapid voltage responses in IHCs: 1) maximum synchronization index to tones at frequencies below 4 kHz (Figure 6.7) and 2) the variance of the first spike latencies (FSLs) to tone bursts presented at 30 dB above threshold (Figure 6.17).

As discussed in previous chapters, data on synchronization index, or phase locking, are difficult to obtain in the mouse AN. This is because, as in other mammals, significant phase locking between AN spikes and the individual cycles of a stimulus sinusoid is only seen for stimulus frequencies below 4 kHz; however, in contrast to other mammals, 4 kHz is close to the low-frequency end of the mouse mechanical frequency map, thus few AN fibers respond to frequencies < 4 kHz (except at very high sound pressures). Nevertheless, the few measures of synchrony-level functions that were obtained from wildtype and knockout ears are consistent with the idea that the degree of phase locking is reduced in the absence of the BK channels (Figure 6.7).

More compelling evidence for disruption of rapid IHC voltage responses *in vivo* was seen in the data on variance of first spike latencies in the AN fibers. As shown in Figure 6.17, many AN fibers in the knockout ears showed increases in FSL variance of two orders of magnitude, and this increased variance was closely tied to a decrease in the onset rates of AN fibers. Because this onset rate is measured with time bins of 0.5 msec, it is exquisitely sensitive to the synchronization, across stimulus presentations, of the first spike after tone burst onset. Clearly, the loss of the BK channel has decreased the degree of synchronization. It is not hard to imagine that this loss of synchronization is a direct result of a slower rate of rise of IHC receptor potential after tone burst onset, as implied by the results obtained in isolated IHC with injection of "transducer currents" (Figure 6.1C and D). As described in the Introduction, this transducer current waveform was derived by passing a 2-kHz sinusoid through a saturating non-linearity of the form described for the transformation between stereocilia bundle displacement and receptor current.

It is less clear why there should be heterogeneity in this aspect of AN response, i.e. why some fibers in knockout ears retained near-normal onset rates coupled with near normal FSL variances (Figure 6.17). The relatively small number of "normal" AN fibers in knockouts were not clustered in particular animals or particular CF regions; rather they appeared to be intermingled at random with the larger population of abnormal fibers. The existence of normal fibers suggests that other channels in the IHC can be up- or down-regulated to compensate for the loss of BK. Their apparent randomness suggest that such compensation is a probabilistic event that occurs only rarely.

Although the decrease in AN onset rates is well explained by a slowing of the IHC receptor potential at tone burst onset, it is not obvious how a decrease in steady-state rates would arise from the same mechanism. The further observation, from Figure 6.17B, that knockout fibers with normal FSL variances still had lower-than normal steady-state rates (despite showing normal onset rates), also strongly suggests that a second mechanism must be invoked to explain the observed changes in steady state rate.

There are a number of IHC-based mechanisms that contribute to the generation of a maximum steady-state rate in the AN, from the saturating non-linearity in mechanoelectric transduction at the apical end of the cell which produces the IHC DC receptor potential, to the synaptic machinery at the basal end of the cell that converts that potential to an equilibrium rate of vesicle release. There are a number of *ad hoc* hypotheses that could be advanced to explain the observed decrease in steady-state AN discharge rate, based on a modification of one or more of these IHC-based processes. For example, the loss of BK channels should lead to a slight depolarization of the IHC resting potential; and such a sustained depolarization might directly affect the efficacy of the afferent synapse or, by reducing stereociliary Ca^{++} entry, shift the transducer set point rightward along the I,x curve, thus reducing sound-driven DC potentials and maximum neural rates. However, in search of the mechanisms underlying decreased steady-state rates in the BK knockout, it is also important to look further "downstream", i.e. to consider the possibility that BK expression in the spiral ganglion cells themselves also shapes important aspects of AN response in the adult ear.

6.4.3 BK channels in spiral ganglion cells

BK channels are known to play important roles in shaping action potential waveform (Edgerton and Reinhart 2003; Faber and Sah 2002; Lovell and McCobb 2001; Smith et al. 2002) and consequently, in shaping the intrinsic firing properties of neurons (Lovell and McCobb 2001; Smith et al. 2002). Action potential waveforms recorded from Purkinje cells in cerebellar slices from BK knockout mice showed a decrease in the after-hyperpolarization, without a significant change in the spike waveform itself (Sausbier et al. 2004). Purkinje cells from BK knockout mice also showed an elevated (depolarized) resting potential and greatly reduced action potential frequency, both in spontaneous activity as well as in activity that can normally be evoked by depolarizing pulses. In otherwise silent Purkinje cells, spikes could be evoked only by preceding the depolarizing pulses with a hyperpolarizing current injection. Thus, the authors concluded that "depolarization block", i.e. inactivation of Na^{+} channels due to the loss of BK channels and concommitant loss of the after-hyperpolarization of the action potential, was responsible for the decreased neural activity observed (Sausbier et al. 2004).

With respect to expression of BK channels in cochlear neurons, *in vitro* studies of murine spiral ganglion cells isolated at post-natal days 3-8 (Adamson et al. 2002) show dramatic effects

of charybdotoxin, a specific BK channel blocker, including increased latencies for the first spike evoked by depolarizing currents near threshold. In pharmacological studies, *in vivo,* of cochlear function in the adult, perfusion of BK blockers charybdotoxin or iberiotoxin can virtually eliminate the neural compound action potential (CAP) while causing little change in the DPOAEs or cochlear microphonics. Such a profound effect on sound-evoked neural activity would not be predicted based on the fractional changes in onset rates associated with loss of BK function in the adult mouse. This discrepancy suggests that there are additional channels in either IHCs or AN fibers that are critical for synaptic transmission and are sensitive to these pharmacological agents.

BK channels have been localized to spiral ganglion cells in the adult guinea pig using *in situ* hybridization (Skinner et al. 2003). Thus, it is likely that BK channels continue to play an important role in adult spiral ganglion cells. Combining these observation with those on the spike-rate reductions seen in cerebellar neurons in the BK knockout, it is tempting to speculate that the dramatic decreases in steady-state rates seen in AN fibers are due to phenomena related to depolarization block in the neurons themselves, rather than to any changes in IHC function associated with the loss of BK channels. Further support for this hypothesis could be obtained by inference of the neural refractory period from construction of "hazard functions" (Li and Young 1993). However, large numbers of spike intervals are required for robust statistics and such long runs are difficult to achieve in recordings from mouse AN.

6.5 Conclusion

BK-channels are known to play a prominent role in hair cell function where their interaction with voltage-gated calcium channels generates an electrical resonance. In the basilar papilla of the chick, it is believed that variations in the number and properties of BK channels, which influences the electrical resonance of each cell, helps establish the tonotopic map in this organ (Navaratnam et al. 1997; Rosenblatt et al. 1997). In contrast to lower vertebrates, little is known concerning the role of BK channels in mammalian hearing. Immunohistochemical studies have located BK channels to several cochlear structures including IHCs, OHCs, spiral ligament and stria vascularis (Ruttiger et al. 2004; Shen et al. 2004; Skinner et al. 2003). A BK channel knockout mouse model has been used to elucidate the role of BK channels in mammalian hearing (Ruttiger et al. 2004). Patch clamp recordings from BK knockout IHCs reveal that these cells have increased membrane resistance and consequently, have larger voltage responses to step currents and longer membrane time constants (see Figure 6.1). In this chapter we show that such changes in IHC responses are reflected in lower AN fiber maximum synchronization indices (Figure 6.7) and larger variance of the first spike latency that is associated with lower AN onset rates (Figure 6.17A). The finding that AN fibers also show a striking decrease in steady-state discharge rates, which cannot be easily inferred from pre-synaptic changes in cochlear function, suggests that there are also post-synaptic changes in cochlear function that are shaping aspects of AN fiber response. Given that BK channels have been shown to play a role in action potential (AP) repolarization and after-hyperpolarization (Edgerton and Reinhart 2003; Storm 1987) and that changes in AP waveform can lead to changes in the intrinsic firing properties of neurons (Lovell and McCobb 2001; Smith et al. 2002), it is possible that loss of BK channels in AN fibers may lead to lower discharge rates. In support of this possibility is the finding that action potential waveforms recorded from Purkinje cells in cerebellar slices in BK knockout mice showed a decrease in the after-hyperpolarization and greatly reduced action potential frequency, both in the spontaneous activity as well as in activity that can normally be evoked by

depolarizing pulses (Sausbier et al. 2004). Finally, results from the present study also show that, despite loss of the BK channels in the mouse cochlea, a number of basic response properties of AN fibers were not significantly altered, including 1) the normal stochastic pattern of discharge in AN fibers (spontaneous or sound-evoked), 2) the distribution of AN spontaneous rates, 3) the shapes of AN tuning curves, or 4) the dynamic ranges of AN fibers. The normality of tuning curve shapes in the knockout mouse strongly suggest that, in the mammalian ear, that BK channels do not play the same key role in establishing frequency selectivity as in non-mammalian vertebrates (Fettiplace and Fuchs 1999).

Bibliography

Abou-Madi L, Pontarotti P, Tramu G, Cupo A, and Eybalin M. Coexistence of putative neuroactive substances in lateral olivocochlear neurons of rat and guinea pig. *Hear Res* 30: 135-146, 1987.

Adams JC, Mroz EA, and Sewell WF. A possible neurotransmitter role for CGRP in a hair-cell sensory organ. *Brain Res* 419: 347-351., 1987.

Adamson CL, Reid MA, Mo ZL, Bowne-English J, and Davis RL. Firing features and potassium channel content of murine spiral ganglion neurons vary with cochlear location. *J Comp Neurol* 447: 331-350, 2002.

Bailey GP and Sewell WF. Calcitonin gene-related peptide suppresses hair cell responses to mechanical stimulation in the Xenopus lateral line organ. *J Neurosci* 20: 5163-5169., 2000.

Birch LM, Warfield D, Ruben RJ, and Mikaelian DO. Behavioral Measurements of Pure Tone Thresholds in Normal CBA-J Mice. *The Journal of Auditory Research* 8: 459-468, 1968.

Blackburn CC and Sachs MB. Classification of unit types in the anteroventral cochlear nucleus: PST histograms and regularity analysis. *J Neurophysiol* 62: 1303-1329, 1989.

Borg E, Engstrom B, Linde G, and Marklund K. Eighth nerve fiber firing features in normal-hearing rabbits. *Hear Res* 36: 191-201, 1988.

Brain SD, Williams TJ, Tippins JR, Morris HR, and MacIntyre I. Calcitonin gene-related peptide is a potent vasodilator. *Nature* 313: 54-56., 1985.

Brown MC, Smith DI, and Nuttall AL. Anesthesia and surgical trauma: their influence on the guinea pig compound action potential. *Hear Res* 10: 345-358, 1983.

Carlisle L, Aberdeen J, Forge A, and Burnstock G. Neural basis for regulation of cochlear blood flow: peptidergic and adrenergic innervation of the spiral modiolar artery of the guinea pig. *Hear Res* 43: 107-113., 1990.

Chimento TC and Schreiner CE. Adaptation and recovery from adaptation in single fiber responses of the cat auditory nerve. *J Acoust Soc Am* 90: 263-273, 1991.

Cody AR and Johnstone BM. Acoustically evoked activity of single efferent neurons in the guinea pig cochlea. *J Acoust Soc Am* 72: 280-282., 1982.

Dallos P and Harris D. Properties of auditory nerve responses in absence of outer hair cells. *J Neurophysiol* 41: 365-383, 1978.

Edgerton JR and Reinhart PH. Distinct contributions of small and large conductance Ca2+-activated K+ channels to rat Purkinje neuron function. *J Physiol* 548: 53-69, 2003.

Ehret G. Age-dependent hearing loss in normal hearing mice. *Naturwissenschaften* 61: 506-507, 1974.
Ehret G. Masked Auditory Thresholds, Critical Ratios, and Scales of the Basilar Membrane of the Housemouse (*Mus musculus*). *Journal of Comparative Physiology* 103: 329-341, 1975.
Ehret G and Moffat AJ. Noise masking of tone responses and critical ratios in single units of the mouse cochlear nerve and cochlear nucleus. *Hear Res* 14: 45-57., 1984.
el Barbary A. Auditory nerve of the normal and jaundiced rat. I. Spontaneous discharge rate and cochlear nerve histology. *Hear Res* 54: 75-90, 1991.
Evans EF. The frequency response and other properties of single fibres in the guinea-pig cochlear nerve. *J Physiol* 226: 263-287, 1972.
Eybalin M, Charachon G, and Renard N. Dopaminergic lateral efferent innervation of the guinea-pig cochlea: immunoelectron microscopy of catecholamine-synthesizing enzymes and effect of 6-hydroxydopamine. *Neuroscience* 54: 133-142., 1993.
Faber ES and Sah P. Physiological role of calcium-activated potassium currents in the rat lateral amygdala. *J Neurosci* 22: 1618-1628, 2002.
Fay RR. *Hearing in Vertebrates: a Psychophysics Databook*. Worcester, MA: Hefferman Press Inc., 1988.
Fekete DM, Rouiller EM, Liberman MC, and Ryugo DK. The central projections of intracellularly labeled auditory nerve fibers in cats. *J Comp Neurol* 229: 432-450, 1984.
Fernandez HL, Ross GS, and Nadelhaft I. Neurogenic calcitonin gene-related peptide: a neurotrophic factor in the maintenance of acetycholinesterase molecular forms in adult skeletal muscles. *Brain Res* 844: 83-97, 1999.
Fettiplace R and Fuchs PA. Mechanisms of hair cell tuning. *Annu Rev Physiol* 61: 809-834, 1999.
Finck A and Berlin CI. Comparison between single unit responses in the auditory nerve amd GSR determined thresholds in mice. *Journal of Auditory Research* 5: 1-9, 1965.
Francis HW, Rivas A, Lehar M, and Ryugo DK. Two types of afferent terminals innervate cochlear inner hair cells in C57BL/6J mice. *Brain Res* 1016: 182-194, 2004.
Francis HW, Ryugo DK, Gorelikow MJ, Prosen CA, and May BJ. The functional age of hearing loss in a mouse model of presbycusis. II. Neuroanatomical correlates. *Hear Res* 183: 29-36, 2003.
Gao J, Wu X, and Zuo J. Targeting hearing genes in mice. *Brain Res Mol Brain Res* 132: 192-207, 2004.
Giniatullin R, Di Angelantonio S, Marchetti C, Sokolova E, Khiroug L, and Nistri A. Calcitonin gene-related peptide rapidly downregulates nicotinic receptor function and slowly raises intracellular Ca2+ in rat chromaffin cells in vitro. *J Neurosci* 19: 2945-2953., 1999.
Greenwood D. Critical bandwidth and the frequency coordinates of the basilar membrane. *Journal of the Acoustical Society of America* 33: 1344-1356, 1961.
Groff JA and Liberman MC. Modulation of cochlear afferent responses by the lateral olivocochlear system: activation via electrical stimulation of the inferior colliculus. *Journal of Neurophysiology* 90: 3178-3200, 2003.
Guinan JJ, Jr. and Stankovic KM. Medial efferent inhibition produces the largest equivalent attenuations at moderate to high sound levels in cat auditory-nerve fibers. *J Acoust Soc Am* 100: 1680-1690, 1996.
Guinan JJ, Jr., Warr WB, and Norris BE. Differential olivocochlear projections from lateral versus medial zones of the superior olivary complex. *J Comp Neurol* 221: 358-370., 1983.

Harrison JM and Irving R. The organization of the posterior ventral cochlear nucleus in the rat. *J Comp Neurol* 126: 391-401, 1966.
Heffner H and Masterton B. Hearing in Glires: Domestic rabbit, cotton rat, feral house mouse, and kangaroo rat. *Journal of the Acoustical Society of America* 68: 1584-1599, 1980.
Hequembourg S and Liberman MC. Spiral ligament pathology: a major aspect of age-related cochlear degeneration in C57BL/6 mice. *J Assoc Res Otolaryngol* 2: 118-129, 2001.
Hibino H, Horio Y, Inanobe A, Doi K, Ito M, Yamada M, Gotow T, Uchiyama Y, Kawamura M, Kubo T, and Kurachi Y. An ATP-dependent inwardly rectifying potassium channel, KAB-2 (Kir4. 1), in cochlear stria vascularis of inner ear: its specific subcellular localization and correlation with the formation of endocochlear potential. *J Neurosci* 17: 4711-4721, 1997.
Irving R and Harrison JM. The superior olivary complex and audition: a comparative study. *J Comp Neurol* 130: 77-86, 1967.
Javel E. Long-term adaptation in cat auditory-nerve fiber responses. *J Acoust Soc Am* 99: 1040-1052, 1996.
Jimenez AM, Stagner BB, Martin GK, and Lonsbury-Martin BL. Age-related loss of distortion product otoacoustic emissions in four mouse strains. *Hear Res* 138: 91-105., 1999.
Johnson DH. The relationship between spike rate and synchrony in responses of auditory-nerve fibers to single tones. *J Acoust Soc Am* 68: 1115-1122, 1980.
Johnson DH. The relationship of post-stimulus time and interval histograms to the timming characteristics of spike trains. *Biophys J* 22: 413-430, 1978.
Juaneda C, Dumont Y, and Quirion R. The molecular pharmacology of CGRP and related peptide receptor subtypes. *Trends Pharmacol Sci* 21: 432-438., 2000.
Kiang NY-S, Watanabe T, Thomas EC, and Clarke LF. *Discharge patterns of single fibers in the cat's auditory nerve.* Cambridge: MIT press, 1965.
Kros CJ, Ruppersberg JP, and Rusch A. Expression of a potassium current in inner hair cells during development of hearing in mice. *Nature* 394: 281-284, 1998.
Lang H, Schulte BA, and Schmiedt RA. Endocochlear potentials and compound action potential recovery: functions in the C57BL/6J mouse. *Hear Res* 172: 118-126, 2002.
Legan PK, Lukashkina VA, Goodyear RJ, Kossi M, Russell IJ, and Richardson GP. A targeted deletion in alpha-tectorin reveals that the tectorial membrane is required for the gain and timing of cochlear feedback. *Neuron* 28: 273-285, 2000.
Li HS and Borg E. Age-related loss of auditory sensitivity in two mouse genotypes. *Acta Otolaryngol* 111: 827-834, 1991.
Li J and Young ED. Discharge-rate dependence of refractory behavior of cat auditory-nerve fibers. *Hear Res* 69: 151-162, 1993.
Liberman MC. Auditory-nerve response from cats raised in a low-noise chamber. *J Acoust Soc Am* 63: 442-455., 1978.
Liberman MC. Central projections of auditory-nerve fibers of differing spontaneous rate. I. Anteroventral cochlear nucleus. *J Comp Neurol* 313: 240-258, 1991.
Liberman MC. The cochlear frequency map for the cat: labeling auditory-nerve fibers of known characteristic frequency. *J Acoust Soc Am* 72: 1441-1449, 1982a.
Liberman MC. Effects of chronic cochlear de-efferentation on auditory-nerve response. *Hear Res* 49: 209-223., 1990.
Liberman MC. Morphological differences among radial afferent fibers in the cat cochlea: an electron-microscopic study of serial sections. *Hear Res* 3: 45-63, 1980.

Liberman MC. Single-neuron labeling in the cat auditory nerve. *Science* 216: 1239-1241, 1982b.
Liberman MC and Brown MC. Physiology and anatomy of single olivocochlear neurons in the cat. *Hear Res* 24: 17-36, 1986.
Liberman MC and Dodds LW. Single-neuron labeling and chronic cochlear pathology. II. Stereocilia damage and alterations of spontaneous discharge rates. *Hear Res* 16: 43-53, 1984a.
Liberman MC and Dodds LW. Single-neuron labeling and chronic cochlear pathology. III. Stereocilia damage and alterations of threshold tuning curves. *Hear Res* 16: 55-74, 1984b.
Liberman MC, Dodds LW, and Pierce S. Afferent and efferent innervation of the cat cochlea: quantitative analysis with light and electron microscopy. *J Comp Neurol* 301: 443-460., 1990.
Lovell PV and McCobb DP. Pituitary control of BK potassium channel function and intrinsic firing properties of adrenal chromaffin cells. *J Neurosci* 21: 3429-3442, 2001.
Lu JT, Son YJ, Lee J, Jetton TL, Shiota M, Moscoso L, Niswender KD, Loewy AD, Magnuson MA, Sanes JR, and Emeson RB. Mice lacking alpha-calcitonin gene-related peptide exhibit normal cardiovascular regulation and neuromuscular development. *Mol Cell Neurosci* 14: 99-120., 1999.
Maison SF, Adams JC, and Liberman MC. Olivocochlear innervation in the mouse: immunocytochemical maps, crossed vs. uncrossed contributions and transmitter colocalization. *Journal of Comparative Neurology*, 2002.
Maison SF, Emeson RB, Adams JC, Luebke AE, and Liberman MC. Loss of alpha CGRP reduces sound-evoked activity in the cochlear nerve. *J Neurophysiol* 90: 2941-2949, 2003.
Melcher JR and Kiang NY. Generators of the brainstem auditory evoked potential in cat. III: Identified cell populations. *Hear Res* 93: 52-71, 1996.
Merchan-Perez A and Liberman MC. Ultrastructural differences among afferent synapses on cochlear hair cells: correlations with spontaneous discharge rate. *J Comp Neurol* 371: 208-221, 1996.
Mikaelian DO, Warfield D, and Norris O. Genetic progressive hearing loss in the C57-b16 mouse. Relation of behavioral responses to chochlear anatomy. *Acta Otolaryngol* 77: 327-334, 1974.
Mountain DC. Changes in endolymphatic potential and crossed olivocochlear bundle stimulation alter cochlear mechanics. *Science* 210: 71-72, 1980.
Mueller M, Huenerbein Kv, Silivi Hoidis, and Smolder JWT. A Physiological Place-Frequency Map of the Cochlea in the Mouse. *Assoc Res Otolaryngol Abs*: 382, 2004.
Mulle C, Benoit P, Pinset C, Roa M, and Changeux JP. Calcitonin gene-related peptide enhances the rate of desensitization of the nicotinic acetylcholine receptor in cultured mouse muscle cells. *Proc Natl Acad Sci U S A* 85: 5728-5732., 1988.
Mullen LM and Ryan AF. Transgenic Mice: Genome Manipulation and Induced Mutations. In: *Handbook of Mouse Auditory Research From Behavior to Molecular Biology*, edited by Willott JF. Boca Raton: CRC Press, 2001, p. 457-474.
Muller M and Robertson D. Relationship between tone burst discharge pattern and spontaneous firing rate of auditory nerve fibres in the guinea pig. *Hear Res* 57: 63-70, 1991.
Navaratnam DS, Bell TJ, Tu TD, Cohen EL, and Oberholtzer JC. Differential distribution of Ca2+-activated K+ channel splice variants among hair cells along the tonotopic axis of the chick cochlea. *Neuron* 19: 1077-1085, 1997.
Nelder JA and Mead R. A simplex method for function minimization. *Computer Journal* 7: 308-313, 1965.

Nistri A and Angelantonio S. Enhancement of neuronal nicotinic receptor activity of rat chromaffin cells by a novel class of peptides. *Ann N Y Acad Sci* 971: 100-107, 2002.
Ohlemiller KK and Echteler SM. Functional correlates of characteristic frequency in single cochlear nerve fibers of the Mongolian gerbil. *J Comp Physiol [A]* 167: 329-338, 1990.
Ohlemiller KK, Echteler SM, and Siegel JH. Factors that influence rate-versus-intensity relations in single cochlear nerve fibers of the gerbil. *J Acoust Soc Am* 90: 274-287., 1991.
Ohlemiller KK and Gagnon PM. Apical-to-basal gradients in age-related cochlear degeneration and their relationship to "primary" loss of cochlear neurons. *J Comp Neurol* 479: 103-116, 2004a.
Ohlemiller KK and Gagnon PM. Cellular correlates of progressive hearing loss in 129S6/SvEv mice. *J Comp Neurol* 469: 377-390, 2004b.
Osterlund M, Fontaine B, Devillers-Thiery A, Geoffroy B, and Changeux JP. Acetylcholine receptor expression in primary cultures of embryonic chick myotubes--I. Discoordinate regulation of alpha-, gamma- and delta- subunit gene expression by calcitonin gene-related peptide and by muscle electrical activity. *Neuroscience* 32: 279-287, 1989.
Ou HC, Harding GW, and Bohne BA. An anatomically based frequency-place map for the mouse cochlea. *Hear Res* 145: 123-129, 2000.
Palmer AR and Russell IJ. Phase-locking in the cochlear nerve of the guinea-pig and its relation to the receptor potential of inner hair-cells. *Hear Res* 24: 1-15, 1986.
Prosen CA, Dore DJ, and May BJ. The functional age of hearing loss in a mouse model of presbycusis. I. Behavioral assessments. *Hear Res* 183: 44-56, 2003.
Relkin EM and Doucet JR. Recovery from prior stimulation. I: Relationship to spontaneous firing rates of primary auditory neurons. *Hear Res* 55: 215-222, 1991.
Rhode WS and Smith PH. Characteristics of tone-pip response patterns in relationship to spontaneous rate in cat auditory nerve fibers. *Hear Res* 18: 159-168, 1985.
Rhode WS and Smith PH. Encoding timing and intensity in the ventral cochlear nucleus of the cat. *J Neurophysiol* 56: 261-286, 1986a.
Rhode WS and Smith PH. Physiological studies on neurons in the dorsal cochlear nucleus of cat. *J Neurophysiol* 56: 287-307, 1986b.
Robertson D and Gummer M. Physiological and morphological characterization of efferent neurones in the guinea pig cochlea. *Hear Res* 20: 63-77, 1985.
Robles L and Ruggero MA. Mechanics of the mammalian cochlea. *Physiol Rev* 81: 1305-1352, 2001.
Rosenblatt KP, Sun ZP, Heller S, and Hudspeth AJ. Distribution of Ca2+-activated K+ channel isoforms along the tonotopic gradient of the chicken's cochlea. *Neuron* 19: 1061-1075, 1997.
Rouiller EM, Cronin-Schreiber R, Fekete DM, and Ryugo DK. The central projections of intracellularly labeled auditory nerve fibers in cats: an analysis of terminal morphology. *J Comp Neurol* 249: 261-278, 1986.
Rouiller EM and Ryugo DK. Intracellular marking of physiologically characterized cells in the ventral cochlear nucleus of the cat. *J Comp Neurol* 225: 167-186., 1984.
Ruel J, Nouvian R, Gervais d'Aldin C, Pujol R, Eybalin M, and Puel JL. Dopamine inhibition of auditory nerve activity in the adult mammalian cochlea. *Eur J Neurosci* 14: 977-986., 2001.
Ruggero MA and Rich NC. Furosemide alters organ of corti mechanics: evidence for feedback of outer hair cells upon the basilar membrane. *J Neurosci* 11: 1057-1067, 1991.

Ruggero MA, Rich NC, Recio A, Narayan SS, and Robles L. Basilar-membrane responses to tones at the base of the chinchilla cochlea. *J Acoust Soc Am* 101: 2151-2163, 1997.
Ruttiger L, Sausbier M, Zimmermann U, Winter H, Braig C, Engel J, Knirsch M, Arntz C, Langer P, Hirt B, Muller M, Kopschall I, Pfister M, Munkner S, Rohbock K, Pfaff I, Rusch A, Ruth P, and Knipper M. Deletion of the Ca2+-activated potassium (BK) alpha-subunit but not the BKbeta1-subunit leads to progressive hearing loss. *Proc Natl Acad Sci U S A* 101: 12922-12927, 2004.
Sachs MB, Winslow RL, and Sokolowski BH. A computational model for rate-level functions from cat auditory-nerve fibers. *Hear Res* 41: 61-69, 1989.
Sausbier M, Hu H, Arntz C, Feil S, Kamm S, Adelsberger H, Sausbier U, Sailer CA, Feil R, Hofmann F, Korth M, Shipston MJ, Knaus HG, Wolfer DP, Pedroarena CM, Storm JF, and Ruth P. Cerebellar ataxia and Purkinje cell dysfunction caused by Ca2+-activated K+ channel deficiency. *Proc Natl Acad Sci U S A* 101: 9474-9478, 2004.
Schrott A, Puel JL, and Rebillard G. Cochlear origin of 2f1-f2 distortion products assessed by using 2 types of mutant mice. *Hear Res* 52: 245-253, 1991.
Sento S and Ryugo DK. Endbulbs of held and spherical bushy cells in cats: morphological correlates with physiological properties. *J Comp Neurol* 280: 553-562, 1989.
Sewell WF. The effects of furosemide on the endocochlear potential and auditory-nerve fiber tuning curves in cats. *Hear Res* 14: 305-314, 1984a.
Sewell WF. The relation between the endocochlear potential and spontaneous activity in auditory nerve fibres of the cat. *Journal of Physiology* 347: 685-696, 1984b.
Sewell WF and Starr PA. Effects of calcitonin gene-related peptide and efferent nerve stimulation on afferent transmission in the lateral line organ. *J Neurophysiol* 65: 1158-1169, 1991.
Shen Z, Liang F, Hazen-Martin DJ, and Schulte BA. BK channels mediate the voltage-dependent outward current in type I spiral ligament fibrocytes. *Hear Res* 187: 35-43, 2004.
Siegel JH and Kim DO. Efferent neural control of cochlear mechanics? Olivocochlear bundle stimulation affects cochlear biomechanical nonlinearity. *Hear Res* 6: 171-182, 1982.
Skinner LJ, Enee V, Beurg M, Jung HH, Ryan AF, Hafidi A, Aran JM, and Dulon D. Contribution of BK Ca2+-activated K+ channels to auditory neurotransmission in the Guinea pig cochlea. *J Neurophysiol* 90: 320-332, 2003.
Sliwinska-Kowalska M, Parakkal M, Schneider ME, and Fex J. CGRP-like immunoreactivity in the guinea pig organ of Corti: a light and electron microscopy study. *Hear Res* 42: 83-95., 1989.
Smith MR, Nelson AB, and Du Lac S. Regulation of firing response gain by calcium-dependent mechanisms in vestibular nucleus neurons. *J Neurophysiol* 87: 2031-2042, 2002.
Smith PH, Joris PX, and Yin TC. Projections of physiologically characterized spherical bushy cell axons from the cochlear nucleus of the cat: evidence for delay lines to the medial superior olive. *J Comp Neurol* 331: 245-260, 1993.
Smith RL. Short-term adaptation in single auditory nerve fibers: some poststimulatory effects. *J Neurophysiol* 40: 1098-1111, 1977.
So E, Kikuchi T, Ishimaru K, Miyabe Y, and Kobayashi T. Immunolocalization of voltage-gated potassium channel Kv3.1b subunit in the cochlea. *Neuroreport* 12: 2761-2765, 2001.
Spoendlin H. Innervation patterns in the organ of corti of the cat. *Acta Otolaryngol* 67: 239-254, 1969.

Spoendlin H and Schrott A. The spiral ganglion and the innervation of the human organ of Corti. *Acta Otolaryngol* 105: 403-410, 1988.
Spongr VP, Flood DG, Frisina RD, and Salvi RJ. Quantitative measures of hair cell loss in CBA and C57BL/6 mice throughout their life spans. *J Acoust Soc Am* 101: 3546-3553., 1997.
Storm JF. Action potential repolarization and a fast after-hyperpolarization in rat hippocampal pyramidal cells. *J Physiol* 385: 733-759, 1987.
Takeuchi S and Ando M. Voltage-dependent outward K(+) current in intermediate cell of stria vascularis of gerbil cochlea. *Am J Physiol* 277: C91-99, 1999.
Tsuji J and Liberman MC. Intracellular labeling of auditory nerve fibers in guinea pig: central and peripheral projections. *J Comp Neurol* 381: 188-202, 1997.
Vergara C, Latorre R, Marrion NV, and Adelman JP. Calcium-activated potassium channels. *Curr Opin Neurobiol* 8: 321-329, 1998.
Vetter DE, Adams JC, and Mugnaini E. Chemically distinct rat olivocochlear neurons. *Synapse* 7: 21-43., 1991.
Vetter DE, Li C, Zhao L, Contarino A, Liberman MC, Smith GW, Marchuk Y, Koob GF, Heinemann SF, Vale W, and Lee K. Urocortin-deficient mice show hearing impairment and increased anxiety behavior. *Nature genetics* 31: 1-7, 2002.
Vetter DE, Liberman MC, Mann J, Barhanin J, Boulter J, Brown MC, Saffiote-Kolman J, Heinemann SF, and Elgoyhen AB. Role of alpha9 nicotinic ACh receptor subunits in the development and function of cochlear efferent innervation. *Neuron* 23: 93-103, 1999.
Watson JD, Gilman M, Witkowski J, and Zoller M. The Introduction of Foreign Genes into Mice. In: *Recombinant DNA* (Second ed.). New York: Scientific American Books, 1998, p. 255-267.
Weakly JN. The action of cobalt ions on neuromuscular transmission in the frog. *J Physiol* 234: 597-612, 1973.
Webster DB and Trune DR. Cochlear nuclear complex of mice. *Am J Anat* 163: 103-130., 1982.
Westerman LA and Smith RL. Rapid and short-term adaptation in auditory nerve responses. *Hear Res* 15: 249-260., 1984.
Winter IM, Robertson D, and Yates GK. Diversity of characteristic frequency rate-intensity functions in guinea pig auditory nerve fibres. *Hear Res* 45: 191-202., 1990.
Ylikoski J, Pirvola U, Happola O, Panula P, and Virtanen I. Immunohistochemical demonstration of neuroactive substances in the inner ear of rat and guinea pig. *Acta Otolaryngol* 107: 417-423., 1989.
Yoshida N and Liberman MC. Sound conditioning reduces noise-induced permanent threshold shift in mice. *Hear Res* 148: 213-219., 2000.
Young ED, Robert JM, and Shofner WP. Regularity and latency of units in ventral cochlear nucleus: implications for unit classification and generation of response properties. *J Neurophysiol* 60: 1-29., 1988.
Zheng QY, Johnson KR, and Erway LC. Assessment of hearing in 80 inbred strains of mice by ABR threshold analyses. *Hear Res* 130: 94-107., 1999a.
Zheng XY, Henderson D, McFadden SL, Ding DL, and Salvi RJ. Auditory nerve fiber responses following chronic cochlear de- efferentation. *J Comp Neurol* 406: 72-86., 1999b.
Zurek PM, Clark WW, and Kim DO. The behavior of acoustic distortion products in the ear canals of chinchillas with normal or damaged ears. *J Acoust Soc Am* 72: 774-780, 1982.